CHARACTERIZATION OF SHAPE MEMORY POLYMERS FOR USE AS A MORPHING AIRCRAFT SKIN MATERIAL

Thesis

Submitted to

The School of Engineering

UNIVERSITY OF DAYTON

in Partial Fulfillment of the Requirements for

The Degree

Master of Science in Aerospace Engineering

by

Robert Sebastian Bortolin

UNIVERSITY OF DAYTON

Dayton, OH

August 2005

CHARACTERIZATION OF SHAPE MEMORY POLYMERS FOR USE AS A
MORPHING AIRCRAFT SKIN MATERIAL

APPROVED BY:

Brian Sanders, Ph.D.
Advisory Committee Chairman
Adjunct Professor, Mechanical and
Aerospace Engineering Department

Geoffrey J. Frank, Ph.D.
Committee member
University of Dayton Research Institute

Margaret Pinnell, Ph.D.
Committee member
Assistant Professor, Mechanical and
Aerospace Engineering Department

Kevin Hallinan, Ph.D.
Chair, Department of Mechanical and
Aerospace Engineering Department

Donald L. Moon, Ph.D.
Associate Dean
Graduate Engineering Programs & Research
School of Engineering

Joseph E. Saliba, Ph.D., P.E.
Dean, School of Engineering

ii

ABSTRACT

CHARACTERIZATION OF SHAPE MEMORY POLYMERS FOR USE AS A
MORPHING AIRCRAFT SKIN MATERIAL

Bortolin, Robert S.
University of Dayton

Advisor: Dr. Brian Sanders

The research presented in this thesis investigated the characteristics of Shape
Memory Polymers (SMPs) for potential use as a skin material on morphing aircraft. Out
of the many possible morphing techniques to investigate, this research centered on in-
plane morphing, which provides the skin with a varying geometry while it must resist the
aerodynamic and structural loads presented to it. For this geometry change, it is necessary
to understand the behavior of the material in shear, as that is how the material will be
deformed. The shear properties were obtained by designing a unique test fixture to induce
pure shear in the SMP. With this fixture, the rate dependence of the material, the amount
of prestrain in the material and varying specimen geometry were tested in order to assist
in the understanding of the behavior of the SMP in shear. Additionally, a Finite Element
(FE) analysis was conducted to better comprehend the observed experimental results. The
tests showed that the behavior of the SMP was that of a nonlinear viscoelastic material,
indicating a high strain rate dependence of the material properties. There was a large out-
of-plane deformation noticed during the testing, and with the use of the FE model it was

possible to identify this as buckling of the material. The results indicated that shape memory polymers are a young technology in need of more research if they are to be used for morphing aircraft skins. The end result is that SMPs are still a strong candidate material for long term goals, but not enough is known about them for their use in the near future as a deformable skin.

ACKNOWLEDGEMENTS

TABLE OF CONTENTS

LIST OF FIGURES

LIST OF TABLES

CHAPTER I

INTRODUCTION

Starting with the first powered flight on 17 December 1903, humans have been interested in changing the shape of aircraft for various reasons. Initially the Wright brothers used wing warping for roll control, but as aircraft began moving faster structures needed to become stiffer, making it harder for the wing to deform. Now aircraft are controlled by distinct control surfaces using rigid body motion, such as flaps and ailerons that change the lift characteristics of the wing, with minimal deformation of the structure.

Figure 1: Aircraft with Variable Sweep Wings. Left to Right: F-111, B-1, F-14

More recently changes in wing shape have been used to improve the aerodynamics of fighter aircraft. This can be observed in the variable sweep wings of the F-14, B-1 and the F-111 in Figure 1. These wings allow the aircraft to have good aerodynamics at multiple points in the flight envelope of the aircraft instead of optimal performance at one point and poor to acceptable aerodynamics at other points. Most noticeably swept wings reduces drag at higher Mach numbers, while long straight wings

are better for performance at low speeds and generally increase the range and endurance of an aircraft. Figure 2 illustrates how the coefficient of drag (CD) for a given wing sweep angle increases with Mach number, but with an increase in wing sweep angle the associated increase in the CD with Mach number is reduced. With variable sweep wings an aircraft can combine the attributes of both straight and swept wings for increased range over a swept wing aircraft and increased speed and maneuverability over a straight winged aircraft.
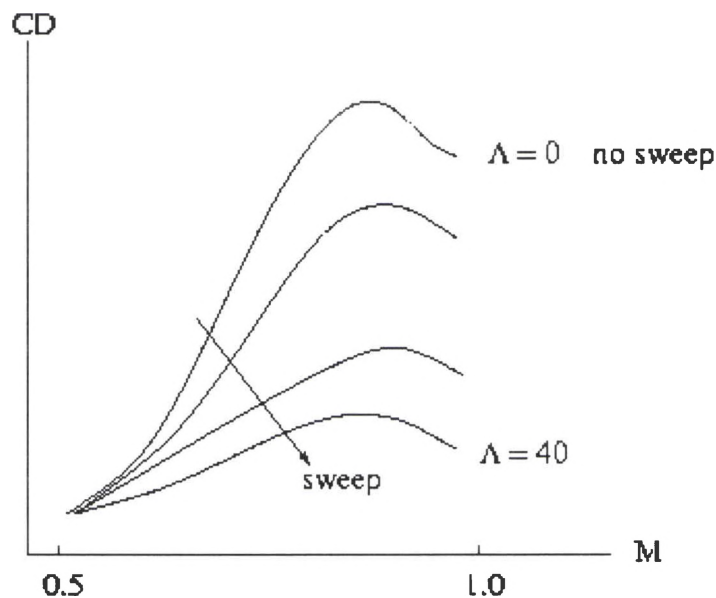
Figure 2: Effect of Sweep on Drag vs. Mach Number
Figure 2 used with Permission from **www.aerodyn.org**

The Air Force Research Laboratory defines morphing aircraft as aircraft that are capable of large scale controlled deformation to allow for a change of state of the aircraft. This change of state allows the aircraft to have improved aerodynamic performance throughout its entire flight envelope, even when compared to multiple aircraft simultaneously. This is because current aircraft are designed with a specific wing geometry that provides optimal performance at one point in the flight envelope that is

considered the most critical point. Performance decreases drastically as the aircraft moves away from that one point in the flight envelope.
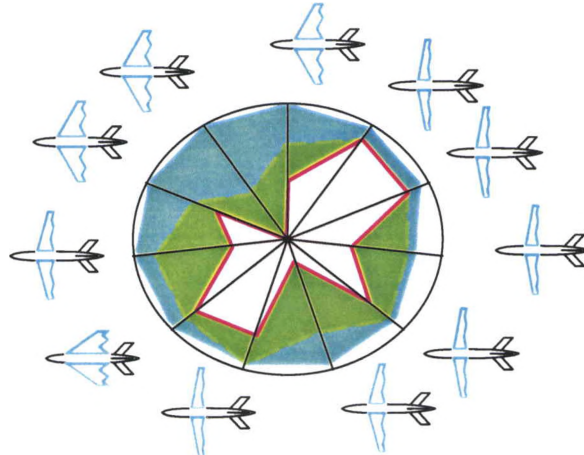
© *NextGen Aeronautics*
Figure 3: Spider Plot

Figure 3 shows what is called a spider plot. This plot compares how efficient different configurations are for different phases of flight, though does not necessarily show all possible flight regimes. The blue plot that almost fills the circle corresponds to the morphing concept shown by the aircraft figures surrounding the circle. Each radial line indicates a different phase of flight, such as take off, cruise, or maneuver, with more efficient configurations filling more of the circle along that direction. As is easily seen the blue plot is the most efficient of the three shown because it fills most of the circle. The green plot bordered by the dashed line is the next smaller plot, representing a less efficient aircraft design, possibly that of a variable sweep wing. The aircraft has good efficiency at most points on the plot, but is not as good as the morphing concept. The smallest plot, shown in red, is more representative of a typical aircraft design, with some

points of decent efficiency, while being almost incapable of obtaining some of the flight regimes shown in the spider plot.

Recent research efforts have focused on large planform changes, on the order of 100% change in area. Key elements to allow these changes are distributed high power density actuators, new structural designs, mechanized structures, and flexible skin concepts, with the latter being the focus of these efforts.

Mechanized structures provide the desired motion to shape the aircraft. These structures are highly engineered to provide one particular motion when it is requested. High power actuators are needed to overcome aerodynamic loads and provide this motion. Keeping the overall weight of the aircraft in mind these items must be as light as possible, while still providing the requisite stiffness. To reduce the weight, composites and lightweight actuators are needed. This results in high power density actuators being used to deform the structure. The deforming structure is covered by a flexible skin that can maintain aerodynamic characteristics while withstanding the air loads and providing minimal resistance to the desired motion of the structure.

There are currently two funded companies working on morphing aircraft concepts, which can be seen in Figure 4 below. Out of an infinite number of ways to achieve morphing, each company has picked one that it is working with. Both of the concepts require the use of many new technologies including flexible skins, mechanized structures, and high power density actuators. Both of the concepts have long straight

wings for cruise and loiter, while the in-flight morphing provides a change in aspect ratio and area to increase speed and improve maneuverability.
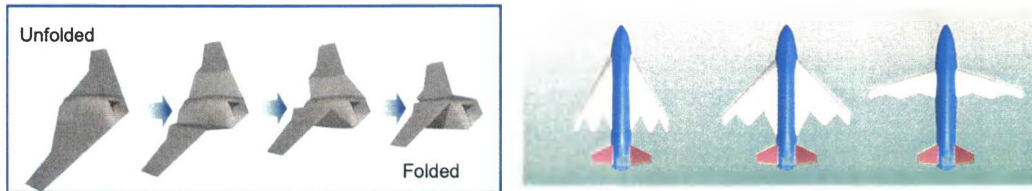
Figure 4: Out-of-Plane and In-Plane Morphing Aircraft Concepts

Lockheed Martin is using out-of-plane morphing for their folding wing concept. By using the different fold angles for the wing the aircraft can achieve the desired aerodynamic performance throughout its flight envelope. At cruise the wing is completely unfolded, providing the largest possible aspect ratio, and low drag. For maneuverability and high speed flight the wing will be folded up against the fuselage in the shape of a "Z" when viewed from the front, with the root and tip sections parallel and the middle section folded past vertical. Finally, for takeoff and landing the proposed configuration hash the middle section of the wing nearly vertical to enable some form of yaw control with the flaps.

The other concept, from NextGen Aeronautics, uses in-plane morphing, which involves complex manipulation of the wing planform to achieve maximum aerodynamic performance throughout the flight envelope. This aircraft varies the sweep of the wing through four key settings in fifteen-degree increments, from 15° to 60° sweep. The low sweep is used for cruise, with the maximum sweep is used for the dash and maneuvering configuration. The other two main settings are used for loiter and landing. In addition to the change in sweep, there is a change in chord as well, with different chord settings coupled to each of the sweep settings.

These are just two of many potential morphing aircraft geometries, and both of these concepts require the use of the aforementioned technologies. High power density actuators are needed to produce motion in mechanized structures, and flexible skins are needed to cover the structure and change shape with it. These skins must be able to carry shear loads while still transferring the aerodynamic pressures to the aircraft structure. Here is where a major problem occurs. A material that allows for the deformation of the structure will not transfer the aerodynamic loads very well. The more compliant the material the more it will need to be attached to the structure to prevent pillowing of the skin [Keihl et al, 2005]. Using an elastic material for the skin also requires a holding force when the skin is deformed because it wants to return to its original shape when strained. With Shape Memory Polymers (SMPs) this is not the case because once the SMP is cooled it will require no input force to maintain its deformed shape, and thus could require less power overall, compared to other candidate materials.

It is crucial that the skin of the aircraft be smooth and continuous, while at the same time allowing for these radical changes in geometry. A significant problem lies in finding a skin that can provide both simultaneously while not siphoning all of the available power on the aircraft to actuate the change in shape. A smooth skin is only possible without any out-of-plane deformation. This allows for laminar, as opposed to turbulent airflow over the wing. Laminar flow is preferred because it produces less drag under the same conditions, which in turn reduces the power required to fly the aircraft, and increases the range and endurance of the aircraft. Having a wavy or inconsistent

6

(layered) skin reduces the velocity at which the airflow over the wing becomes turbulent causing the aerodynamic detractions associated with turbulent flow to appear faster and have a larger impact.

Possible skin concepts to allow for the deformation while still maintaining a smooth skin are: scales, sliding panels, elastomers, and SMPs. A skin of scales would operate much like the scales on a fish; they would overlap enough to allow the desired motion through expansion of area and flexure of the wing and not be limited to a particular motion. A sliding skin would operate in a similar manner, but would be on a larger scale with fewer, more intricate panels used to allow a specific motion. Elastomers can be stretched in any direction to a point of maximum strain to allow wing deformations, but must be held in place because when in tension they constantly exert a force to return to their initial position. The final potential concept is to use shape memory polymers, with their ability to be soft and ductile when heated above their glass transition temperature, but be rigid and strong when below that temperature.

SMPs are just one of a long list of potential materials for use as skins in morphing aircraft. Other investigations have compared certain physical properties of SMPs, to various polyurethanes, copolyesters (a type of thermoset), and woven materials such as Spandex® [Kikuta, 2003]. Whatever material is investigated there are two key properties that should be present. First, the material must be able to deform to allow for the large shape changes that most morphing concepts see, and secondly, the material must be able

to withstand the aerodynamic loading that is applied on them with minimal out-of-plane deformation.

Shape Memory Polymers, with their ability to change shape and desire to return to their original, or lowest potential energy, shape are a very promising material to be used for the skin of a morphing aircraft wing. This research provides a foundation to make an initial assessment of just how promising SMPs are by determining their ability to be deformed in shear in both rigid and ductile states.

In order to help make this assessment this research had four main goals; the first was to devise a repeatable test process for large amounts of shear strain using a tensile loading machine, the second was to perform basic characterization of an SMP, next it was desired to model the behavior of the SMP, specifically in the tests preformed, and finally to understand the effect of prestrain on the SMP.

Shape Memory Polymers (SMPs) exhibit different properties at different times, or under different external conditions. This ability has the potential to allow a material to be rigid enough to carry loads, and also soft enough to allow deformations. These materials do not solve all of the problems, but instead limit the scope of the problems to specific intervals instead of throughout the entire flight envelope. When the material is soft to allow morphing it still must be able to resist the aerodynamic loads that allow the aircraft to fly. Many people believe that these materials are the primary candidate for a morphing skin material, as they can handle the required loadings, and need to be reinforced only at

specific times, thus changing the requirements of the reinforcement because it does not

see a constant load, but rather only sees a load for a brief amount of time.

CHAPTER II

BACKGROUND

This section will provide the reader with an idea of some of the possible materials and desired characteristics for skins on morphing aircraft. The materials must be able to deform to large strains, while carrying the aerodynamic loads that are applied to the structure. There is a brief history of some previous attempts at morphing, in a broader sense of the term, and how new materials provided the solutions to enable them, so the reader can understand where the program is coming from. Finally, there is an in-depth discussion about polymers, specifically shape memory polymers, and their properties.

All of the historical examples mentioned below shared many of the same problems that are being seen with the morphing aircraft program today. Each program needed a flexible skin to allow the desired deformations. These skins needed to be rigid enough resist the aerodynamic loads seen by the aircraft while allowing the deformations to be actuated with minimal power.

2.1 Previous Component Shape Control Demonstrations with Flexible Skins

In the early 1980's Boeing and the United States Air Force began work on a program call the Mission Adaptive Wing (MAW). The objective was to use a fly-by-wire technique to improve the aerodynamic efficiency of the F-111. This manifested itself in the form of a computer program that would act autonomously to control the camber of the wing by using leading and trailing edge variable camber devices that were connected to a fixed wingbox. Constraining the program to a fixed wingbox would allow the MAW to be installed on any F-111 without any significant structural changes being made to the wing.

At a weight penalty of 1% actuators were added inside the wing to deform the structure with a deformable fiberglass skin. The inputs to these actuators were reviewed multiple times a second to ensure that the wing was constantly at its optimal performance, according to predetermined calculations. These calculations were based on the coefficient of lift, wing sweep, and Mach number, and other parameters, and tabulated within the computer for referencing. The optimal camber for different variations in these factors was determined during many hours of wind tunnel testing, and tabulated for the flight control computer to read [DeCamp et al, 1987].

The deformable fiberglass skin is not what is thought of today as deformable, but was rather a flexible sliding skin. The skin did not need to deform over a large range of motion, but more accurately only over a few degrees of bending at a specific location on

11

the wing. This allowed for materials of the day, such as fiberglass, to be used for the deformable part, while a standard aluminum skin could cover the majority of the aircraft.

Even though the skin did not deform on the scale of what is desired today it was an achievement of the times. The skin was needed to deform, in this case primarily through bending, while still maintaining contact with other structural elements, which was done by allowing the skin to slide. Proper design of this component allowed for a near seamless integration with the existing skin. Their solution was to use specifically constructed fiberglass sections that would allow for a bending deformation when requested by the flight control computer.

During the testing it was proven that this concept with a flexible skin could be used for almost any size aircraft over a range of wing thicknesses. The concept also proved that it could be used to either increase the wingloading to a maximum allowable value for a given structure, or minimize the weight of the structure at a given loading [DeCamp et al, 1997]. Because the computer used a set of tables to determine the deflection of the various control surfaces many people do not see this as true morphing, but as an early proof that morphing can provide the desired results.

Another program investigated changing the inlet geometry during flight, as the optimal inlet geometry for an aircraft is highly dependant upon where in the flight envelope the aircraft is. At low speeds a larger inlet with blunt lips is desired, while at higher speeds sharp lips produce less drag and a smaller area can provide the necessary

airflow to the engines. The DARPA funded Smart Aircraft and Marine Project System demonstratiON (SAMPSON) project goal was to design a smart inlet that would change shapes to optimize engine performance over the flight regime, while avoiding the high life-cycle cost commonly associated with variable geometry inlets.
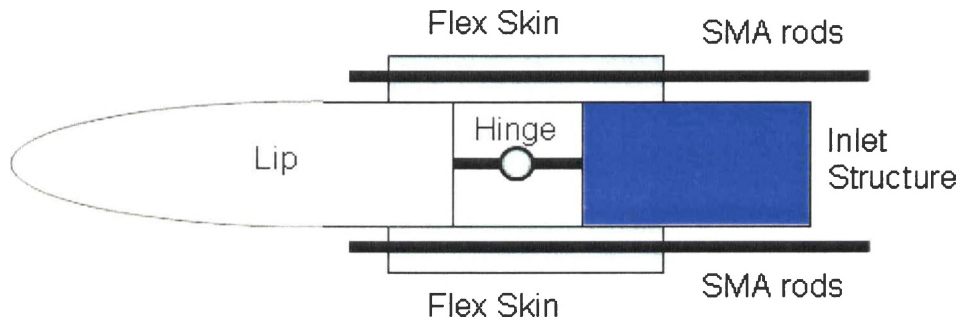
Figure 5: SAMPSON Lip / Flexskin / Cowl Geometry

The lip / flexskin / cowl interaction of the SAMPSON inlet can be seen in Figure 5. This smart inlet uses Shape Memory Alloy (SMA) wire bundles to act as actuators to induce motion in the inlet cowl. The system also has an SMA rod integrated into a reinforced elastomeric structure, called flexskin. The flexskin is compliant enough to allow deformation, while still maintaining its shape under the applied aerodynamics [Dunne et al, 2000]. With the flexskin / SMA composite attached on either side of a rigid lip and affixed to the lower edge of the cowl the inlet geometry could be controlled.

The flexskin covered the hinge and provided a smooth cover to the lip hinge line. In order to remain smooth and resist the aerodynamic loads placed on it the elastomer had structural rods as well as the SMA imbedded in it [Pitt et al, 2001]. Knowing the pressure loads that the flexskin would see it was possible to determine the number, strength, and

13

location of the structural rods that were added to increase the out-of-plane strength of the material.

The SAMPSON inlet was designed using smart materials to achieve near optimal performance from the inlet over the entire flight envelope. A flexible skin was needed to allow the rotation of the bottom lip of the inlet that was needed for the optimal performance. The loads on the skin were known from wind tunnel testing, and thus the skin could be designed so that it would withstand the out-of-plane loads while still allowing actuation to the desired positions.

More recently, the DARPA / AFRL / NASA sponsored smart wing program (1995 – 2001) was created to develop control surfaces to optimize aerodynamic performance, and ultimately lead to an aircraft wing with seamless control surfaces [Kudva, 2004]. A seamless control surface will improve the overall pressure distribution along the wing and reduce the chances of premature flow separation that is often seen with hinged control surfaces [Sanders et al, 2001]. To allow for the seamless deformation of a wing a sliding skin, like that used in the MAW program, or a flexible skin, similar to the one employed with the SAMPSON project, must be used at the hinge and along the control surface.

A sliding skin would be rigidly attached to the deformable structure but not to the skin of the rest of the wing. Instead it would run through a seal just under the skin in front of the trailing edge, so that when the control surface moved, the skin could slide in and

out. This configuration would be the same on the top and bottom of the control surface, and would allow a rigid material to be used in order to resist the air loads seen on the control surface. This method creates additional complications because it requires joints and slides to be added. These complications drove the designers to use a flexible skin for the control surface because it was thought the complications associated with such a skin would be easier to overcome [Wang, 2001]. The wind tunnel model that was used for the phase II testing of the smart wing can be seen in Figure 6, with the smart wing on one side and a traditional control surface on the other wing.
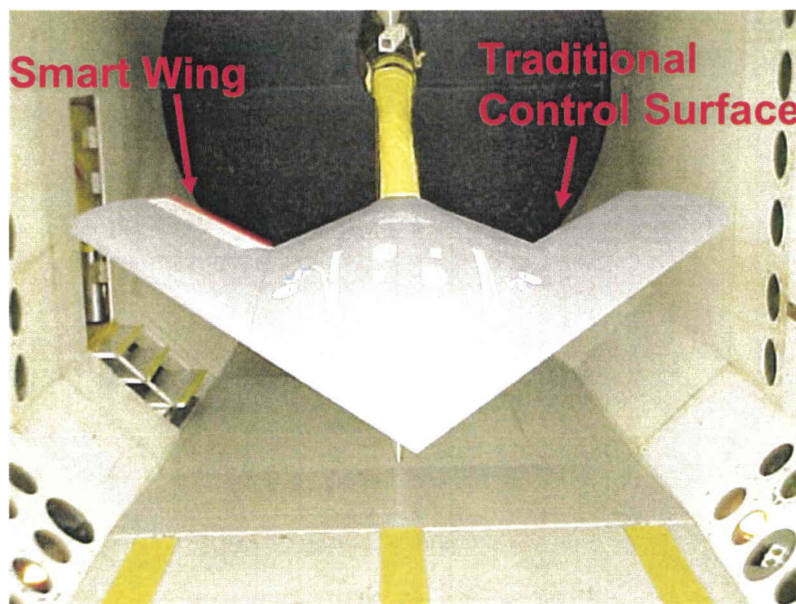
Figure 6: Smart Wing Phase II Wind Tunnel Model

The smart wing control surface consisted of ten independent segments, each actuated by an ultrasonic pizeo-electric motor. By actuating different segments different amounts allows for various shapes to be obtained, such as the 'bathtub' or sine wave shapes seen in Figure 7, instead of only the traditional uniform deflection of the entire control surface. All ten segments of the smart wing were covered with one continuous high strain silicone skin on the top and bottom to provide a smooth continuous surface.

15
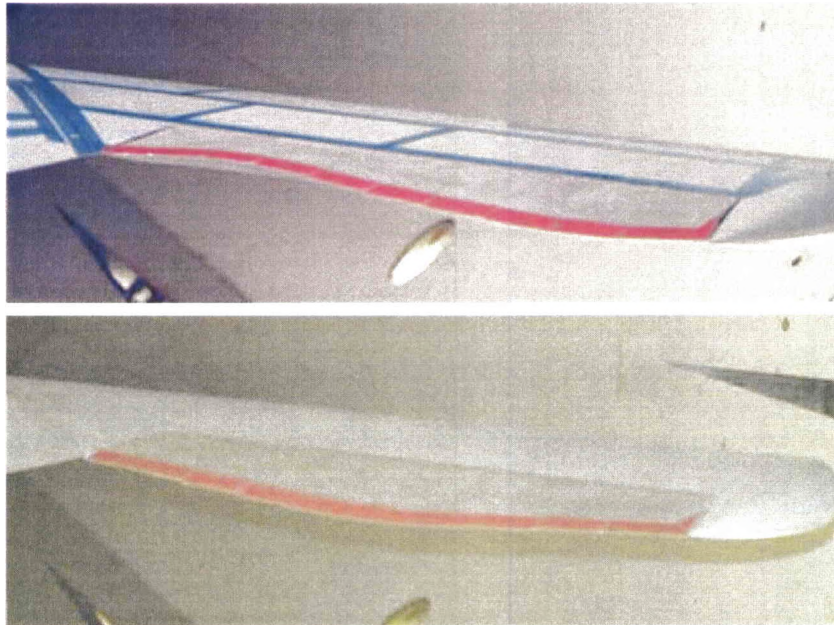
Figure 7: Two Different Configurations of the Smart Wing Control Surface
Top - Sine Wave; Bottom - Bathtub

There were minimal worries about out of plane deformation of the elastomer because the skin was attached to each section and the spaces between sections were quite small. The gap at the hinge line that the elastomer covered was quite small as well allowing for a smooth skin in the chordwise direction. The fact that the elastomer was attached at almost every location on the wing means that there is a minimal chance of the material being deformed out-of-plane, even under dynamic pressures of 300 psf that the wing was tested in.

2.2 Morphing Aircraft Skin Materials

The skin of a morphing aircraft must be flexible enough to obtain specific targeted shapes and have a repeatable behavior. Currently, the targeted shapes require skin deformation up to 300% while carrying the out-of-plane aerodynamic loads. The

primary candidate materials for this application are categorized as elastomers or shape memory polymers.

There are many potential skin materials for morphing aircraft. These materials possess the capability to change their shape and surface area significantly, some with almost no applied force. The majority of materials that are being investigated are compliant materials that will allow deformation to occur. This leads to a problem of preventing unwanted deformation due to aerodynamic loads on the aircraft.

There have been a number of investigations into the potential materials that can be used for morphing aircraft skins, primarily different elastomers and shape memory polymers. These studies generally select a few materials and perform standard tests on the materials to determine their physical characteristics in tests that are believed to approach the real world use of the material for a morphing aircraft skin. The material properties are compared to each other, and often to an ideal, but non-existent, material to determine which materials would be appropriate for the skin of a morphing aircract. For more on the various potential materials the reader is referred to Kikuta [2003.]

Maintaining the desired shape of the airfoil is crucial to an aircraft. The airfoil shape directly affects how much lift the aircraft produces, and how much total drag is acting on the aircraft. Once the shape of the airfoil is obtained, preserving it's smooth cross section is necessary to keep the lift and drag properties optimal. Out-of-plane

deformation of the aircraft skin would interrupt the smooth cross section, reducing lift and increasing drag.

To prevent out-of-plane deformation of a complaint material, like Spandex®, there are a few possibilities. One is to attach the material to the underlying structure in many locations. This limits the amount of material that can deform due to the out-of-plane loads, therefore limiting the total deformation. A second possibility is to stretch the material so that it is very taught over the spaces where it is not attached, which would increase the loads required to deform the material. A third approach would be to add a substructure to the material itself to help prevent out of plane deformations from occurring by increasing the out-of-plane stiffness of the material.

The first possibility requires a significant, and intricate, underlying wing structure. This may increase the weight and cost of the aircraft considerably. The second idea might end up limiting the amount of possible morphing deformation that is available from the material because it is pulled so tight over the structure that the skin can not deform much more. The final theory has the most potential, in that while it will increase the weight it can be done so that there is only a minor increase in the weight of the aircraft and minimal, if any, limiting of the possible deformation of the material.

Polymers are a prime candidate for morphing aircraft skins because they have a large range of properties, which can be tailored for a specific task. This section will

explain some of the behavior of polymers, and provide a more in depth look at shape memory polymers specifically.

With such a large number of polymers available, there are many ways to classify and group them. For this research the familiar classification used by Keihl et al [2005], dividing polymers into four groups based on their molecular structural alignment, was used.

The first group is natural polymers occurring in plants and animals, such as cellulose and protein. The behavior of these polymers varies greatly. Next come thermoplastics, which are also known as linear polymers. This group typically behaves in a ductile fashion. The third grouping is that of thermosets, which are made by combining a resin and hardener and curing the mixture at temperature. This set of polymers has many crosslinks, which help to increase the strength of the polymer. The last classification consists of elastomers, or rubbers, that have some crosslinks, and a nearly linear elastic behavior. This allows the elastomers to elastically deform very large amounts without permanent deformation. The crosslinks induce a form of memory effect in the material that allows it to return to its original shape when the loads are removed.

The different materials have different mechanical properties, as can be guessed from the descriptions above. Overall, polymers appear to have a combination of viscous fluid and elastic solid properties, and are called viscoelastic materials. Different groups of

polymers have different combinations of these properties, among other properties, that allow for the different classifications of polymers.

By definition, viscoelastic materials flow internally when there is an applied force, but they return the energy and recover elastically. The amount of energy imparted to deform the material and the amount and speed of the elastic recovery are highly dependent on the temperature of the material and the rate of deformation imparted on the material. At higher rates or lower temperatures polymers display elastic characteristics, while at low deformation rates and higher temperatures they display more viscous characteristics. When at a high rate and temperature, or low rate and temperature the material's reaction depends on which characteristic dominates at that particular rate and temperature combination.

All of these materials have a glass transition temperature, which is where the viscous characteristics begin to dominate over the elastic ones, at a constant middle range rate of deformation. In thermoplastics the glass transition temperature, or T_g, can be increased with increasing molecular weight. The T_g is always less than the melting temperature of the polymer though, because it does not require all of the bonds to melt, and therefore it requires less energy to arrive at the T_g, molecularly speaking.

For thermosets the same trend of increasing the T_g is seen with increasing the number of crosslinks in the material. These materials do not have a melting temperature

because of their manufacturing process, but as the temperature increases well above the T_g the material degrades, and will eventually burn [Strong, 1996].

When a material is considered an elastic material all of the energy from the applied force is stored in the material, and is then used to return the material to its initial position, very similar to a spring. The stress / strain plot of an elastic material can be either linear or nonlinear, as long as the material fully returns to its undeformed shape when the load is fully removed. Elastomers are in this state at room temperature.

Viscous materials show no recovery when the force is removed, rather all of the force gets dissipated into making the material move or generating heat. Often the viscous properties of a material are dependant on the rate of deformation. If the material becomes thinner, or less viscous, with higher shearing rates the material is said to be pseudoplastic. This characteristic is often seen in polymers, and is the result of the applied force increasing the internal energy of the material, which encourages movement and untangling of the polymer chains, which reduced the viscosity of the material. If a material gets thicker with increasing shear rates it is said to be shear-thickening, or dilatant. As a general rule, an increase in the temperature of a material decreases the viscosity of a material. Finally, the force relationship of a viscous material is similar to that of a dashpot, where the force is equal to a material constant multiplied by the rate of deformation.

Figure 8 shows various ideal force / displacement relationships for elastic, viscous, and viscoelastic materials in response to a step force. An elastic material will strain a finite amount immediately after the force is applied, and remain at that strain until the force is removed, providing there is no creep. A viscous material will deform at a constant strain rate, dependent upon the viscosity of the material, until the force is removed, at which point it will remain at a constant strain until another force is applied. A viscoelastic material will be strained, linearly or nonlinearly, until the force is removed, at which point it will return to a state of zero strain after a period of time under no load.
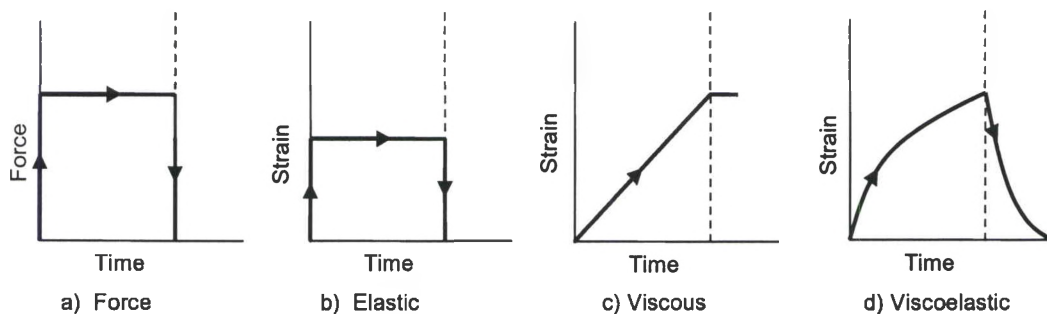
Figure 8: Mechanical Response Curves of Various Materials to an Imposed Constant Force
Figure redrawn from Strong [1996]

A viscoelastic material can be either a solid or a liquid, with a force / displacement curve somewhere in the middle of the two previously mentioned models. If the rate of displacement is increased polymers offer a stiffer, or more viscous reaction. This is because the polymer chains have less time to untangle and slide past each other, so they are forcibly pulled past each other, which requires a higher force.

The long-range, or viscous, effects take more energy to activate, generally done by heating the polymer above its T_g. Upon recovery to zero displacement, viscoelastic

materials usually show hysteresis. Also, once the material is pulled beyond its yield point it will not completely recover, but rather return to zero stress at slightly less strain than the strain when the load was removed. The modulus that the material exhibits upon recovery in either case is the same modulus exhibited in the elastic region.

Depending on whether the viscoelastic material is a liquid it can be approximated by a Maxwell, or series, model. If a material is a solid it can be approximated by the Voigt/Kelvin, or parallel, model. Within the solid model plastic deformation is represented with a pick & notch that slips at a particular force [Strong, 1996]. This model does not catch all of the details of a viscoelastic-viscoplastic model with all of the intricate relationships between the molecules in different states. To fully capture all of the behavior of a viscoelastic-viscoplastic material one would need to perform a number of tests at various conditions to obtain the large number of constants needed to understand and model the material. These materials also have a very good resistance to impact due to their high ductility (near and above the T_g for SMPs), but this is also what makes them hard to model [Frank and Brockman, 1998].

SMPs do not fall into any of the polymer groupings mentioned above, but can exhibit characteristics similar to different groups at different times. In fact, depending on the kind of crosslinking that is present within the SMP it can be molecularly considered to be in any of the groups mentioned earlier, except that of natural polymers [Cullen et al, 2002]. Many currently available SMPs are a combination of thermoplastics and elastomers, but not all SMPs are combinations of existing polymers, they are actually

new polymer formulations that exhibit a shape memory effect. The material used for this research is a one of the few SMPs that is a thermoset, even though it is based on polystyrene, which itself is an amorphous linear thermoplastic.

As a linear material, the polystyrene will soften as it is heated because the secondary bonds in the material melt, allowing the polymer to flow viscously within itself. Being an amorphous material, the T_g, shown in Figure 9, is not a distinct value, but is actually a range of temperatures over which the secondary bonds melt, because of different molecular weights (chain length) inside the material [Keihl, et al, 2005]. When obtaining properties of an SMP there is a distinct value for the T_g (the green vertical line in Figure 9,) which is actually a value at the upper end of the range over which the modulus changes.
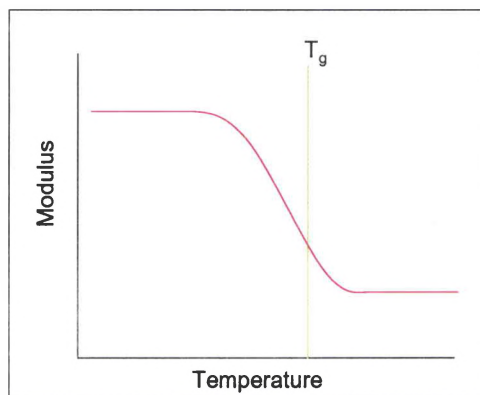
Figure 9: Typical Modulus vs. Temperature Plot for an SMP

Shape Memory Polymers have a unique set of characteristics that allows them to be rigid and carry air loads, while at another point being soft enough to deform with minimal force, allowing for a change in the shape of the underlying structure. These polymers take advantage of a property change at the glass transition temperature, in that the material can be reformed with minimal force at temperatures above it's T_g. Once

cooled below the T_g the SMP becomes rigid again, with crosslinks rejuvenated by the lowering temperature, maintaining the shape that was given it in its viscous state. The induced strain gets frozen in the material. This frozen strain can be recovered by heating the SMP back above the T_g, which reduces the number of crosslinks present, allowing the material to flow in its viscous form again. The unique property of SMPs is that the few remaining crosslinks drive the material to return to its original manufactured shape. Additionally, SMPs can be deformed plastically while below their T_g, storing the induced strain imparted to it in this form as well. When it is heated back above the T_g the same recovery effect is noticed [Abrahamson et al, 2002].

When an SMP is deformed at temperature creating a stress-strain plot one can see that there appear to be two stiffnesses, one in the elastic range and one in the plastic range. This is a result of the viscous properties of the material, and unlike plastic deformation in most materials, the deformation in the plastic range of an SMP can be fully recovered. If there is any residual strain from the loading cycle (usually from loading well below T_g) it can be recovered by heating the SMP back above its T_g for a short time, allowing the material to flow back to its original shape.

SMPs provided by Cornerstone Research Group (CRG) of Beavercreek, OH were used for this research. With these styrene-based SMPs from CRG the T_g is controllable over a large operating range. This is done by varying the ratio of the styrene, vinyl monomers and a crosslinking agent in the composition. The material properties, such as storage modulus, can also be adjusted by varying the composition of the monomer matrix

that is used to make the SMP. Lastly, these SMPs are of a fairly low cost and easy to process, especially when compared to metals that are currently used as aircraft skins [Cullen, et al, 2002].

2.3 Chapter Summary

Throughout the years there have been many attempts to control the wing shape while in flight. As technology and materials advanced, larger and more difficult controlled deformations, have been desired and achieved. With the continued advancement of materials and technology, concepts that were impossible a decade ago are becoming possible. Theses concepts introduce new ideas and improve on old ones to allow for an aircraft that can have optimal performance over an ever expanding flight envelope.

The mechanical behavior of SMPs is well understood, however the material is not well characterized for use in aerospace structural applications. This research will provide insight into the structural capabilities of shape memory polymers, specifically for in-plane, large shear loading for morphing aircraft applications.

CHAPTER III

EXPERIMENTAL SETUP & EXPERIMENTS

In this chapter the test set-up and fixtures are described, and the experiments performed are discussed as well. In-plane, large shear deformation tests were performed on specifically sized specimens that mimicked the desired geometry and deformations of a skin panel on a potential morphing aircraft to characterize SMPs as a prospective skin material. This experiment required that the entire test be performed within an environmental box, and it also needed a unique fixture to allow a tensile machine to perform a shear test with a large amount of shear strain. Another set of experiments was performed using ASTM tensile standards to obtain material properties that could be compared to data taken on any other material.

3.1 Experimental Setup

In order to conduct the experiments the SMP needed to be heated above it's T_g and have it's temperature held constant. The first specimens obtained had a T_g of approximately 95°C, so it was decided that the tests would be run at that temperature. Ideally it would have been run at a temperature slightly above the T_g to ensure that all of the material was adequately heated, but limits on the equipment prevented the use of higher temperatures. The specimen needed to be maintained at this elevated temperature for the duration of the test, and since the temperature is so close to the T_g, the temperature

must also be accurately measured and controlled. This led to the construction of an environmental box that was able to hold the specimen at a constant temperature throughout the test.

The experimental setup for the shear characterization of shape memory polymers consisted of an environmental box set inside a loading unit, fixtures to hold the specimens during testing, and the specimens themselves. The environmental box and the fixtures provided unique problems based on the desired size and geometry of the test. Once a load frame was designated for these experiments, the other components could be designed to ensure the setup was capable of the full range of motion.
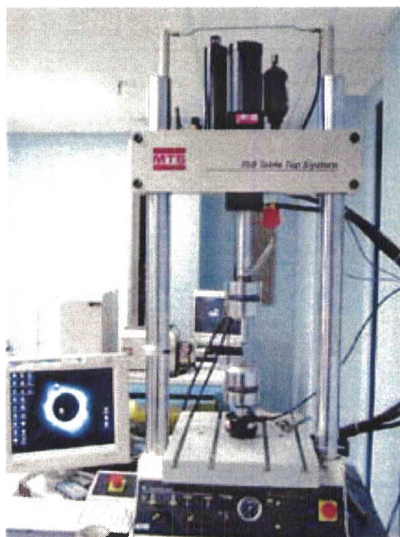
Figure 10: MTS 858 Table Top Load Frame

The loads unit was an MTS 858 Table Top System, Model 359, seen above in Figure 10, which used an MTS Force Transducer, Model 661.19F-01 load cell, with a force capacity of 1100 pounds. MTS provided their TestStar IIs Control System to control the load unit and for use as a data acquisition system. The TestStar IIs is described by MTS as

"an automated digital system used to control single station, single channel closed loop dynamic testing systems. TestStar IIs uses graphical, mouse-driven system software to set up and manage tests and to collect data. Time-critical processes such as closed loop control, limit detection and data acquisition take place in the controller firmware," [MTS website].

The user specified what data was recorded and the rate at which it was recorded. For this experiment the force, displacement and time were recorded at a set rate, which was varied depending on the rate that the sample was loaded (2Hz for a rate of 2" per minute.) All of the desired data was recorded to a user specified file, which was later imported into a spreadsheet to ease the calculations.

The environmental box, which can be seen below in Figure 11, was needed to maintain a heated environment that the SMP was submersed in to obtain and maintain a desired temperature within the specimen. The box itself was fabricated from 0.25 inch Plexiglas, with one aluminum side that would be used to attach inline heaters. 16 inches wide, 21.5 inches high and 18 inches deep, the box was insulated with 0.4 inches (1 cm) thick R3 Styrofoam insulation on three sides (excluding the access door / viewing window) and the top, to help limit heat loss. There was a small hole on the top of the box to allow a connection between the load frame and fixture, and another small hole in the back of the box that was filled with the front end of the thermometer. The bottom had five small holes, four of which were used to attach the grip plate for the bottom grip to the box and both the grip plate and box to the base of the load frame. The fifth hole was

to allow space for the bolt that held the grip to the grip plate that was attached to the box and frame. The temperature was controlled with the use of an infra-red laser thermometer - a Raytek Thermalert IV, Model RAYT4BALT, with a Model RAYSHLTSFLS1 sensor that was accurate within ± 2° F. The green circle at the middle left in Figure 11b shows the location of the thermometer. The output from the thermometer was displayed on a control box which controlled the power to one of two inline heaters. The inline heaters, seen in the yellow oval on the right side of Figure 11a, were AHP-5051 model, 0.5 inch diameter, 4.5 inch heated length, capable of delivering 88 watts/inch heated length at 10 cfm. These were fed room temperature air at 40 psi, which they heated as it passed through them into the environmental box. The heater that was not linked to the thermometer was on continuously, as this was the best method found for maintaining the specimen at a constant 203° F. The air inside the box was circulated by an exhaust fan, indicated by the red circle on the rear view, pulling air out near the top, and reintroducing it to the box on the bottom via a 2.5 inch diameter, 3.5 foot long rubber feedback hose. The rubber hose was insulated with a thermal wrap to help prevent heat dissipation. The recirculation fan was a Cooltronic, Inc. #716-0931, type U62B1 AO, 2500/300 rpm. The load cell mentioned above is visible in the blue oval at the top of Figure 11a.

a) Front   b) Back
Figure 11: Front and Back View of Experimental Set-up
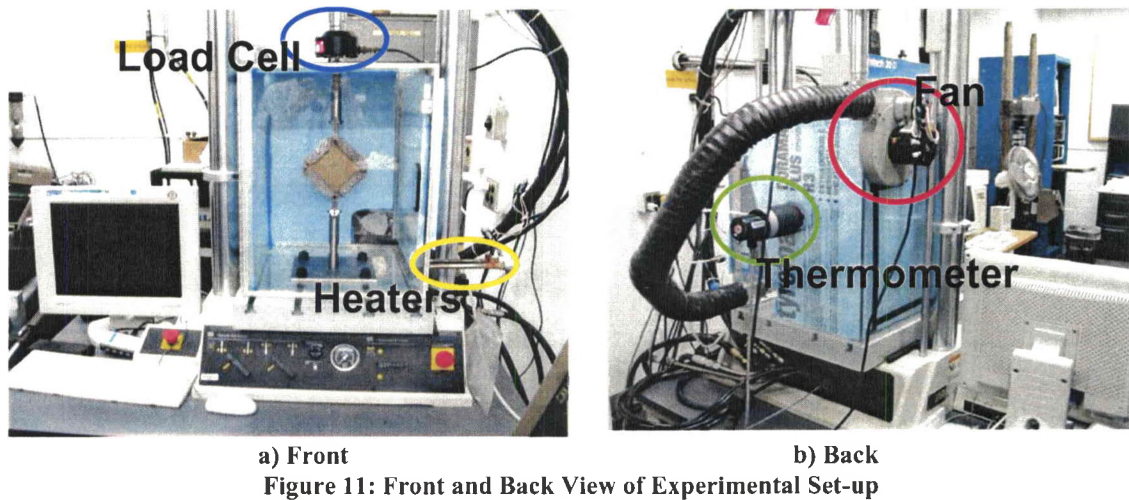
Within this setup three different fixtures were used, one for the shear tests and two, seen below in Figure 12, for prestraining the SMP. The tensile fixtures consisted of two pairs of semi-triangular plates, with each pair being attached to opposing edges of a small sheet of SMP by use of nuts and bolts clamping the SMP between the plates through two rows of offset holes in the fixture, and subsequently in the SMP. The first fixture had a few large holes, and could accommodate a specimen up to five inches across. The second fixture had many more holes, at approximately half the diameter, spread along a plate that allowed for specimens up to thirteen inches across to be pulled. After using both fixtures it was noticed that the material was held better with more, but smaller, bolts clamping it, so the second fixture was used much more than the first.
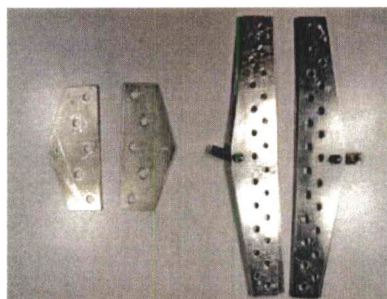
Figure 12: Prestraining Fixtures

31
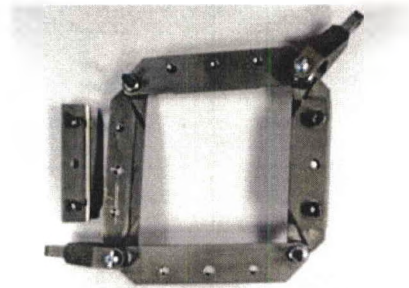
Figure 13: Shear Test Fixture

The fixture to test the SMP in pure shear within a tensile machine had the basic geometry of four bars pinned at the corners, generally in the shape of a square (Figure 13), and allowing deformation along either axis to the shape of a diamond with smaller interior angles of just less than 30°. This geometry allows the area of the sample to change without any change in the length of the sides, as is shown in Figure 14, with a maximum when the bars are perpendicular in the shape of a square. This also allows the specimen to be attached along its edges, except in the immediate vicinity of the pins. For the test it was decided to vary the angle of the small corner between 90° and 30°, which allows for a change in area of 100%, which meets the requirements for the area changes on the in-plane morphing aircraft concept that was seen in Figure 4.
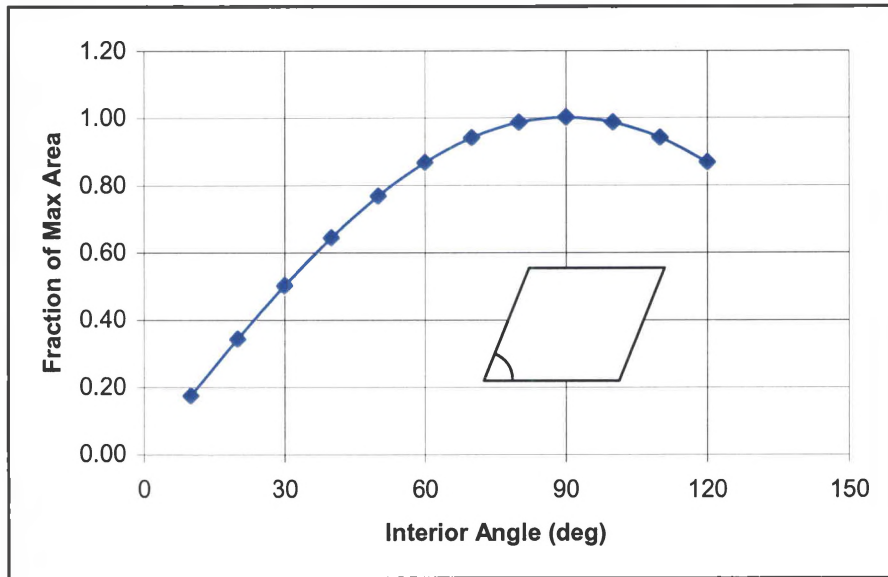
Figure 14: Geometry Changes and Associated Area Changes
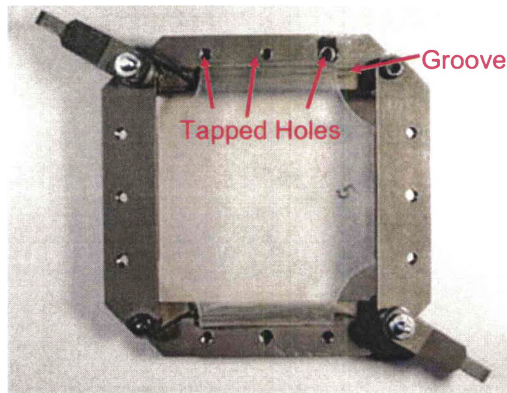
Figure 15: SMP in Shear Fixture; Not Clamped

To clamp the specimen into the fixture each of the four bars had a groove down the length near the inner edge, and three tapped holes near the outer edge of the bar. The specimen was clamped with four smaller bars, which had a lip to match the groove in the base fixture, and three holes drilled through that lined up with the tapped holes. The fixture was sized so that the SMP could be placed on the fixture covering the grooves, while not covering any of the holes, as in Figure 15. When bolts were put through the smaller bars and tightened into the threaded holes the SMP was pressed between the two

33

bars, with the lip and groove combination adding extra clamping force to the fixture. Even with the extra clamping of the lip and groove combination, the fixture had to be tightened twice during heating of the SMP because of the softening of the material associated with the rise in temperature.
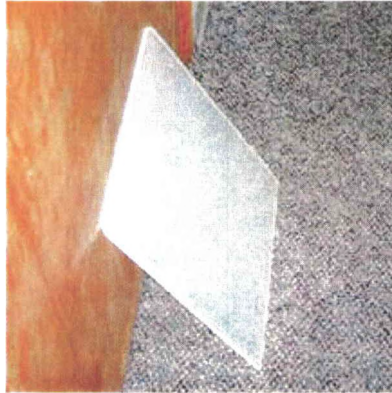
Figure 16: SMP Bulk Sheet

All of the specimens were cut out of flat sheets of the bulk SMP that were approximately 0.154 inches (~4 mm) thick (Figure 16.) Each sample had a variation in thickness of up to 0.02 inches (~0.5 mm) from the minimum to maximum thickness. The specimens that were used for the shear test were cut into squares with 4.25 inch sides, with a two inch diameter hole centered on each corner cut out in order to limit the possibility of the specimen getting caught in the corners of the fixture during testing. Specimens 1, 2, 5, 6, 7, and 8 were cut out of bulk sheets of SMP as received. Specimens 3, 4, 9, 10, 11, and 12 were cut from material that had been prestrained various amounts. The first four specimens were cut out of the first formulation received, that had a T_g of approximately 95° C, whereas the remainder of the specimens were cut from a second formulation that had a T_g of about 65° C. All other properties of the two different SMP formulations were comparable. Using this second formulation allowed the tests to be run at a higher increment above the T_g while not changing the actual temperature of the test.

34

For the tensile tests the test specimen configuration of ASTM D-638 Type I was used, with an extended overall length. This shape was chosen because the material was deemed rigid or semirigid over most of the temperature rage, and only nonrigid at the highest temperatures, and it was desired to use the same shape for all of the tests.

As seen below in Figure 17, the narrow section had a width of 0.5 inches and a length of 2.25 inches, allowing for a gauge length of up to 2 inches to be used. The wider section had a width of 0.75 inches, and was set so that the overall length of the specimen was 9 inches. This allowed for the specimen to be within a clamshell furnace with the grips comfortably far away so that they would not be endangered by any excessive heat. A radius of 3 inches was used to change between the sections of the specimen with different widths. All of the specimens were cut from the same stock SMP that provided the shear and prestrain specimens, with a thickness of 4 mm that varies up to 0.5 mm from minimum to maximum thickness.
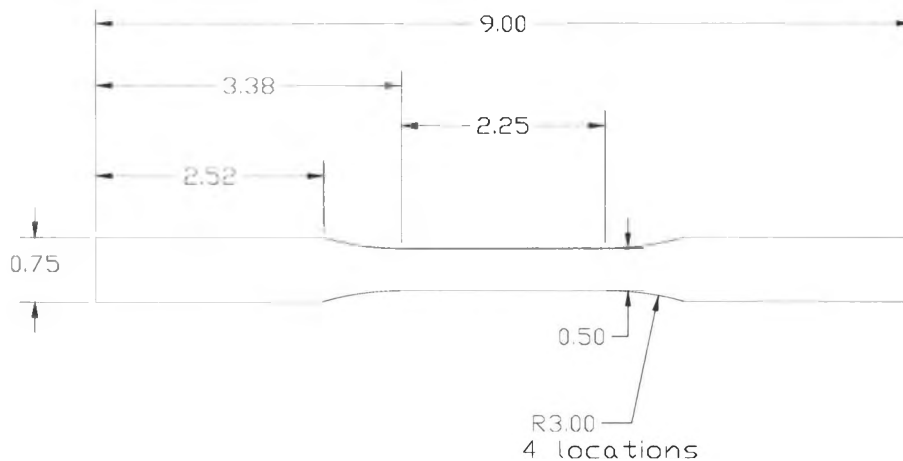
Figure 17: ASTM D-638 Type I Specimen Geometry

The tests were run on the same machine as the shear tests, with a distance of 6 inches between the grips between which a clamshell oven was used to heat the middle of the specimen. The load frame with the oven in place for tensile testing can be seen in Figure 18. The oven used to heat the SMP was an Applied Test Systems, Inc. (ATS) series 3210, with one heating zone capable of temperatures up to 1650° F. To heat itself the oven used 610 Watts of 115 Volt electricity, drawing 5.3 amps. The temperature control system was an ATS temperature control system series XT16 single zone TCS that drew up to 20 amps of 115 Volts and controlled the power going to the oven.

The machine controls and data acquisition were the same for the tensile tests as they were for the shear tests.

Figure 18: Load Frame Setup for Tensile Testing

3.2 Test Procedures

Since there are no current test procedures for SMPs the procedures used had to be extrapolated from other work done on SMPs [Abrahamson et al, 2002]. Much of this work generally follows standards for plastics, with some modifications to accommodate

the differences between normal single-state plastics and SMPs. As SMPs continue to grow in popularity, dedicated testing procedures will be developed, quite probably based on the efforts that were reviewed at the beginning of this research.

The procedures explained here created a repeatable test used to obtain information over a large amount of shear strain with a tensile machine. During these tests it was desired to obtain the shear properties of the material to characterize it for potential use as a morphing aircraft skin material. Also, the reaction of the material to different amounts of prestrain was desirable as well.

The output from the tests in the form of load, displacement, and time at each data point was saved. The load and displacement data from each experiment was operated on within a spreadsheet to obtain the shear stress and shear strain. The shear strain can be defined as 'the change in angle between two originally perpendicular line segments that intersect at a corner' [Craig, Jr., 2000]. The segments obviously have an initial angle of 90° between them, so the shear strain can be measured and the difference between $\pi/2$ (90°) and the angle, in radians, at the top or bottom of our test specimen. With the large magnitude of shear strain seen in the testing, it was not possible to use small angle assumptions for this calculation, but rather it was required to calculate the interior angle based on the displacement of the load frame with basic geometry.

In order to determine the shear stress acting on a specimen, one must first determine the resultant forces. Figure 19 depicts a unit vertical force whose resultants

along both sides must each have a downward component of 0.5 lbs, which leads to a resultant of 0.707 lbs on each side at the beginning of the test. Figure 20 shows the resultant force as a percentage of the total applied force. One can see that it decreases from 71% of the applied force down to 52% of the applied force over the range of the test This is because as the test continues the vertical component of the resultant must remain one half of the applied load, but with the changing angle more of the resultant vector is in the vertical direction, making the overall resultant less. To obtain the shear stress, this shear force was divided by the area it was acting on. The specimens were 0.154" thick, and the sides were 2.125" long after the corners were removed, creating an area of 0.327 in^2. The geometric relations used to make the above calculations are shown in Appendix A.
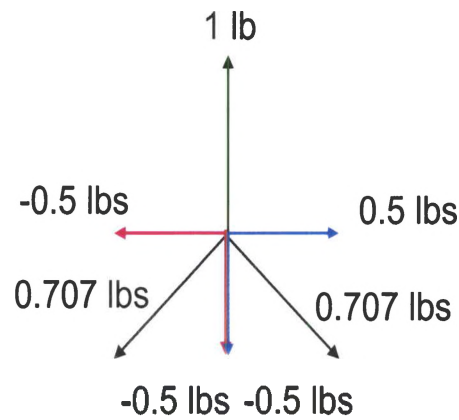
Figure 19: Resultants from a Unit Force
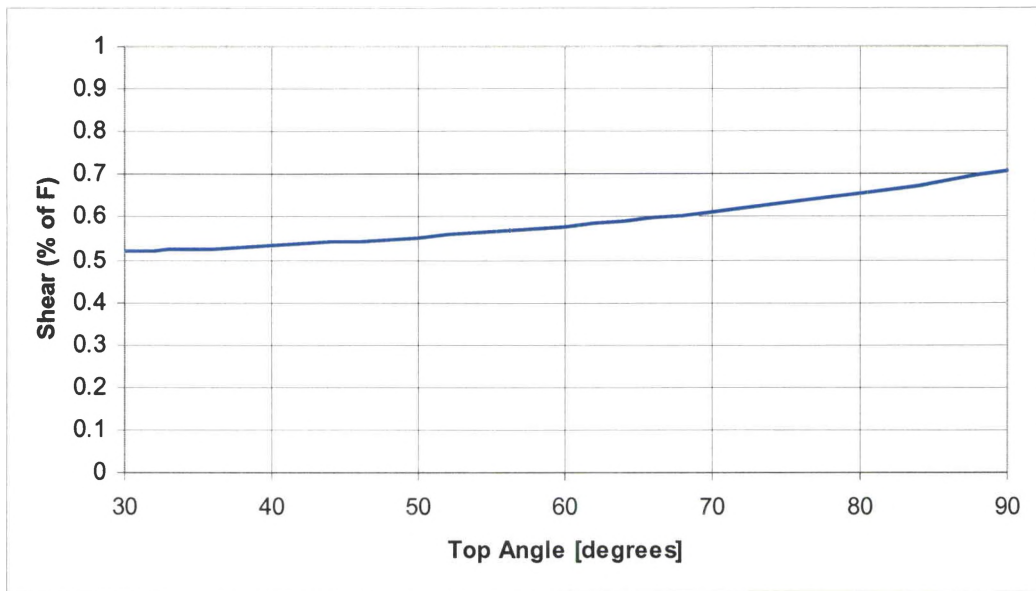
Figure 20: Shear Force, in % of Applied Force

The vertical force in the above explanation corresponds to the force applied to the test fixture. As the applied force increases so do the resultants, or shear forces, but they maintain in fixed relation to the applied force, as a function of the interior angles at the top and bottom of the test fixture.
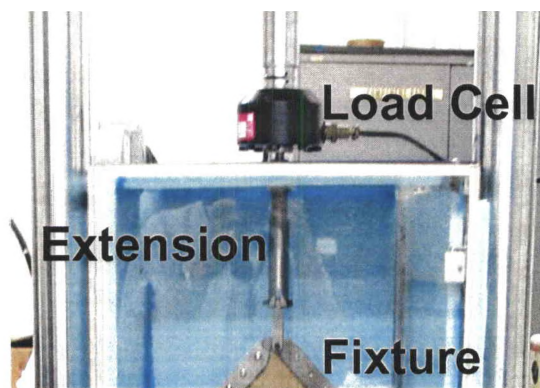
Figure 21: Extension from Load Frame Connecting the Fixture to the Load Cell

A summary of the shear tests that were performed and some of the variables can be seen in Table 1. For any given test the four-inch square specimen is placed in the shear fixture, and attached to an extension of the load frame inside the environmental

39

box, shown in Figure 21. On top of the extension was the load cell to record the force. The whole unit was actuated by hydraulics. The basic setup allowed the sample to be deformed from a square to a diamond, with interior angles of 30° and 150°, by pulling on the end (top corner) of the shear fixture to a displacement of 2.07 inches.

Table 1: Tests and Test Variables, With Specimens Used

|	Type	Sample Status	Temp (° F)	Rate (in/min)	Angle at Fixture Top (deg.)	Test Purpose	Sample Numbers
1	Monotonic Shear	Bulk	203	2.0	90 to 30	Prove set-up	1, 2, 7
2	Uni-axial Pre-strain	Bulk to prestrained	203	2.0	Pure tensile	Poisson's ratio Young's Modulus	3, 4, 9, 10
3	Monotonic Shear	Prestrained	203	2.0	90 to 30	Eliminate sample folding	3, 4, 9, 10
4	Monotonic Shear	Prestrained	203	2.0	30 to 90	Eliminate sample folding	11, 12
5	Cycled Shear	Bulk	203	2.0	90 to 30 to 90	Repeatability	1 (X8), 2 (X16)
6	Cycled shear at varied rates	Bulk	203	0.2, 2.0, 20.0	90 to 45 to 90	Rate Dependency	5, 6
7	Extreme Reverse Shear	Bulk	Room	0.05	90 to 87	Load Limit	1
8	Extreme Reverse Shear	New shape	Room	3.0	45 to 27	Load Limit	2
9	Extreme Positive Shear	Bulk	Room	0.05	90 to 68	Load Limit	5
10	Extreme Positive Shear	New shape	Room	0.05	45 to 51	Load Limit	2
11	Low load, High cycle	Bulk	Room	0.05	90 to 89	Repeatability, Shear Modulus	7 (X10) 5 (X25)
12	Low load, High cycle	New shape	Room	0.05	45 to 43	Repeatability, Shear Modulus	7 (X10)

Figure 22: Shear Fixture (Without Specimen), Setup to Run Diamond to Square Shear Test

The initial tests were done monotonically, but could easily be reversed for cyclic testing. For all of the shear tests, except those done on rate dependence, the specimen was deformed at a rate of 2" per minute [Ram, 1997; Anon, 2005.]. As testing progressed it was desired to run the test in the opposite direction as well, pulling the SMP from a diamond to a square. Figure 22 shows how the same test fixture could easily be used, but a new, taller, bottom grip was needed because the extension to the load frame was not long enough to reach the specimens with the new geometry, and the bottom grip was easier to fabricate.

All the samples except sample #7 were allowed to recover to their original shape between tests, either rapidly in a boiling water bath or slowly lying on the floor of the test set-up environmental box during other testing at $T>T_g$. This was done so that each test would begin with a flat specimen, even if it were not freshly cut from the bulk material.
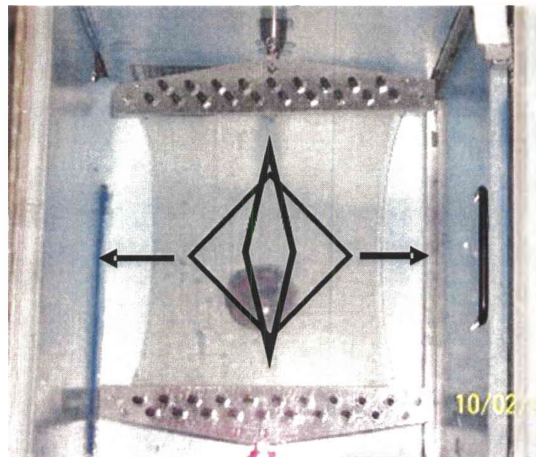

Figure 23: Prestrained Specimen Showing Where Shear Specimens Are Cut

Once the test process was validated by our initial tests it was expanded to include some investigation of prestrain effects, cycling, and rate dependency of the SMP. Figure 23 shows prestrained material, with images of the shear test specimens drawn where they

would be cut out. The arrows indicate the direction of the applied force during the shear testing. The prestraining was accomplished with the tensile fixtures described above by pulling a small sheet of the bulk material to a predetermined percent strain. The SMP was then allowed to cool in this new shape, and the shear specimen was then cut out of the material. The shear tests on these specimens were done so that the direction of prestrain was perpendicular to the direction of tension for the shear tests. This was so that the prestrain would be relaxed as the two sides of the shear fixture acted in compression on the specimen.

The tensile specimens were cut from bulk material as received from Cornerstone Research Group. All of the tests were performed on the same load frame as previously described, with some preliminary comparison tests done elsewhere.

To perform the ASTM tensile testing, an accurate way to measure the strain was needed in order to compute the modulus. Normally this is done with a laser extensometer and reflective tape for polymers, but the cost of an extensometer prevented the purchase of one for these experiments. A Tinius Olson load frame packaged with a laser extensometer was available for some tests, but the laser would not be able to obtain data when the specimen was in the oven attached to the load frame.

It was noted that Abrahamson, et al. [2002] had a similar problem with their work on elastic memory composites. In their research, they showed that using the displacement of the load frame crosshead to measure strain resulted in only a minor difference in the

strain, and that was only below approximately 3% strain. Above 3% strain data from a video system and the crosshead were identical, and since they were concerned about data at greater strains it was not crucial as to what measurement they used.

It was decided that, faced with a similar problem, a similar solution would be sought. Having access to the Tinius Olson frame and laser extensometer combination provided the means to run the tests. The software that came with the machine was not able to read two displacement inputs, so multiple tests were run using each of the two measurement devices. The results are tabulated below in **Error! Reference source not found.**, with the average and standard deviation calculated as well. The "L" and "CH" columns indicate which method was used to measure the displacement, Laser or CrossHead.

Table 2: Summary of Comparison Test Results

SMP	E (psi)	L	CH
10	182139		x
11	204793		x
12	205000	x	
13	180580	x	
14	174890		x
15	202024		x
16	200338		x
17	176842		x
18	206279		x
20	217411	x	
21	205663	x	
22	205079	x	
23	237000	x	
24	202500		x
AVG modulus	200038.43	208456	193726
SD	16850	18456	13330

43

Based on these results, a correction factor for the specimen was calculated to be 1.076. As long as the tests use the same specimen geometry and distance between the grips the correction factor holds true. This is more critical to these tests than the ones mentioned above because these tests are concerned with the modulus as well as material properties and reactions at other locations along the stress-strain curve.

To perform these tests, the cut specimens were clamped into the load frame with a thermocouple taped to the specimen approximately one-third of the length from the bottom. The output from this thermocouple was used to determine the temperature of the specimen. There was a second thermocouple imbedded in the oven that was used to help prevent overheating of the specimen from the oven becoming too hot. Once the straining had begun, the thermocouple taped to the material came off, preventing the tape from effecting the strength of the material.

The oven was closed around the specimen, with insulation added in the gap at the side where the two halves of the oven locked together. The temperature was then set at 250° F for the thermocouple on the oven itself. When this value was obtained the set point was increased to 265° F. Once the oven held stable at this temperature control was switched to the thermocouple taped to the specimen, which at this point would be nearly the desired 203° F.

This form of temperature control was used to prevent a large overshoot of the desired temperature that was likely to occur because of the low conductivity of the

specimen and the rapid temperature change the occurred in the ovens heating elements. If the thermocouple on the SMP were to be used alone the temperature within the oven would be well over 300° F before the specimen was at temperature, and it would not cool off quickly, and therefore continue to raise the temperature of the specimen well over the desired test temperature, and possibly above the degradation temperature of the material.

Once the specimen was stable at the desired temperature the tensile test was preformed, which involved the bottom of the specimen remaining fixed, while the top was pulled out of the oven. While not desirable, this occurrence was inevitable because the heating area of the oven was only four inches high. During testing at the slower rates this could allow the material to cool enough to increase the stiffness slightly, which would also drive up the calculated modulus at these rates as well. At higher rates the material would not have enough time to cool off while the test was being conducted.

3.3 Chapter Summary

The above pages described the setup for the shear and tensile tests that were performed, the items critical to the test in addition to the load frame, and the procedures used during those tests. There were three fixtures designed to be used for the tests, two for prestraining the material and one for the shear tests. In the end, to simplify data acquisition, the same load frame was used for both kinds of testing, with the gripping mechanism changed from pinning to hydraulic, and the heating device changed between the environmental box and a small clamshell oven for the shear / prestrain tests and the tensile tests, respectively.

CHAPTER IV

RESULTS

Chapter four discusses the experimental results of the individual experiments that were conducted to obtain the shear properties of the material. These properties are a function of the specimen geometry, the rate at which the specimen was sheared, and how much the specimen was prestrained. This chapter will also show how the desired properties were calculated from the experimental data.

4.1 Monotonic Shear Testing

In order to determine how well the test fixture worked the initial tests were monotonic. By performing a simple test over the full range of shear strain, it was possible to work out most of the problems that otherwise would have occurred during the more important and complicated testing. This also allowed familiarization with the load frame and the associated data acquisition and control software.

A small flaw in the specimen / fixture combination was noticed during the testing. The specimen would begin folding almost as soon as the test began because the sides were in compression. Beyond approximately 100% shear strain it was possible for the folded specimen to become pinched in the fixture at one of the corners. This increased the

46

required force to continue to strain the specimen because in addition to straining the specimen, the applied force also had to compress the folded specimen. This phenomenon can be noted in Figure 24, "Specimen1_Test2" with a sharp increase in shear stress seen starting at approximately 120% shear strain.
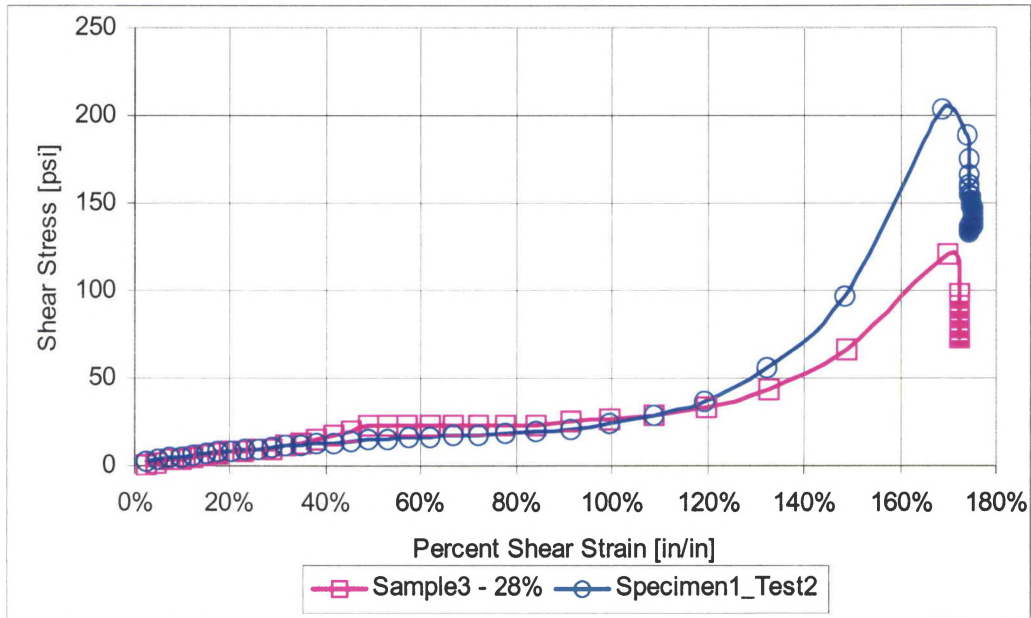
Figure 24: Data from Monotonic Testing

Moving past these learning experiences, data from the first specimen and third specimen (after being prestrained 28%) was successfully obtained from the monotonic testing. Figure 24 shows the data from these tests, with the specimen being pulled so that the smaller interior angle was 30° at the end of the test, and the fixture was held briefly at the resulting final strain. The first specimen tested shows a fairly smooth curve until it begins to be pinched in the test fixture. The specimen that was prestrained has a plot that can be divided up into three sections. The initial, linear, section, which lasts until 50% shear strain; the second section is identified by the nearly constant stress until almost 100% shear strain; the last section is where the shear stress increases again, until

maximum strain is obtained. This test will be discussed in more detail with other tests done on prestrained specimens, in section 4.4.

To alleviate the pinching mentioned above it would be possible to run the tests to only 100% shear strain (45° / 135° interior angles) but that would not cover the full range of motion that was desired. Another possibility was to cut out the corners. Initially the corners were all clipped slightly to allow the fixture rotation to occur about a pin located on each corner. This problem led to the final specimen shape described earlier, and shown below in Figure 25, with a one-inch radius hole centered on each corner being cut out of the originally square specimen. This cutout allowed the specimen to fold while significantly reducing the possibility of the fold being pinched in the fixture during testing.
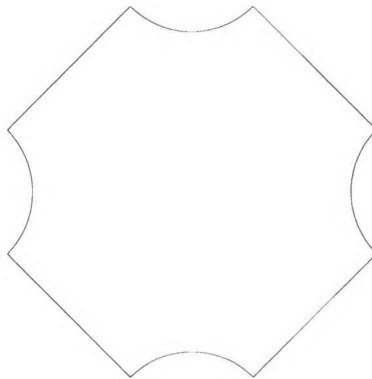
Figure 25: Final Shear Specimen Geometry

4.2 Cyclic Testing

Cyclic tests were conducted in the same manner as the monotonic, but with the specimen being returned to the original position. For many of the tests this was done

multiple times without cooling the specimen. The results from these tests indicated that the test was highly repeatable.
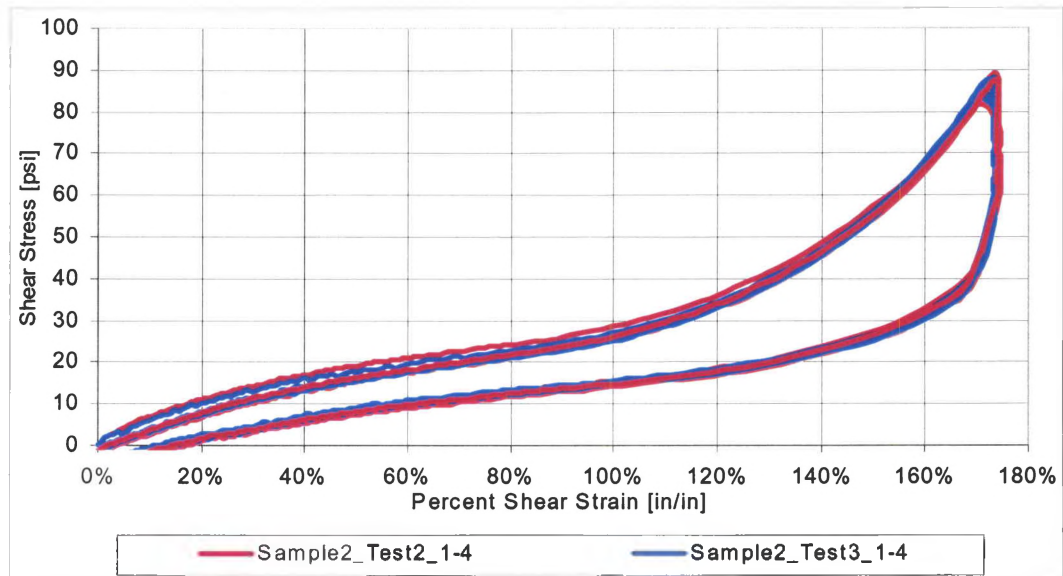

Figure 26: Stress-Strain Curve Showing Repeatability of Tests at 203°F

Two different specimens went through a total of 24 cycles, with typical results shown in Figure 26. To reduce clutter in the graph, stress-strain data for only two tests are shown. The samples were cycled four times in the fixture without being cooled. All four cycles of both specimens are essentially the same. The set of curves beginning near the origin are from the loading portion of the test. Once the maximum strain was reached, seen at the peak stress, the specimens were immediately returned to zero strain at the same displacement rate. The curves for each test are continuous, dropping to negative stress at low strains during the unloading portion of the test. The steep decline in shear stress near the maximum strain shows that by simply removing some of the applied force the material will reduce its strain. This plot indicates that not only is the test repeatable between specimens, but also that the test does not change the properties of the SMP or induce plastic strain, and that the specimens did not slip out of the fixture.

49

Knowing that the test was fully repeatable allowed data from different cycles to be compared, not just data from corresponding cycles. This shows that the test, and material, can be deformed numerous times, similar to the operating requirements that the skin would see.

For measuring the rate-dependence of the SMP properties, rates an order of magnitude on either side of the test standard of two inches per minute vertical displacement were used (0.2" / min, 2.0"/ min and 20.0" / min.) For these tests, two different specimens were cycled twice each at each rate, and held for 15 seconds at zero displacement between the two cycles and again after the test. The zero displacement condition was held to allow the SMP to return to its initial state, should it be needed, before being tested again. This was done for each of the three rates, as shown in Figure 27. As expected, there is a high rate dependence of the SMP properties. With each increasing rate, there is more hysteresis and more relaxation during the hold. The increase in hysteresis with rate was expected and is caused by forcibly deforming the SMP back to its original shape faster than the material wants to return solely due to the memory effect. Additionally, one can see that the slopes of the curves are different for the different rates. A slower rate allows the material to flow at it's own pace and not be pulled out. The faster rate pulls the material initially, shown by the higher slope at the beginning of each pull. Once the material reaches a certain strain, the slope levels off to nearly that of the slowest rate. Also, at the higher rates, the repeatability between tests decreases, as seen by the larger variation among the plots within the higher rates.

For both samples at each rate the second cycle had slightly lower stresses throughout the entire cycle, indicating a lower force was needed to deform the material for the second cycle. This is most prevalent at the highest rate, and is possibly the result of the material not having a complete viscoelastic recovery between cycles. The small peak near the maximum strain point for one of the tests (2 cycles) at twenty inches per minute vertical displacement indicates that specimen was pinched slightly at the end of the test. Other than the small peak, the data is indistinguishable between the two different tests.

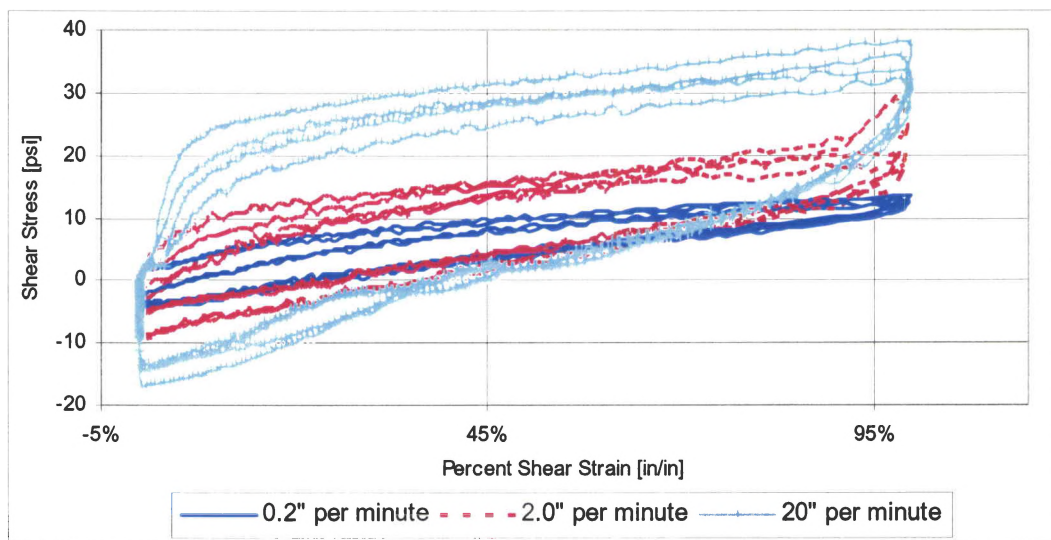**Figure 27: Stress-Strain Curve at Each of Three Different Rates for Four Cycles Going From 90° to 30° at 203°F**

4.3 Post Test Observations

Once cyclic testing began, it was apparent the SMP would not return to its initial flat form at the end of these tests; rather, it would have a slight out-of-plane deformation, as shown in Figure 28. Later use of finite element analysis tools indicated that this

phenomenon was from the material buckling during the testing. The buckling happened with every specimen cycled and resulted in the need to heat the SMP in an unfettered situation to gain the full benefit of the shape memory effect and reacquire a flat sample. It is possible this occurred because of the restriction of the test fixture, preventing the out-of-plane deformation that occurred during the test from returning to a flat position. Another possibility is that once buckled the material requires more energy input to fully remove the buckle. One of the specimens had an out-of-plane deformation occur during heating with no stress or strain (Figure 29.) It is believed this out-of-plane incident was a function of the sample geometry (too much of the corners were removed,) and prestrain. Further testing to prove either of these two hypotheses is warranted.
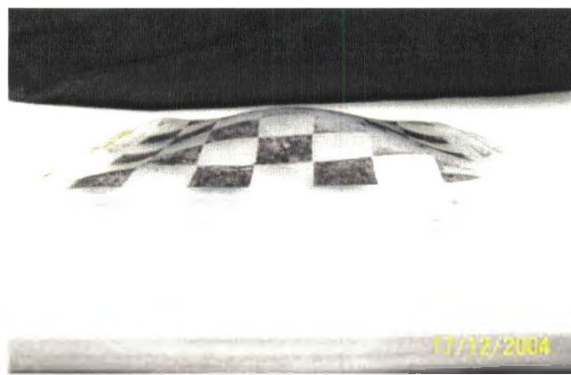

Figure 28: Sample #2 after cycling

Figure 29: Sample #4 Showing Relaxation at T>Tg, Before Deformation

Additionally, it was noticed that the force required to hold the SMP in its deformed shape, while minimal at temperature, increased as the SMP cooled, as seen in Figure 30. Before the SMP is cooled there is a relaxation of the applied force, seen as a reduction in shear stress at maximum strain. As the SMP cools below its Tg the force required to hold the same displacement doubles the initial force required to bring the material to that displacement. Once the SMP was completely cool the force would be removed with no significant change in shape of the specimen. This indicates that there is a small coefficient of thermal expansion in the SMP, and that as the specimen cools it also shrinks a small amount, exerting a force. This must be taken into account when designing a deformable structure that is covered with this material, because more power will be needed to hold the material in place unless the structure is designed to deform slightly more than required and upon cooling of the material obtain the desired shape.
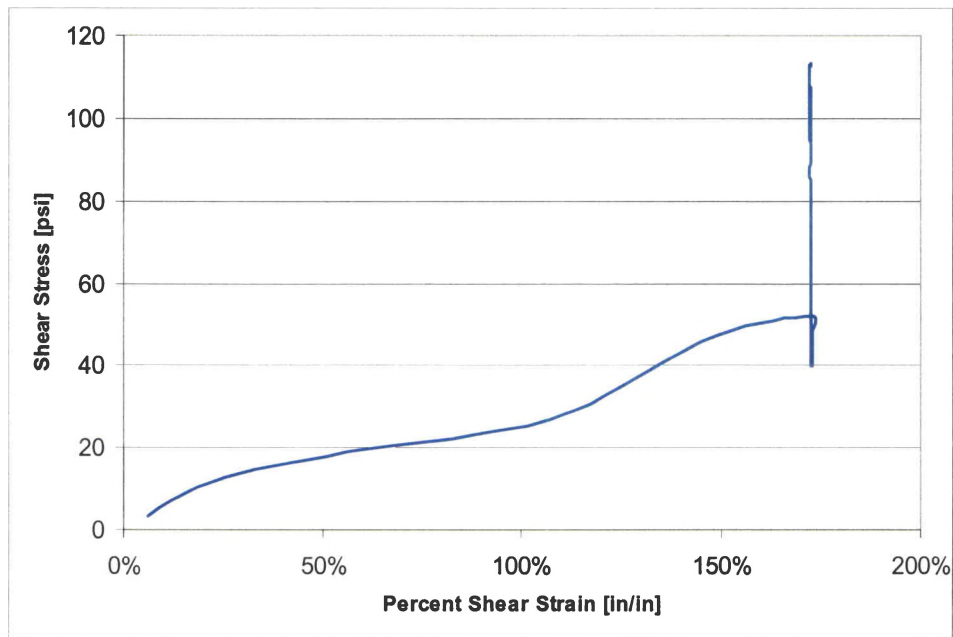

Figure 30: Specimen #1, Strained then Cooled Under Displacement Control

This phenomenon might be controlled with different forms of activation. Currently, some material research companies are looking into light activated SMPs, where, instead of heating the SMP over its T_g, the T_g of the SMP is actively changed between two values by shining UV light of a specific wavelength on it [Snyder & Tong, 2005]. Since this does not involve heating and cooling of the material, thermal expansion would not be an issue.

4.4 Pre-strain Effect on Out-of-Plane Deformation

The initial results from monotonic testing showed promise. At temperature the SMP was viscous and could act like a membrane because of its very low modulus. Because the specimen is in tension in one direction and compression in the other, compression of the membrane would result in an immediate out-of-plane deformation. The other possibility was that the specimens were buckling, and because the modulus was so low the critical force required to induce buckling was extremely low as well. Either theory produced an out-of-plane deformation which continued into a folding of the specimen, seen in Figure 31 at interior angles of both 45° (left) and 30° (right.) The folding that occurred was later proven to be buckling with the use of a finite element analysis.

Figure 31: Samples #2 and #1 Showing Folding of SMP During Testing

It was desired to determine if reduction and prevention of this buckling was possible. The initial method investigated for reducing the folding was uni-axially prestraining the SMP. Prestraining was accomplished by pulling the material in tension in one direction and letting it cool in the deformed shape. Then a shear specimen would be cut out of the deformed material, and located in the shear fixture so that the direction of prestrain was perpendicular to the direction that the shear fixture was loaded in. This placement resulted in a shear sample that wants to reduce its length along the horizontal, or prestrained, axis, and at the same time slightly increase its length along the vertical axis because of Poisson's ratio effect. The logic used is that as the shear fixture is pulled, the prestrain in the material will hold it in tension along the horizontal axis, even as it is constricting, thus reducing or eliminating the buckling that was witnessed. As part of the pre-straining, the Poisson's ratio was also measured. To review how the specimens were cut out of prestrained material the reader is referred back to Figure 23, on page 41.

By prestraining the SMP to 28% strain the buckling was delayed, but not removed completely, as expected by the comparably small amount of prestrain. The data from the

sample that was prestrained 28% had a very identifiable knee that began at approximately 45% shear strain, representing where the sample buckled (Figure 32.) The presence of buckling indicated that the prestrain in the sample had been recovered, and although the magnitude of the buckle (out-of-plane displacement) at the final displacement was less severe than the fold in any of the non-pre-strained specimens, it was not removed completely. The plot does not provide much useful information from a mechanical standpoint, but rather helps to understand prestrain by indicating when the prestrain has been fully recovered from the material, allowing buckling to occur.
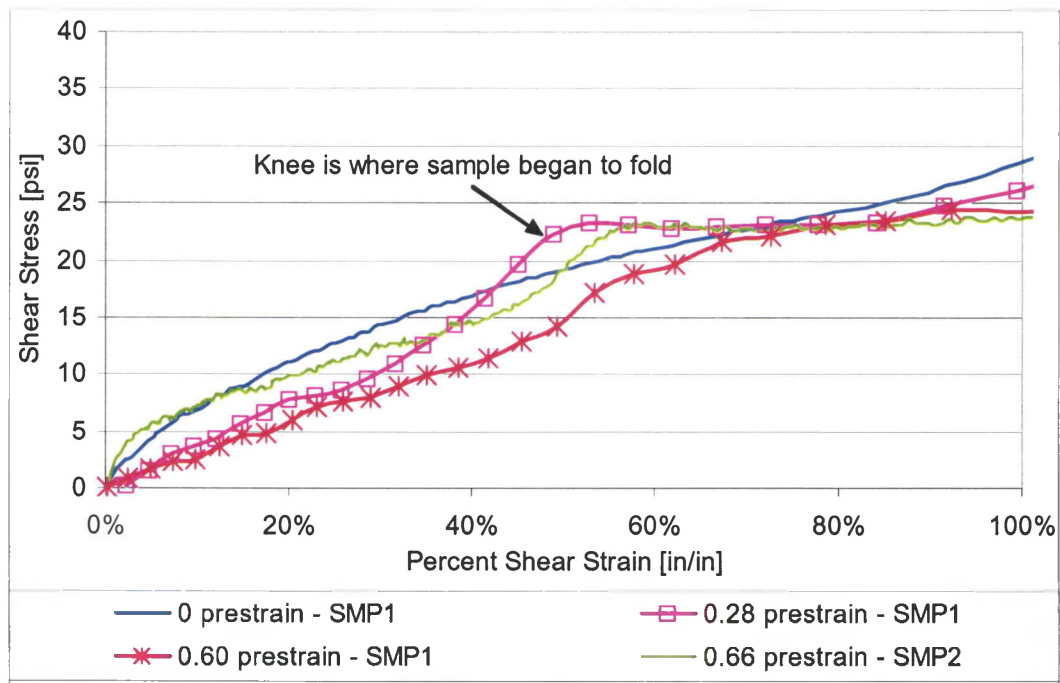

Figure 32: Shear Stress vs. Strain for samples in shear with different pre-strains

Sample #4 was pre-strained 60% and tested. This specimen showed a significantly longer delay in the folding with a much gentler knee in the plot, indicating that the buckling occurred at different times in different locations of the specimen as the prestrain

was eliminated in that section. At the maximum displacement, the fold of this specimen was significantly smaller than in any other specimen.
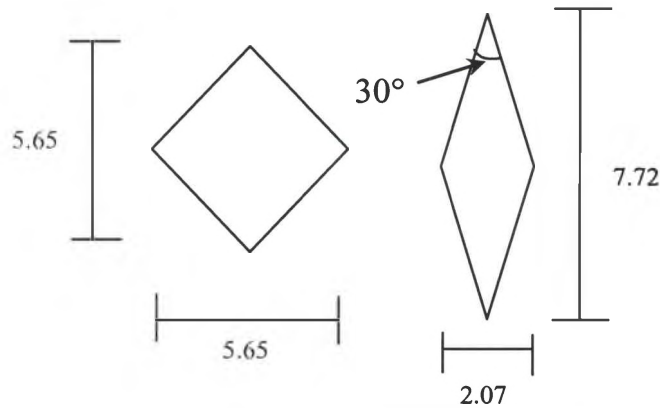

Figure 33: Illustration of Test Fixture Changes Which Induce Strain in the Sample

Sample #9 (from SMP2) was prestrained 66%, just above the -63% the SMP is strained along the horizontal during the test when the distance between the corners is reduced to less than 2.1 inches (Figure 33.) With this new formulation, there is a small change in the physical properties of the SMP, but the overall data is still very useful in understanding prestrain and its ability to remedy the buckling. This specimen began to buckle near 50% shear strain, which is earlier than the specimen that was prestrained only 60%. These results, however, were only single samples and that difference could be reduced, or even changed, with a large number of tests at each amount of prestrain. Another possibility would be that the different formulations account for the small difference in properties. In either case there was not enough material available to fully investigate this anomaly to the theory that increased prestrain would delay the onset of buckling in the specimen.

After testing, the pre-strained samples recovered back to their shape before prestraining which rendered them smaller than the 4 inch square tested, specifically in the direction of the pre-strain. This phenomenon can be seen in Figure 34.

Figure 34: Samples with Increasing Prestrain, From Left to Right (0%, 28%, 60%) Recovered to Their Original Shape after Testing

Specimens 11 and 12, which were prestrained 66%, and were tested from a diamond shape to a square instead of vice versa, did not fare well with the test fixture. The reader is referred back to section 3.2 to see how the diamond was cut out of the material, and the test conducted for this geometry. The clamping method used to hold all four sides of the SMP artificially increased stresses at the edge of the clamp, which was verified in the finite element modeling. The additional stress, combined with the sharp corners of the fixture, the SMP's memory effect, and soft material, led to tearing of both samples that were prestrained. The first one that was tested was torn beyond use during heating, as seen in Figure 35. The second specimen had only a minor tear when heated to temperature, so it was tested. During the test the tear increased a small amount, and another small tear appeared on the opposite side of the specimen. Using a different sample connection to the fixture, or a different fixture, may prevent this occurrence during the test. It would be possible to fasten the SMP with an epoxy, but the specimen

58

would have to be burnt off to remove it. This solution could work for a final product where the SMP would not be removed prior to replacement, but it is not practical for testing samples intended for reuse.
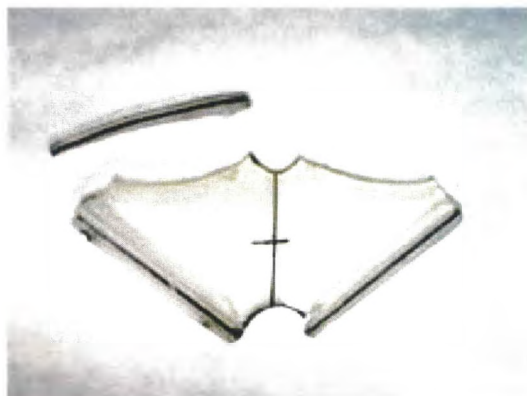

Figure 35: Specimen 12 after Tearing During Heating

One test that was desired, but beyond the scope of this work at this time was the use of bi-axial prestrain, coupled with a different starting geometry. To properly induce a constant bi-axial prestrain requires a complicated mechanism capable of expansion in two directions, with attachment points that move with the specimen. With the specimen held rigid at any location, especially in the corners, there will be a gradient in the amount of prestrain in the surrounding areas, which could lead to faulty tests.
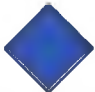
30°	Initial Strain	90°
	$\varepsilon_x = 35\%$ $\varepsilon_y = 35\%$	
	40°	

Figure 36: Requirements for Symmetric Bi-axial Prestrain

Figure 36 shows the required geometry for symmetric bi-axial prestrain that will theoretically keep the material in tension over the range of the test, therefore preventing the buckling from occurring. Using bi-axial prestrain reduces the total amount of

59

prestrain needed to keep the specimen in tension throughout the test because the material is initially pulled in two directions. With the corresponding change in test geometry (starting with 40° corners, then apply positive and negative displacement to achieve 30° and 90° corners) the material should never be in compression, and therefore not be susceptible to buckling. Also, the smaller amount of prestrain introduced into the material will allow for larger strains during the actual testing.

4.5 Cold Testing

One part of this research is to understand what happens to the SMP during the shape change, and what forces it can withstand. Another part is to understand the materials' behavior while it is cool, in both the undeformed and deformed positions. To achieve this, the material would have to be cycled in each position while at room temperature. First, the load limits of the material had to be known, so the during the cycling tests the material would not be readily fractured. To find these limits a basic load-to-fracture test was conducted.

For the load-to-fracture test, two samples were heated above the T_g, formed into the new shape, and cooled. As plotted in Figure 37 the specimens were pulled in tension, bringing the load cell near its upper limit, and pulling the fixture as far as it would allow, but the samples did not fracture. Shear compression was applied by trying to return the sample to its original state while cooled. The loads were then allowed to increase until the sample fractured. The fractured sample, loaded in compression from the top and bottom in the picture, can be seen in Figure 38, while the plot of the compressive fracture

test is shown in Figure 39. For the compression plot the shear strain is a function of the original shape of the material, which is why it starts at 90% and decreases. Once the specimen has been reduced to below 88% strain it becomes weaker, taking less force to reduce the strain the same amount, as is noticed by the change in slope of the plot at that strain.
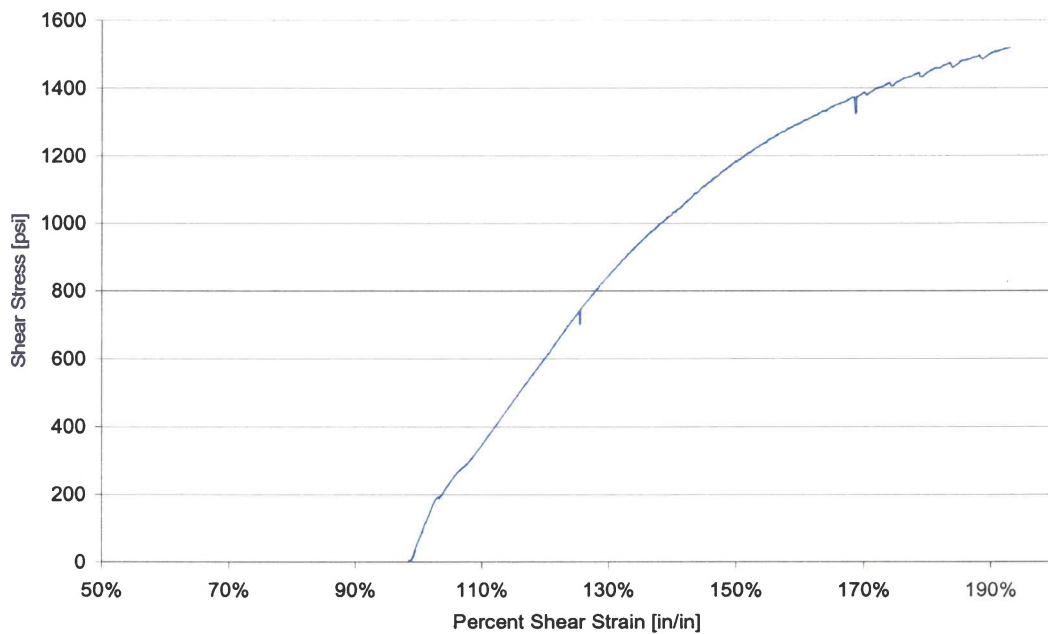

Figure 37: Tensile Test After Specimen was Deformed and Cooled

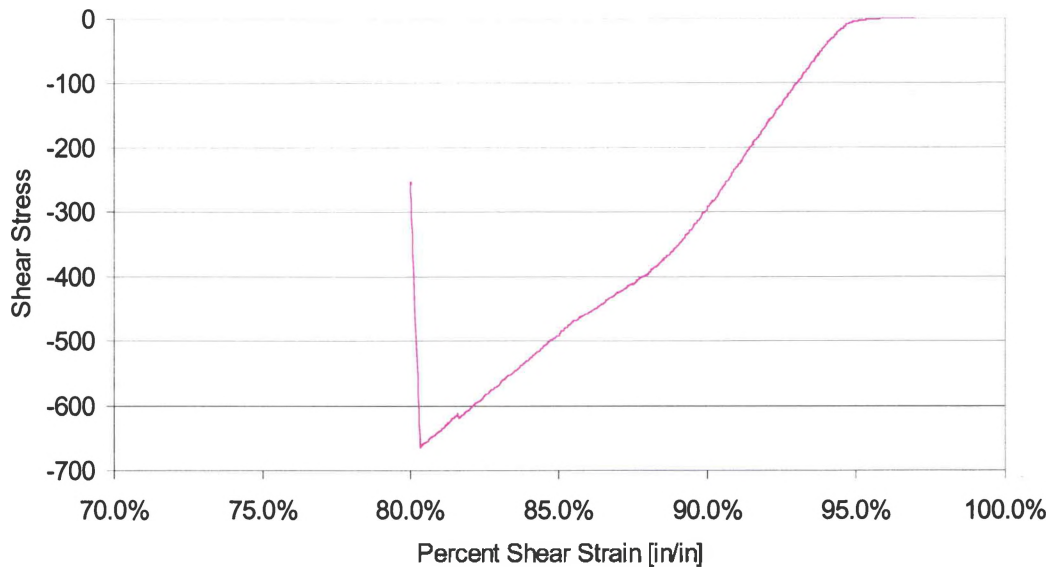**Figure 38: Specimen 2 Fractured from Compression**

Figure 39: Fracture Plot of Specimen 2 Cold

For low-load testing, sample #7 was cycled to a small deformation while at room temperature ($T<T_g$.) This was done to simulate real-world use and flexing of the morphing structure. After the cycling at room temperature, the specimen was heated, shaped, cooled back to room temperature, and cycled again. The sample was then heated above the T_g again in the test fixture, and reshaped again, this time from the diamond back to it's original position in the shape of a square. The data from the low-load cycling indicates there is some hysteresis as the deformed material is cycled, but it appears to converge during the last two cycles. The same trend was found during the load-cycling of the bulk SMP.

Figure 40 shows the results of SMP being cold cycled to a small displacement while deformed. The material requires slightly less load each cycle to achieve the set displacement of 0.05 inches from the starting position.
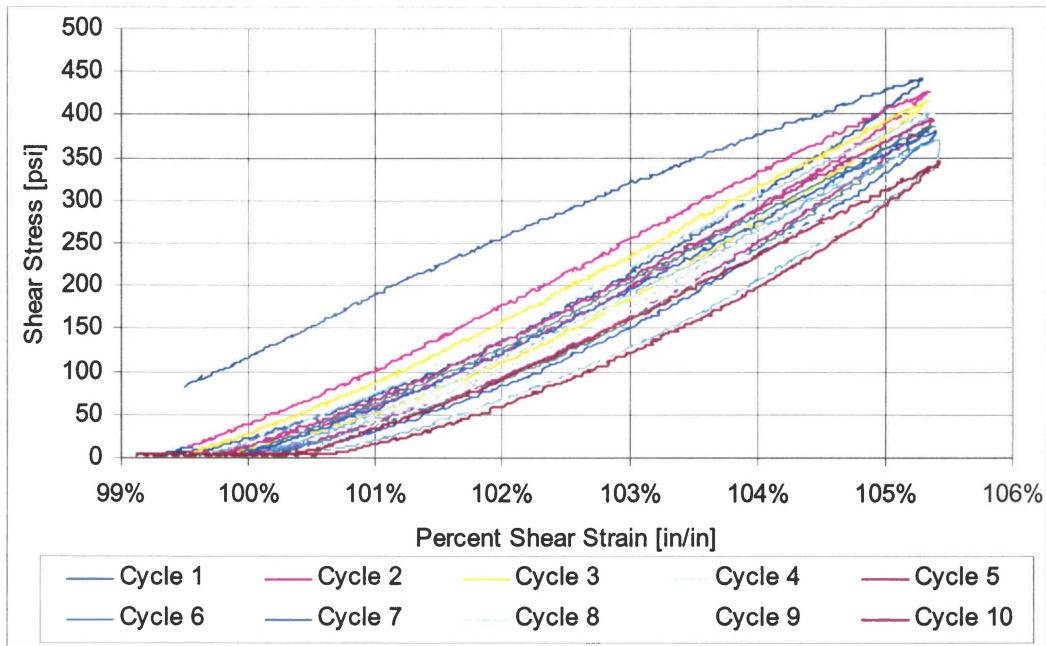
Figure 40: Shear Stress-Strain Curve for Sample 7, Cycled to 0.05" Displacement, After Deformation and Cooling Below Tg

Figure 41 contains the results from the material being cold cycled in the undeformed condition. Since the material did not appear to require any force to obtain part of the displacement it was decided to run the test again with a different specimen, and for more cycles to determine if there is convergence in the load reduction trend mentioned above. From the results in Figure 42 below, it was noted that after approximately 20 cycles this force reduction trend stopped, indicating that the material had stabilized. This can be seen by the abundance of data plotted on top of each other. The one line cutting across the plot is from the first cycle. After that initial cycle the second specimen shows the same trend that led to the decision to test a second specimen, almost no force is required to move the initial displacement. One possibility for this is that the material is settling into the fixture on the first cycle, and therefore has a small amount of freedom of motion. Also, there could be some free play in the fixture,

specifically in the pinned corners, allowing a small amount of motion to occur at no load. Another possibility is that the cycling imparts a small amount of plastic strain or into the material in the first cycle, but if this were the case there should be some negative stresses compressing the plastic strain during the unloading part of the cycle. Additionally, the material could buckle slightly during the initial cycle, thus changing shape and creating a slight amount of free play in the fixture.
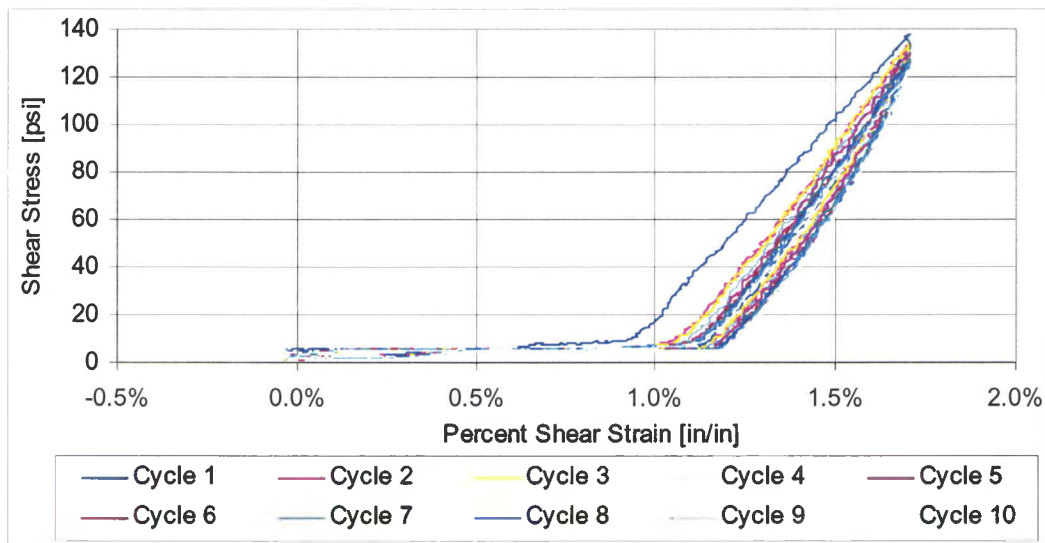

**Figure 41: Shear Stress-Strain Curve for Sample 7 in Undeformed State, Cycled to 0.05"
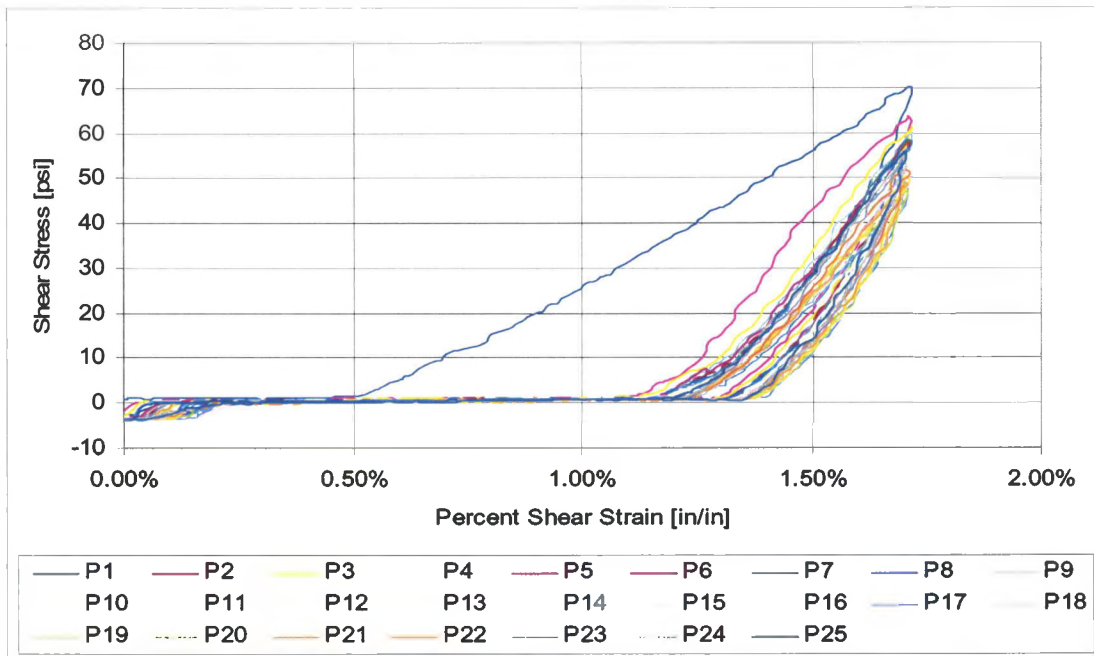Displacement**

Figure 42: Sample #5, Cold Cycled 25 Times

During this test regimen the SMP appears to soften during loading, in that it takes less force to strain it the same amount. This could be the result of a small amount of plastic strain being induced each cycle, or from the material cracking under the load. Whatever the reason, there was no cracking observed, and as noted above, there appears to be a convergence in this behavior, which indicates that there is a finite amount that the material will 'soften' during use.
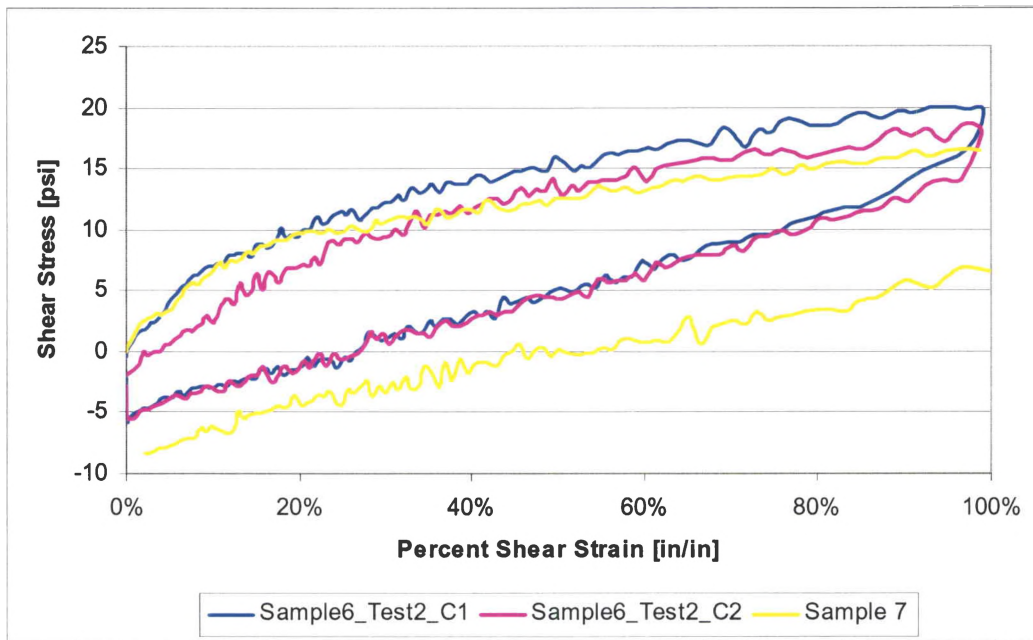
Figure 43: Deformation Plots of Sample #7, Shown With Both Cycles from Sample #6 Test2

When undergoing the series of tests for the cold cycling, the SMP performed similarly to other tests during the heated deformation process; but when it was heated to be returned to its initial position, there was some discrepancy that can be seen in Figure 43. The start of the unloading curve, after sample #7 was cooled, cycled and reheated, is much lower than the end of the loading curve. A potential source of error in this test was the intermittent data acquisition; instead of gathering data constantly, it was collected only during the actual testing. At least one hour is needed to both heat and cool the specimen. Currently the temperature control is done by an external controller, not one linked to the MTS machine. Had the data acquisition run the whole time, one would notice an increase in force as the SMP cools as mentioned previously, and the force would stabilize again once the SMP is well below its T_g, and no longer experiencing a change in temperature. These force and temperature changes that were not recorded could produce the difference in forces seen in the figure.

Since the natural aerodynamic loads cause a structure to flex slightly during flight, the SMP will experience cycling similar to the cold cycling test. When this test is done on more samples, it can be determined if the SMP will experience a permanent change or if it will recover completely every time it is heated up. Should the SMP experience a permanent change, over time it will be able to carry less of the shear loads. The implication for an aircraft wing's design is that it would require a stronger internal wing structure to prevent failure. If the SMP recovers fully after heating, the structure can be designed to allow the SMP to carry some of the shear loading, allowing the planform to change.

Each of the above described tests provided information on the properties of the SMP. The averaged results for the basic material characteristics obtained from each test are shown in **Error! Reference source not found.**. It is noted that prestraining the material appears to have an effect on the shear modulus, though more tests are needed at each amount of prestrain to verify the significance of prestrain on the modulus. Another important point is that if one were to calculate the shear modulus from the tensile properties (E = 87 psi, ν = 0.28) it would be slightly higher than the one listed in Table 3. The most likely cause of this is error in the property measurements, especially in Poisson's Ratio, as it was not measured in a controlled experiment for tensile properties but rather was obtained during a prestraining of the material, where the specific properties were not as important as the final shape obtained.

Table 3: Basic Structural Material Properties of an SMP

Shear Modulus, G, of bulk material at 203°F	25.8 +3.0 / - 3.5 psi
Shear Modulus, G, of pre-strained material – 28% pre-strain at 203°F	38.9 psi
Shear Modulus, G, of pre-strained material – 60% pre-strain at 203°F	28.8 psi
Shear Modulus, G, of bulk material at room temperature	17385 psi
Poisson's ratio from 60% pre-strain at 203°F	0.28
Extreme Positive Shear Load Limit to fracture with formed samples at room temperature	3855 psi

4.6 Tensile Test Results

Tensile tests were conducted to determine the modulus of the SMP over a range of temperatures, determine the strain mechanism of the material. It was only possible to conduct a few of the desired tensile tests, so the testing was limited to tests performed at the same temperature at which the shear tests were performed. This would allow for an improved value for the modulus at temperature to be determined, when compared to the properties obtained from prestraining, but of primary interest was the ascertainment of the materials reaction, be it linear or non-linear, and viscoplastic (VP) or viscoelastic (VE.)

Of the five tensile tests that were run, three were done at a deformation rate of 2 inches per minute, which was the same rate used for the majority of the shear tests. The stress-strain plots resulting from these tests are seen in Figure 44. After analyzing the data it was found that the SMP provided for this research has a modulus of 87 psi when heated to 203° F.
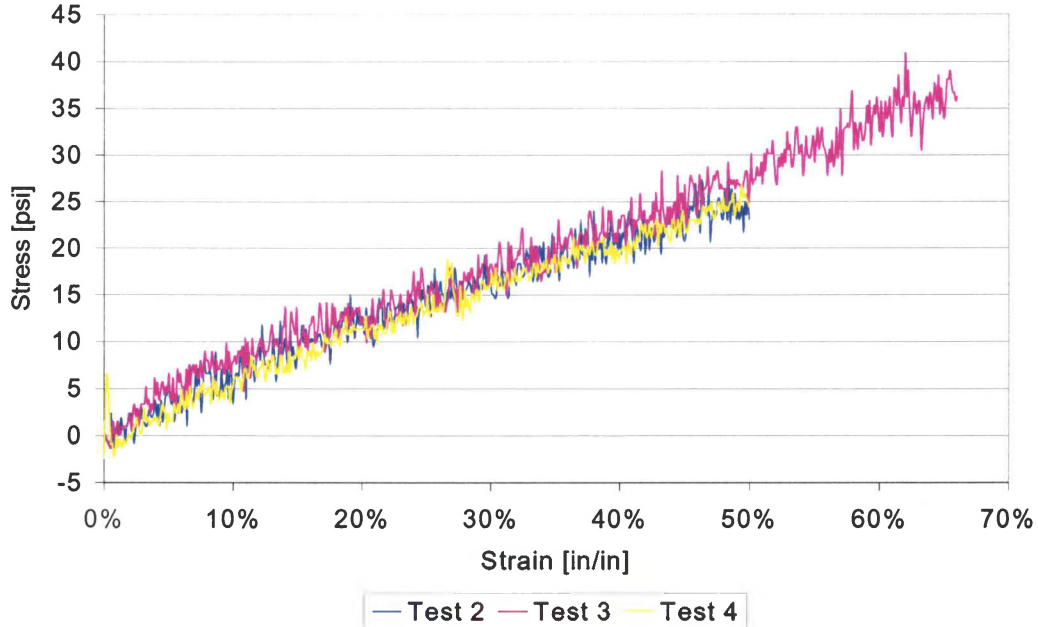
Figure 44: Tensile Data from 3 Tests at 2" /min Deformation Rate

Generally, to determine the linearity of a materials strain behavior a specimen is tested at multiple rates. The results are plotted on stress-time and strain-time graphs, and at least one time of interest is used. The strain of the material from each rate, and the corresponding stresses at this time are recorded, and plotted on what is called an isochronous stress-strain plot. If the material is a linear viscoelastic the resulting stress-strain plot will be linear, and pass through the origin. In order to determine linearity and whether the material went through a VP or VE straining process two higher deformation rates, each an order of magnitude faster than the last (2 inches per minute, 20 inches per minute, 200 inches per minute,) were used (Figure 45.) The smoothed curves shown were obtained by placing a curve fit over the data, then plotting the equation obtained from the curve over the range of strain from the actual data.
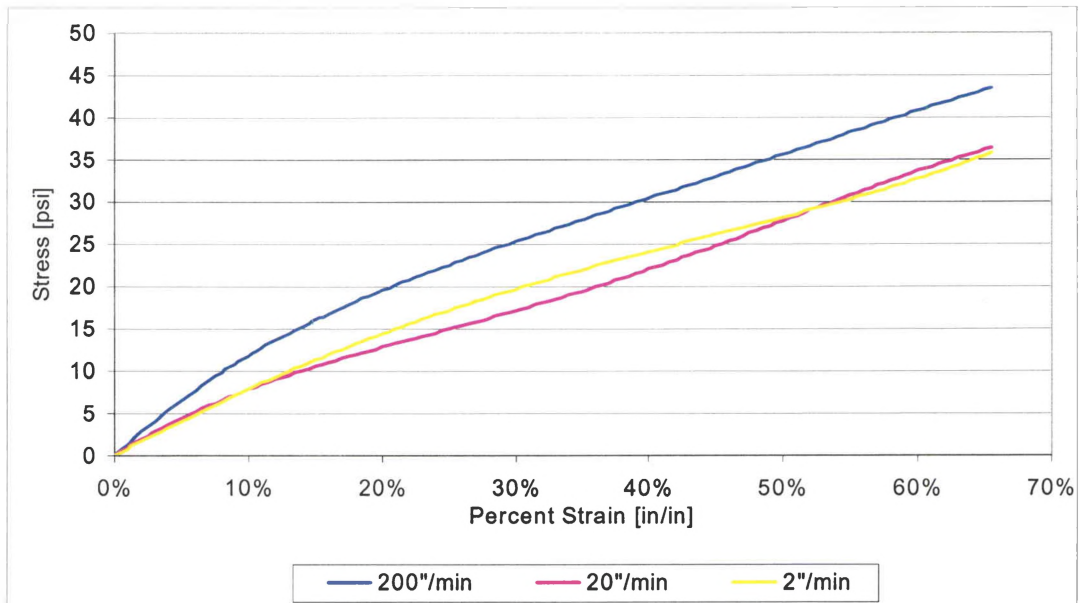
Figure 45: Tensile Results from Different Rates (Smoothed)

The rates that these tests were performed at limited the times available at which all three rates has useful data, as the first data point at the slowest rate corresponds to nearly the last data point at the highest rate, preventing a large sampling range over which the data could be used.

With the use of the curve fit equations used in Figure 45 stress-time and strain-time plots were made, with the only overlapping physical data point being at a time of 0.0025 seconds. The resulting isochronous stress-strain plots are shown in Figure 46. From Figure 46b one can see that the material is linear VE up to at least 5% strain. Figure 46a shows that somewhere between 5% and 50% strain the material goes nonlinear or plastic. By testing other rates it would be possible to obtain data to fill in the spaces between the data points on Figure 46 to confirm the linearity, and to determine where the material stops its linear behavior.

a) All Data Points   **b) First Two Data Points**

Figure 46: Isochronous Stress-Strain Plots

To determine if the SMP is VP or nonlinear VE is a simple matter of observing what happens to the material when it is returned to zero strain. If, after a time, the material returns to zero stress it would be considered a viscoelastic material. If it does not return to zero stress, then there was some plastic deformation that occurred. The test can also be conducted by returning the material to zero stress and waiting to see if it returns to zero strain over time.

The shape memory effect of the SMP is such that, when above T_g and with no applied load, the material will return to the initial shape that it was formed in, which was a flat sheet for this research. Based on this knowledge, and observations made in returning the material to its initial condition after tests, it would be safe to say that, at temperature, SMPs are most likely a nonlinear viscoelastic material.

4.7 Chapter Summary

This chapter broke down the results of the various experiments performed, describing the behavior of SMPs. Some observations were made during the testing that were not expected, so the tests were expanded to help understand these phenomena. At the end of the chapter there is a table summarizing the results from the shear testing, which indicate the SMPs ability to function structurally. The final section, on the tensile tests, provides a more accurate value of the modulus of the SMP at temperature, and evidence for SMPs to be a nonlinear viscoelastic material, when heated above their T_g.

CHAPTER V

MODELING

A Finite Element (FE) analysis was conducted to aid in the understanding of the experimental analysis. PATRAN was used as the visual interface, and ABAQUS used to do the nonlinear material analysis. Even though the model was symmetric, due to the translational complexity of the problem, and it's comparably small size, a full model was used. The model build up, various constants, elements used and the process in going from the initial elastic model to a more accurate elastic-plastic model are explained. Additionally, a buckling analysis was done to determine at what force and displacement buckling would occur in the model, if at all.

5.1 Basic Geometry and Model Development

Figure 47 shows the FE model, and an example mesh. The outer square in the figure represents the fixture, while the other areas represent the material. In the cutout at each corner there is no material, as is noticed by the lack of mesh for those regions on the right side of the figure.
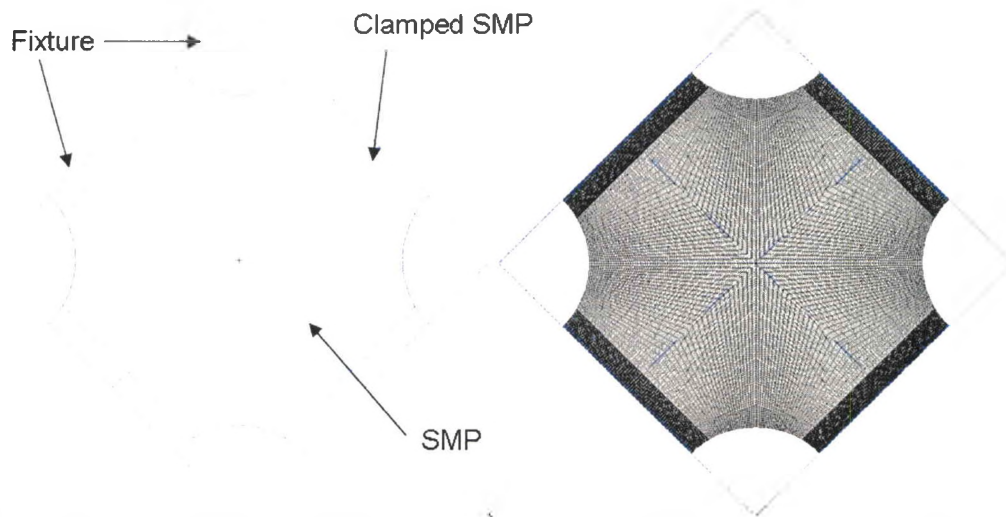
Figure 47: Drawing of the SMP / Fixture Used for Modeling & Early FEM Model

The model was initially meshed with the automatic edge length calculation feature in PATRAN recommending an edge length for the elements. This was done for all of the surfaces and all of the curves that were meshed. The surfaces were all meshed with two dimensional shell elements. The edge surfaces, where the SMP was held into the fixture, had a thickness of 0.5 inches and a modulus of 29,000,000 psi, which is the modulus of steel. This was done to represent the fact that the SMP was being held rigidly between two pieces of steel. The rest of the SMP was modeled with a thickness of 0.154 inches, which is equivalent to 4 mm. As the model progressed data from prestraining the SMP 60% was used to obtain a value of 115 psi for the modulus of the SMP. This value was used on all models until the tensile testing was completed, which provided a slightly lower modulus of 87 psi (Figure 48).
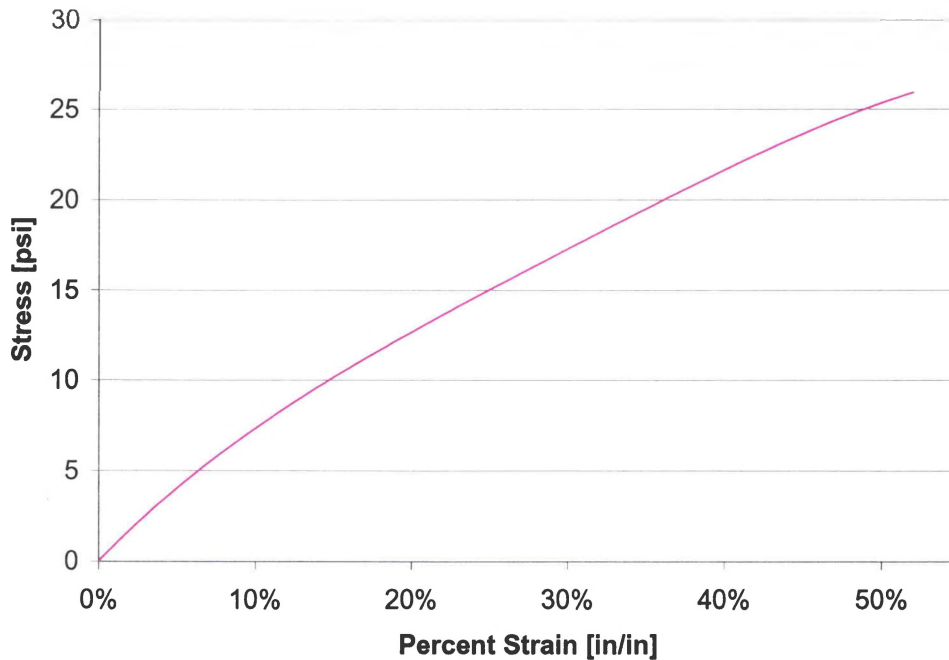
Figure 48: Stress-Strain Plot from Tensile Testing

The fixture was modeled with the B31 element in ABAQUS, which is a one-dimensional beam element. These elements were given a cross-sectional area of 0.45 in^2 and a moment of inertia of 0.0152 in^4.

The model is made of multiple areas, and each area must be meshed separately, creating extra nodes where the surfaces met, or where surfaces and curves, which represent the fixture, overlapped. Once the model was meshed all nodes that were meshed twice had to have the second mesh removed. Removing these duplicate nodes essentially glues the different areas, or areas and curves, together, creating a solid model. In order to allow the fixture to move realistically, rotating around the corners, each corner needed to have two nodes to represent the two different sides of the fixture. If a corner had only one node it would be equivalent to making that corner rigid instead of making it

out of two bars pinned together. This resulted in all of the duplicate nodes, except those at the four corners, being removed.

Since the four sides of the fixture were now modeled as four separate entities they had to be pinned at their corners. This was done with the use of Multi-Point Constraints (MPCs.) An MPC requires that motion of a set of independent nodes be exactly copied by the set of dependant nodes. Four MPCs were used, one for both the 'x' and 'y' directions at each of the two side corners.

To prevent the model from pure translation the two bottom nodes were constrained from all motion except rotation about the 'z', or out-of-plane axis. The corners on the two sides were constrained from out-of-plane translational motion, while allowing a rotation about the 'z' axis only. The top corner of the model was only allowed to move vertically, or in the 'y' direction, while the only allowable rotation was once again about the 'z' axis. These boundary conditions ensured that the model would rotate about pinned corners, with motion of the fixture in the x-y plane only. Finally, a displacement was prescribed at the top corner. This displacement was originally only one inch to validate the model, but as the model progressed the displacement was increased to 2.07 inches, which was the final displacement in the shear tests, and resulted in an interior angle of 30° at the top and bottom corners.

Many model iterations were required to advance the fidelity of the FE model due to the complexity of the test being modeled and in properly quantifying the actual

properties of the material for the analysis. The FE analysis was first done on a purely elastic material, with the thought that as the model was refined the material would progress to an elastic-plastic model, and finally some form of a viscoelastic-viscoplastic model, based on the properties obtained from the testing that was conducted in parallel with the modeling.

The first models used S4R5 elements for the shells. This indicates that the shells had four nodes, used reduced integration, and were allowed five degrees of freedom. Reduced integration means that the element stiffness matrix was calculated with a lower order integration, which greatly reduces running time for large analyses. Generally speaking, instead of using four points within the element for integration, only one is used. This method also often provides more accurate results when the elements are not distorted [ABAQUS, 1995].

Initially the models had a singularity at the boundary between the two material models of the SMP. There was an increase of modulus of multiple Orders Of Magnitude (OOM's) at the intersection, as well as a thickness change, because the edge of the SMP was modeled as being the steel fixture since it was held rigidly. This singularity caused the softer elements on the boundary to deform greatly and eventually enough that the element could not be integrated across and the analysis had to be stopped.

The modeling progressed with a few small changes at each iteration to improve the fidelity of the model and ensure the proper inputs to ABAQUS. The next model had

the mesh refined to approximately one third the size suggested by the automatic edge length calculation feature. The initial displacement was set to 0.05 inches to ensure that the model would run. Once the model ran smoothly the next model was made with no changes, other than increasing the desired displacement to the full 2.07 inches. Failure occurred at approximately 0.5 inches of displacement, with the softer elements at the singularity deforming beyond use. This is the failure mechanism for the analysis at every iteration unless otherwise noted.
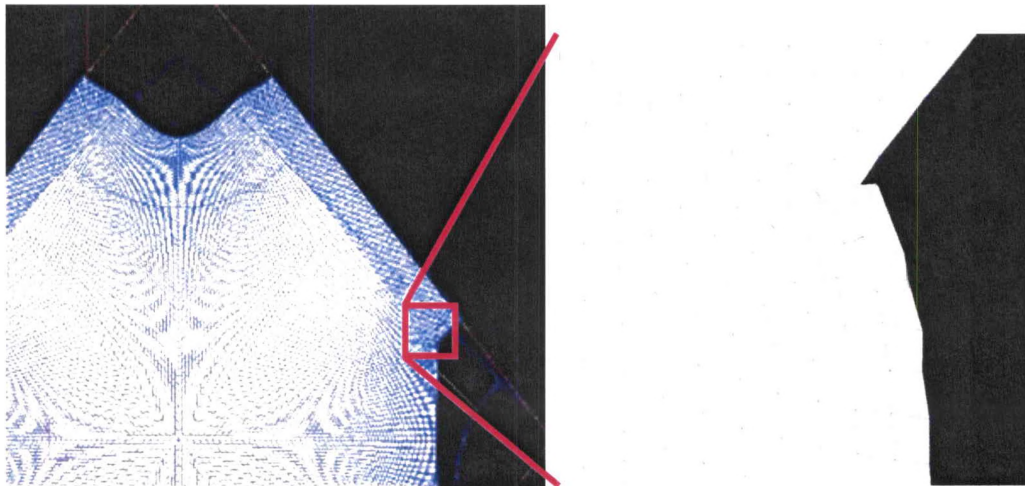
Figure 49: Close-up of Element Failure

Figure 49 shows part of the model and a close-up of a corner where the elements failed. All of the blue lines on the left picture indicate different elements. In the close-up one can see the individual element shapes. All of the elements were initially square like the elements at the top or bottom of the figure. At the material discontinuity it is easy to see that the soft elements deformed significantly to various forms of trapezoids and triangles. When the elements degrade to triangles and beyond (arrowhead shapes), usually from the straining of the material, the stress and strain equations that are solved for the element can no longer be solved, preventing the analysis from continuing.

78

For the next iteration the S4R element was used instead of the S4R5 element. This new element has a full six degrees of freedom, and is geared towards use in large strain situations, such as those observed in the experiments. Additionally the model was not seeing any out of plane deformation like that noticed in the testing, so a very small pressure in the 'z' direction was placed on the eight elements at the center of the model. It was hoped that this small pressure would provide a catalyst to the out of plane motion that was witnessed. This still did not have the desired effect so the pressure was increased two orders of magnitude to 0.001 psi. When this did not provide the desired outcome the original pressure of 0.00001 psi was placed over the entire surface.

The tenth iteration, being the first one with the full surface pressure, also had mesh seed of sixty placed along each side where the change in SMP properties was located. This sets a requirement that there be sixty elements along that line between the two different properties. Also, because of the failure mechanism that has been witnessed, and the fact that in reality there is no clear jump between properties, but rather a gradient between them, a small variation in the modulus was placed at the corners where the elements were degrading. Instead of a jump of six OOMs the four elements on the stiffer side of the corner were set at an intermediate modulus with the hope that they would deform slightly providing something akin to the gradient that occurs in reality.

For the next iteration the variation in modulus at the corners of the edge where the two properties met was increased. The element in the corner itself was the same modulus

as before (400 psi), but the three elements surrounding it were changed to a modulus of 4000 psi, once again with the hopes that it would more closely resemble the changes that are naturally seen in the test. The twelfth iteration added plastic effects to the previously elastic model. The stress-strain relations that were needed as input for the plastic deformation were obtained from the same stress-strain curve as was used for determining the modulus.

With continued failure to obtain the full range of desired motion it was decided to limit the property variation of the SMP at the junction between the material and the fixture. At first the modulus was modeled with an order of magnitude variation between the two surfaces. The next iteration the entire SMP model had the same modulus of 115 psi. The fifteenth iteration had a mesh refinement along the edge of the SMP, as the failure location moved from the joint between the two properties within the SMP to the joint between the fixture and the SMP, as this is where the property variation now occurs. The mode of failure was still the same.

With the increased refinement of the mesh on the edge of the SMP and a mesh seed of thirty there were many elements that were not square shaped. The mesh seed was increased to 67 so that the elements would more closely resemble squares for the next iteration. Also, the modulus was set to vary over a range of elements and the edge of the SMP would not be set with the properties of the steel that was holding it in place. This led to expanding the variation in modulus from the corner to the whole quarter-inch wide edge of the SMP. Since it did not appear possible to vary properties over a range of a

material easily, the properties were set as a function of temperature, with the temperature varied on the edge of the SMP. This is possible because the modeling is taking place with the properties of the SMP above its T_g, not across a range of temperatures. The temperature was set to vary linearly from 0° to 100°, with the modulus being a function of temperature, ranging from 115 psi to 11500 psi.

By the next iteration the tensile testing had begun and a newer, more veritable, modulus was determined to be 87 psi. Over the same 100° temperature variation the modulus would now vary from 87 psi to 8700 psi. Also, due to the minimal out-of-plane deformation in the model a material defect was added. The material defect came in the form of the center of the model being given an out-of-plane displacement of 0.01 inches. During these later analyses the STABILIZE command was added to the displacement step, and the out of plane deformation was finally properly captured in the model. It is notable enough to mention that the out-of-plane deformation in the model actually occurred opposite the direction of the induced displacement from the material defect.

The final model had a modulus of 87 psi, which varied quadratically along the clamped edges up to 8700 psi where the material was held in the grooves of the fixture. A total of 41,845 nodes were used to create the 41,808 elements needed for the model. This model was not able to obtain the full desired displacement, but did provide some insight into the testing. Further mesh refinement, and obtaining a full set of viscoelastic properties for the material could lead to the model obtaining the full 2.07 inch displacement that was used in the experiments.

5.2 Analysis & Results

Even though the model was unable to complete the full displacement that was performed during the physical testing, it was able to provide some useful information. Using the results from these models it was possible to construct a stress-strain plot similar to the ones obtained from the tests performed. This was done taking the resultant forces at each step, and the associated displacements, which is the same basic output that was used to perform the calculations for the tests. Also, useful plots of the stress and strain distribution within the specimen could be obtained from the model. Finally, a buckling analysis was conducted in order to determine if the out-of-plane deformation observed during the tests was buckling behavior, or membrane folding. Knowing what mechanism creates the deformation will be useful in the efforts to prevent it from occurring in the future.

Due to the failure of the analysis, it was impossible to complete the full stress strain plot, but the data that was available results in a stress-strain plot very similar to that from the tests, as seen in Figure 50. The data for the higher modulus started very near the origin then runs slightly above the data obtained from the experiments. The data using the lower modulus actually began with a negative stress and was corrected to a near zero origin, where is lies within the test data. If the curves were all corrected so that they all had the same approximate origin they would lie very close to the results obtained from the ABAQUS model.

82
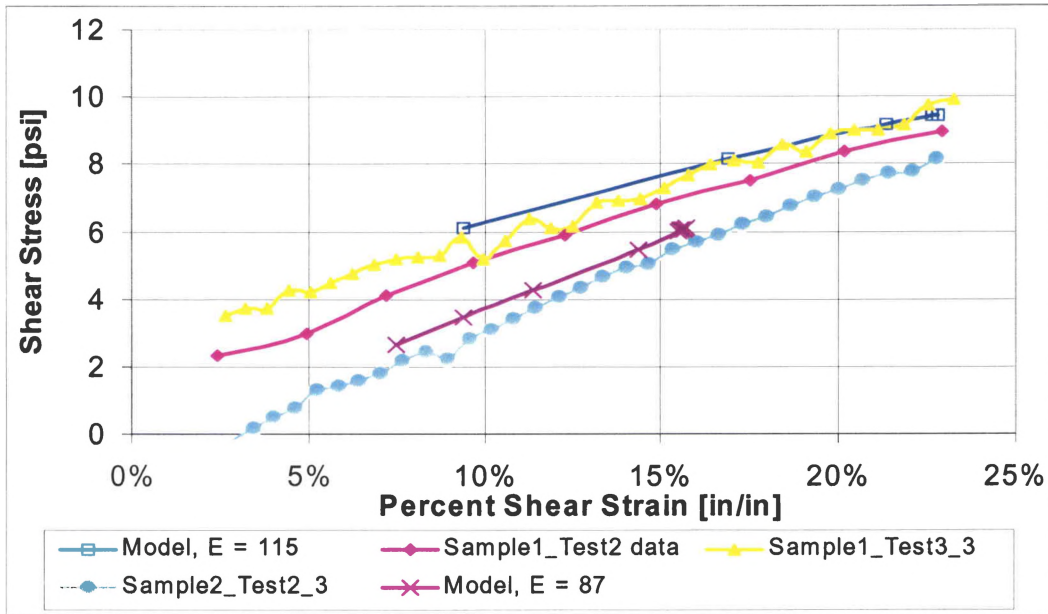
Figure 50: Modeling Stress-Strain Compared to Test Results

This proves that the ABAQUS model provides a good representation of what is happening during the tests because the forces and displacements are similar, though it will be nearly impossible to get an exact model because of the different displacement rates that the material sees at different points of the specimen, which has a direct effect on the effective modulus of the material. One would have to determine the displacement rates and associated moduli at different locations on the specimen in order to obtain an exact model of what occurs during the testing.

Figure 51 is a plot of the von Mises stress in the specimen at a displacement of approximately 0.65 inches, plotted on an undeformed view to more easily show where the stress concentrations occur. The right hand side indicates the value of the stress for each color, and while it is difficult to read, the important fact is that the stress increases from blue to red. While the majority of the specimen is a shade of blue, the eight corners

show stress concentrations, especially the four corners at the top and bottom, where the force is directly applied (or the reaction occurs.) The edges of this model are located at the center of the grooves in the fixture that rigidly hold the SMP. This figure indicates that there is a stress concentration at the corners of the material, as previously mentioned.
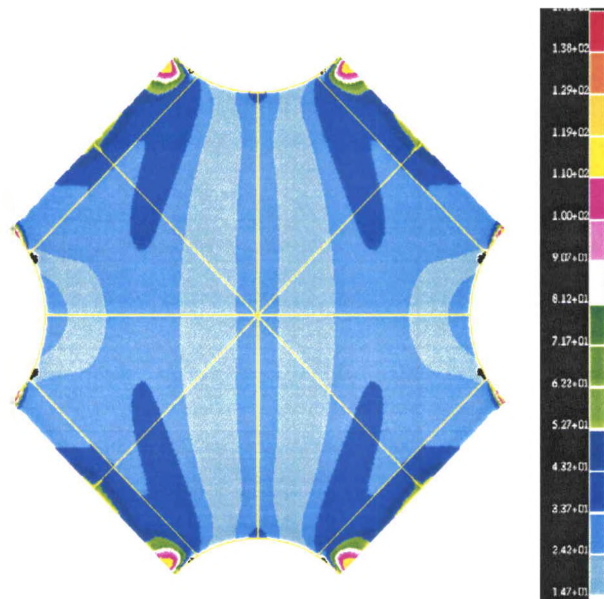
Figure 51: von Mises Stress Plot at a Displacement of 0.65 Inches

The buckling analysis was originally done on a perfectly square model so that the analysis itself could be properly understood before beginning the more complicated problem at hand. This plate model was the same shape of the actual model, with some of the dimensions rounded off for simplicity (i.e. thickness of 0.16 instead of 0.154.)

Because this was not being used for actual forces, a modulus of 1150, an order of magnitude larger than the actual models (before tensile testing), was used to ensure buckling, and not folding, would occur. The entire model was made of shell elements with the same properties, creating a flat plate instead of the multi-material (steel and

SMP) true model. A density of this material was arbitrarily chosen somewhere between the actual densities of the two materials, at 0.0005 slug/in^3.

For a simple buckling analysis a fine mesh is not required, so a very coarse mesh of 10 elements per inch was used. Boundary conditions preventing the bottom from translating at all, allowing the sides 'x' and 'y' translation and the top 'y' translation only were applied. Additionally, all four sides were constrained from any out-of-plane, or "z" displacement to mimic the clamped boundary conditions in the physical test.

The shear force was applied as a force of 6 pounds on each node, which results in an equivalent of 348 pounds force pulling on opposing corners. The entire model had a pressure of 0.0001 applied on one face of the material, as in some of the earlier modeling attempts, to try and induce some out-of-plane deformation that had not yet been captured by the model. The results in this case were not important except to show that the analysis ran correctly, and to aide in the interpretation of the results, but they did show that the first buckling mode was of the same shape as the out-of-plane deformation that was witnessed during the testing.

Once the buckling analysis deck and the resulting eigenvalues were understood a buckling analysis was done on the actual model that was being analyzed for the stresses and strains. This model had the material at the corners removed, and included the fixture as well. The modulus was set at a constant value of 87 psi and not varied at the edges for simplicity. Since the buckling modes occur generally in the center, especially the mode

that that analysis is concerned about, the variation in modulus along the edge was deemed insignificant.

The meshing of the buckling model was once again coarse compared to the analytical model, but was acceptable for a buckling analysis. There were 52 elements along each of the sides of the model, with 66 elements along the circular edges where the corners were cut out. The thickness of the shell elements and the properties associated with the beam elements used for the fixture were the same in this as in the actual analytical models.

The ABAQUS user manual describes buckling as the following eigenvalue problem:

$$\left(K_0^{NM} + \lambda_i K_\Delta^{NM}\right)v_i^M = 0 \tag{1}$$

Where:

K_0^{NM} is the stiffness matrix corresponding to the base state, including preloads P^N

K_Δ^{NM} is the differential initial stress and load stiffness matrix due to the incremental

       load Q^N

λ_i are the eigenvalues

v_i^M are the buckling mode shapes, or eigenvectors

M & *N* refer to degrees of freedom M and N of the whole model

i   refers to the *i*th buckling mode

Using the first eigenvalue, the critical buckling loads are then

$$P^N + \lambda_i Q^N \qquad (2)$$

Where P^N is the preload on the material and Q^N is the incremental load applied for the buckling analysis.

The results from the buckling analysis indicated that the first buckling mode occurred at an eigenvalue of 0.04946. The eigenvector associated with this mode can be seen in Figure 52. The analysis that was performed had no preload, so P^N was zero, and had a constant perturbation load pattern, Q^N. For this scenario Equation (2) states that the eigenvalue is multiplied by the perturbation force to obtain the force at which the buckling shape associated with the eigenvalue occurs. This results in the first buckling mode occurring at a load of 1.19 pounds, based on the applied perturbation force of twenty-four pounds.
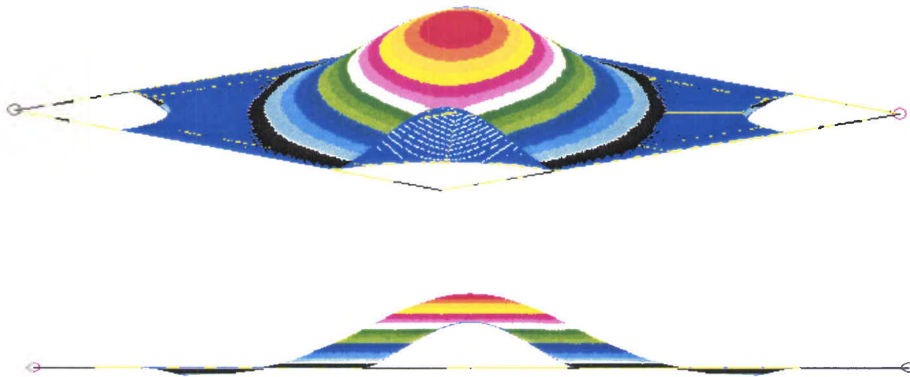
Figure 52: Two Views of First Eigenvector (Buckling Mode)

Additionally, hand calculations were done to determine the theoretical buckling load from Timoshenko's exact solution for a clamped square plate buckling under shear.

The following derivation can be found in its full form in *Theory of Elastic Stability* by Timoshenko and Gere [1961].

First, it is assumed that the plate buckles in two half-waves, one representing the deflection along each pair of parallel sides. With this assumption the total deflection can be represented by the following equation:

$$w = a_{21} \sin \frac{2\pi x}{a} \sin \frac{\pi y}{b} \tag{3}$$

Expanding the assumption so that the out-of-plane deformation can be represented by multiple half waves in each direction leads to

$$w_{mn} = a_{mn} \sin \frac{m\pi x}{a} \sin \frac{n\pi y}{b} \tag{4}$$

This is similar to expanding a Taylor series. To get the actual deflection one must sum Equation 4 over a significantly large range of m and n. Therefore the total deflection is written as

$$w = \sum_{m=1}^{m=\infty} \sum_{n=1}^{n=\infty} a_{mn} \sin \frac{m\pi x}{a} \sin \frac{n\pi y}{b} \tag{5}$$

From this equation one can determine that the strain energy of bending will be

$$\Delta U = \frac{D}{2} \frac{\pi^4 ab}{4} \sum_{m=1}^{m=\infty} \sum_{n=1}^{n=\infty} a_{mn}^2 \left(\frac{m^2}{a^2} + \frac{n^2}{b^2} \right)^2 \tag{6}$$

Next the equation for the work done by external forces is found to be

$$\Delta T = -N_{xy} \int_0^a \int_0^b \frac{\partial w}{\partial x} \frac{\partial w}{\partial y} \, dx \, dy \tag{7}$$

Substituting Equation (5) into Equation (7) gives two results in integral form, one for $m \pm p$ being an even number, and the other for $m \pm p$ being an odd number. When these are solved we obtain

$$\Delta T = -4N_{xy} \sum_m \sum_n \sum_p \sum_q a_{mn} a_{pq} \frac{mnpq}{\left(m^2 - p^2\right)\left(q^2 - n^2\right)} \tag{8}$$

Equating the work from external forces (Equation (8)) and the strain energy of the system (Equation (6)) we obtain an equation for determining the critical value of the shearing forces seen in Equation (9).

$$N_{xy} = -\frac{abD}{32} \frac{\displaystyle\sum_{m=1}^{m=\infty} \sum_{n=1}^{n=\infty} a_{mn}^2 \left(\frac{m^2 \pi^2}{a^2} + \frac{n^2 \pi^2}{b^2}\right)^2}{\displaystyle\sum_m \sum_n \sum_p \sum_q a_{mn} a_{pq} \frac{mnpq}{\left(m^2 - p^2\right)\left(q^2 - n^2\right)}} \tag{9}$$

The critical shear force is that which occurs when Equation (9) is at its minimum. To determine this point one must take the derivative of Equation (9) with respect to each of the coefficients and set them equal to zero. This provides a system of linear equations than can be divided into two groups: equations with constants a_{mn} where $m + n$ are odd numbers, and one for which $m + n$ are even numbers. For square plates both sets of equations are needed, resulting in mn equations. As more of the equations are used the results become more accurate. Using five equations and setting their determinant equal to

zero one can find an equation for the calculation of the critical shear stress, which is introduced when solving for the coefficients in Equation (9).

$$\tau_{cr} = k \frac{\pi^2 D}{b^2 h} \tag{10}$$

where:

k is a constant depending on the aspect ratio of the plate, $\frac{a}{b}$, and the boundary conditions

(14.71 for our case)

a and b are the length and width of the specimen, respectively

h is the height, or thickness, of the material

$$D = \frac{h^3 E}{12(1 - v^2)}$$

E is Young's Modulus

v is Poisson's Ratio

This results in:

$$\tau_{cr} = \frac{k \pi^2 h^2 E}{12 b^2 (1 - v^2)} = 1.714 = \frac{N_{cr}}{A} \tag{11}$$

Based on the properties of the test specimen, Equation (11) indicates a critical shear force of 1.056 pounds, which translates to a vertical force of 1.49 lbs at zero displacement for the shear test. The FE buckling model and eigenvalue problem, discussed above, produced results indicating that a vertical force of 1.19 pounds would be required to induce buckling. As expected, the FE results indicated a lower force because Timoshenko's equation is for a square plate, and the actual specimen is not square, but rather a square with corners cut out, which should reduce the specimens ability to carry shear loads, resulting in a lower actual force.

90

Taking this data back to the model an analysis was run to determine at what force and displacement the out-of-plane deformation first occurs. This was done by reviewing results showing that the deformation occurred before 0.2 inch displacement. The analysis was run to that displacement, with a small initial step size, and reaction forces requested at each step.

The results were reviewed to see at which step the out-of-plane deformation was first visible. The displacement at this step was 0.112 inches, which occurs only six seconds into the minute long straining of the material. The resultant force at this step was looked up, and found to be 1.42 pounds. The step before the displacement was noticed is at 0.08 inch displacement, with a force of 0.72 pounds. So the deformation is first noticed in the model at a step that has a load slightly above the predicted buckling load, which indicates that buckling had just occurred. This means that the out-of-plane deformation that is witnessed during the testing is buckling, not membrane folding.

The same model was run again, with the same initial time step, but a maximum time step of 0.1, which requires that there would be a minimum of 10 data points. The resulting 13 data points were broken into the resultant force and the "z", or out-of-plane, displacement and plotted against the "y" displacement of the specimen in Figure 53. This plot is shown with the "z" displacement on the primary axis and the force on the secondary axis. The horizontal red line indicates a force of 1.19 lbs, which occurs at approximately 0.09 inches of displacement in the "y" direction.
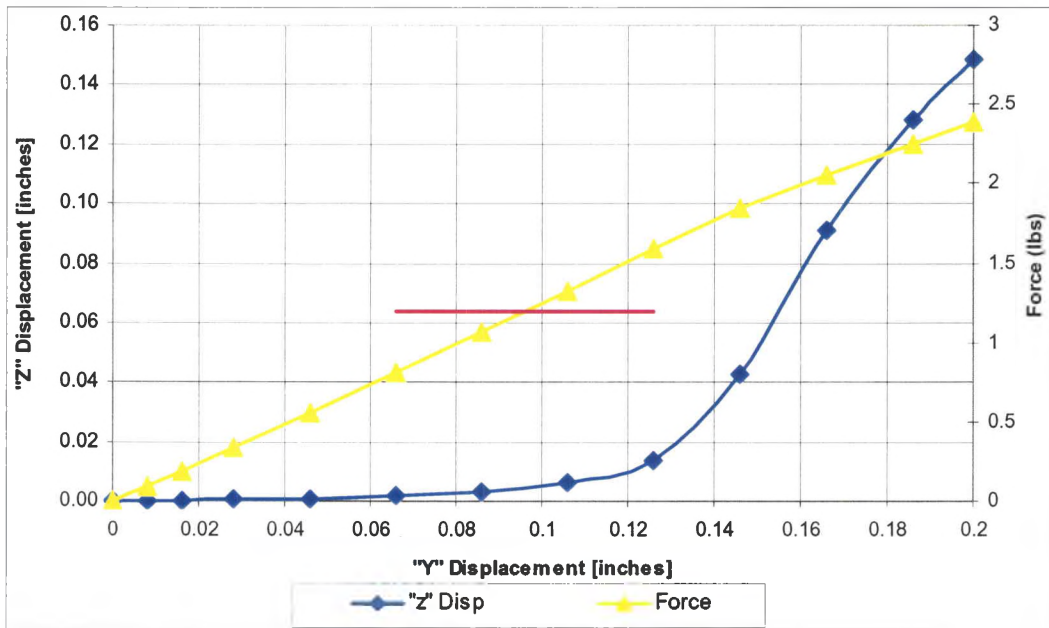
Figure 53: Force and Displacement Data from Model

From the plot it is easily seen that the force increases at a nearly constant rate through the buckle, while the "z" displacement increases significantly after the bucking has occurred. Visually this states that once the SMP buckles, it simply continues to fold in the shape of the first buckling mode as it continues to be compressed in the first mode, and not progress to other eigenvectors. This is believed to be stable buckling – when there is no distinct 'snap through' of the material. Figure 54 shows a cooled specimen after being tested to the full displacement. When compared to Figure 52 (or the top of Figure 55), one can see that the first mode shape has been compressed, with larger out-of-plane displacements resulting and that the specimen has not snapped to the next mode shape with the continued application of force, which would be characteristic of unstable buckling. The first and second mode shapes, or eignvectors, are compared in Figure 55.

92
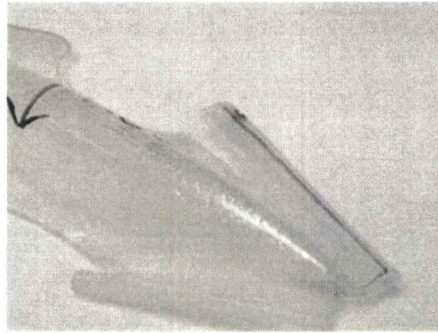
Figure 54: Folded Specimen
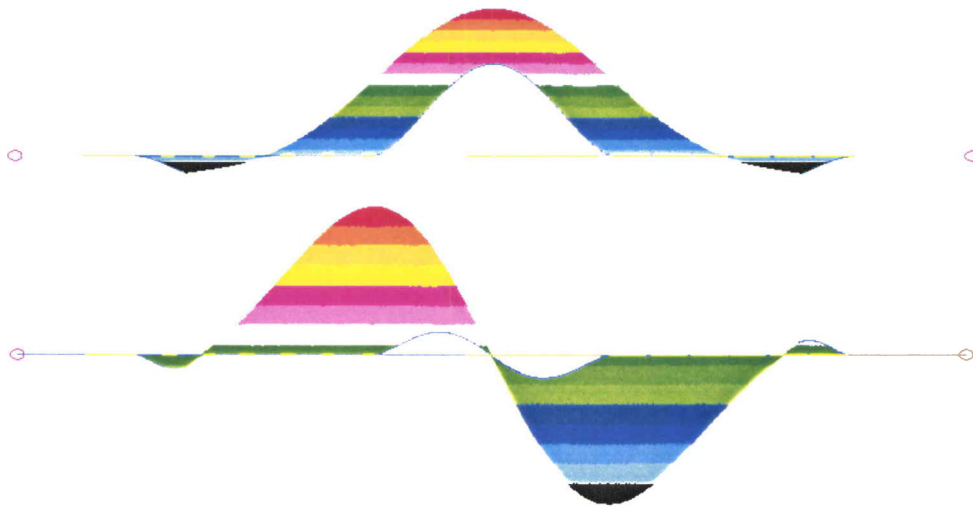
Figure 55: First (top) and Second (bottom) Mode Shapes Seen Together

Stable buckling is so named because once the system has deformed it can still be in equilibrium in its deformed position; it is just not the exact same shape as before the buckling occurred. Essentially the equilibrium equation is continuous, and it's first derivative is positive, over an appropriately large enough range when plotted on a force-displacement graph. Unstable buckling would occur if there were multiple stable buckling curves for the equilibrium equation, and at least one unstable curve (when the derivative is negative) that intersects multiple stable curves at their critical force. When the load along one of the stable curves reaches its critical value, the structure will buckle from one stable mode to another nearly instantly, and with a noticeable change in force.

Since, for the case presented here, there is no distinct change in slope of the force, and the buckling deformation appears smooth this cannot be unstable buckling [Hjelmstad, 1997].

5.3 Chapter Summary

This chapter established that it is possible to model shape memory polymers with a finite element model, but only for small strain situations where the material strain mechanism is nearly elastic. Under high strains the strain mechanism is more complicated, and is therefore harder to model. The modeling was able to verify that the out-of-plane deformation noted in the testing is in fact buckling. It was possible to verify the fidelity of the model through comparison of shear stress-shear strain curves, and by noting at what applied force and displacement the buckling occurred at during the testing.

CHAPTER VI

CONCLUSIONS

This final chapter provides a brief summary of the thesis and the conclusions that were obtained from the research. This includes potential future work that can be used to expand on the data presented here, and items to pursue to more fully model the phenomena occurring in the SMPs during these tests.

6.1: Thesis Summary

This thesis began with an introduction to morphing aircraft and their inherent advantages over current designs, including some current aircraft that exhibit a shape change on a very small scale that improves their efficiency, speed, and range. A review of some shape control concepts illustrated the types of shape control required. These program descriptions focused specifically on their use of different technologies to provide the flexible skin needed to achieve the project goals. The oldest program, the F-111 Mission Adaptive Wing, used new technology of the time, with engineered fiberglass skins to flex where needed. The two newer programs used elastomers attached nearly continuously along actuators producing small deformations (Smart Wing) and a reinforced elastomer actuated by a shape memory alloy (SAMPSON.) Key technologies to enable these morphing aircraft in the near future include distributed, high power

density actuators, mechanized structures, and flexible skins. To allow for flexible skins there are many technologies available, including a scaled skin (i.e. like a fish), sliding skin panels, or making the skin out of elastomers or shape memory polymers, though recent trends have been leaning away from scales and sliding panels due to their added complication and hardware requirements.

The procedures used during the experimental process were described so they could be repeated in the future, should one have access to the same equipment and materials. This includes the environmental box that was designed to bring the test specimen up to temperature and maintain the desired temperature throughout the test. Also, a unique test fixture was needed to induce pure shear, from a tensile machine, over a large range of shear strain. Chapter four provided the results of the experiments, and a description of the material reactions to the experiments, ending with a brief list of material properties.

Finally, a description of the modeling is provided. This includes the geometry, elements, mesh, boundary conditions and constants for the initial models, and the variations in mesh refinement, and modulus distribution with the use of temperature dependent properties, that followed with each improvement to the model.

This research produced a number of 'firsts' in SMP testing. A shear fixture was designed and manufactured to test shear in a tensile machine over extremely large deformations, with shear strain up to and over 150%. A CRG employee who visited to

watch some of the testing indicated that it was the first time anyone at the company had seen such a large amount of SMP strained so much (a 5" x 5" specimen strained 60%,) all other tests witnessed by CRG employees were conducted on much smaller size specimens (1" x 0.5".)

The tensile tests were the first known testing of this SMP to specifically determine the modulus at temperature. Previous testing was done with a Dynamic Mechanical Analysis machine with one specimen tested continually over a range of temperatures.

The procedures used were often modifications from some of the references, helping push towards a core standard for testing shape memory polymers, which is crucial to expanding use of the material and for properly classifying different formulas.

Finally, this research provided a solid base for further SMP testing and expanding capabilities for modeling SMP behavior.

6.2: Conclusions & Recommendations

Based on the research conducted and the results obtained, shape memory polymers remain a strong candidate material for skins on a morphing aircraft. There are still some hurdles to clear with this young technology before it will be able to be used for a full scale, large deformation aircraft, but many of the needed advancements are already being researched.

To assist in the carrying of aerodynamic loads when above the T_g without deforming there should be some form of reinforcement added to the material. In addition to allowing higher pressures, this could have the added benefit of hindering the buckling that was witnessed during testing. Additionally, prestrain should continue to be investigated, including bi-axial prestrain. It is now known that it has an effect on the buckling, but complete control of the buckling was not realized during this research, though it appears to be possible. Finally, by advancing light activated SMPs and moving away from thermally activated SMPs any effects of thermal expansion will be negated.

As was noted earlier the shear fixture increased the stress on the material at the edge of the fixture. Creating a new design that does not do this would improve the experiment by allowing a greater range of tests to be performed without premature material failure. Also, with a larger supply of material more tests could be performed. This is especially needed for prestrained specimens and for the tensile tests, as these two tests lead to a better understanding of minimizing the buckling that occurs and providing a more complete understanding of the strain mechanism seen in the material.

The analytical solution, while proven to have high fidelity at low strains, requires more information from testing in order to provide accurate results at higher strains. Once the strain mechanism is fully understood constants can be calculated to input into the model to produce better results at high strains, and thus fully model the SMP during the shear test.

APPENDIX A

Geometric Relations Used to Calculate Shear Stress
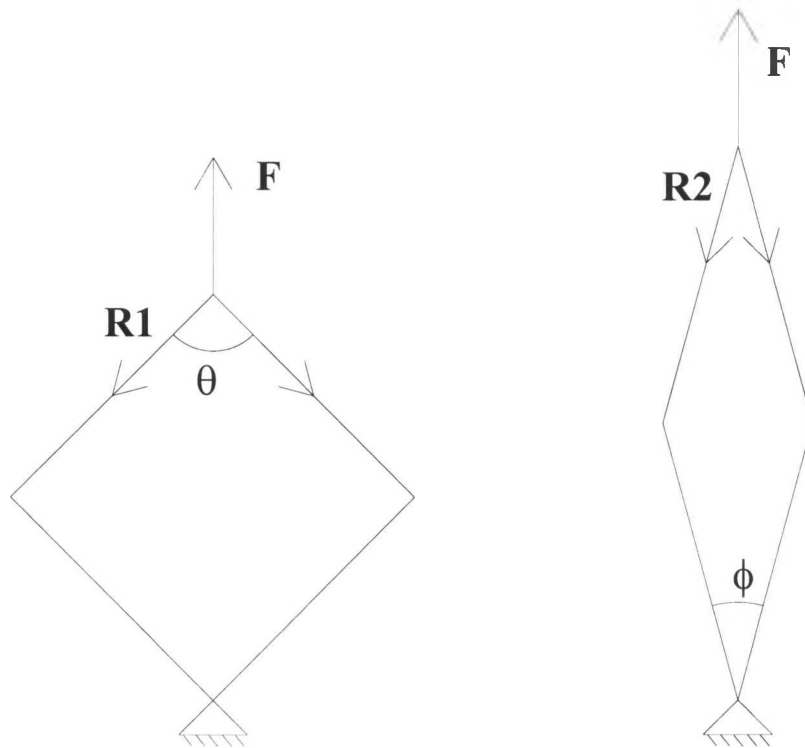
Figure 56: Reaction Forces & Geometry

In Figure 56 above, with equivalent forces acting on the two different geometries the vertical components of each reaction, $R1y$ and $R2y$, must be the same, ½ F.

$$R1 * \cos\theta = 1/2\,F = R1y$$
$$R2 * \cos\phi = 1/2\,F = R2y$$

A1

With differing angles ϕ and θ, the resultants will be different, and can be found by rearranging equations A1 and solving for $R1y$ and $R2y$.

$$R1 = \frac{1/2\,F}{\cos\theta}$$

$$R2 = \frac{1/2\,F}{\cos\phi}$$

A2

These reaction forces are acting down each side of the fixture and are transferred to the specimen as shear forces. To get the shear stress one must divide by the area the force is acting on. Since equations A2 are of the same form, removing characters that identify with a specific geometry will give the governing equation for the shear forces as a function of the applied force and the smaller interior angle. The final equation to obtain the shear stress for the specimens is shown as Equation A3.

$$\tau = \frac{R}{Lt} = \frac{1/2\,F}{Lt\cos\theta} = \frac{F}{0.327\cos\theta}$$

A3

The interior angles of the specimen can be found as a function of the displacement using the relationships in Equation A4, known as the law of sine's.

Using the notation from Figure 57,

$$\frac{A}{\sin a} = \frac{B}{\sin b} = \frac{C}{\sin c}$$

A4
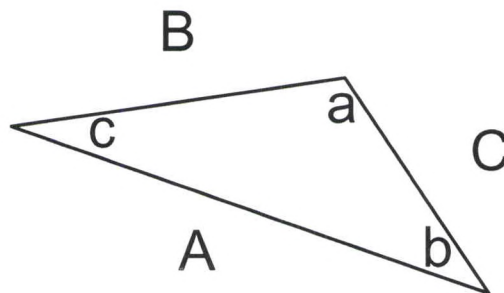
Figure 57: Triangle Side and Angle Naming for Law of Sine's

The specimen can be divided into four right triangles at any point during the test by drawing a line between the two sets of opposing corners, with all four right angles occurring at the center, and the hypotenuse of each triangle equal to four inches. Using the top right of the four triangles as an example, with the notation below in Figure 58:

$$\frac{H}{\sin h} = 4 = \frac{X}{\sin x} = \frac{Y}{\sin y}$$

A5
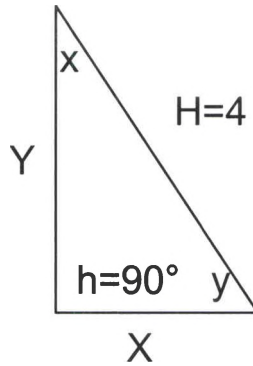
Figure 58: Law of Sine's Definitions for Test Specimen

The value for Y is simply the one half of the initial height of the specimen (corner to corner), plus the displacement, stated mathematically in A6. Where l_0 is the initial height ($sqrt(32)$ = 5.65) and Δl is the displacement.

$$Y = \frac{l_0 + \Delta l}{2}$$
A6

With two of the interior angles known, it is simple to find the third. Combining all of the above, the interior angle θ is found from Equation A7.

$$\theta = 2x = 2(180 - 90 - y) = 2\left(90 - \sin^{-1}\left(\frac{Y}{4}\right)\right)$$

$$= 2\left(90 - \sin^{-1}\left(\frac{\frac{l_0 + \Delta l}{2}}{4}\right)\right) = 2\left(90 - \sin^{-1}\left(\frac{l_0 + \Delta l}{8}\right)\right)$$
A7

Now the shear stress can be calculated as a function of the applied force and the displacement of the specimen.

APPENDIX B

Shear Data

     This appendix contains the plots of each individual shear test, with notable events pointed out under the respective plot.
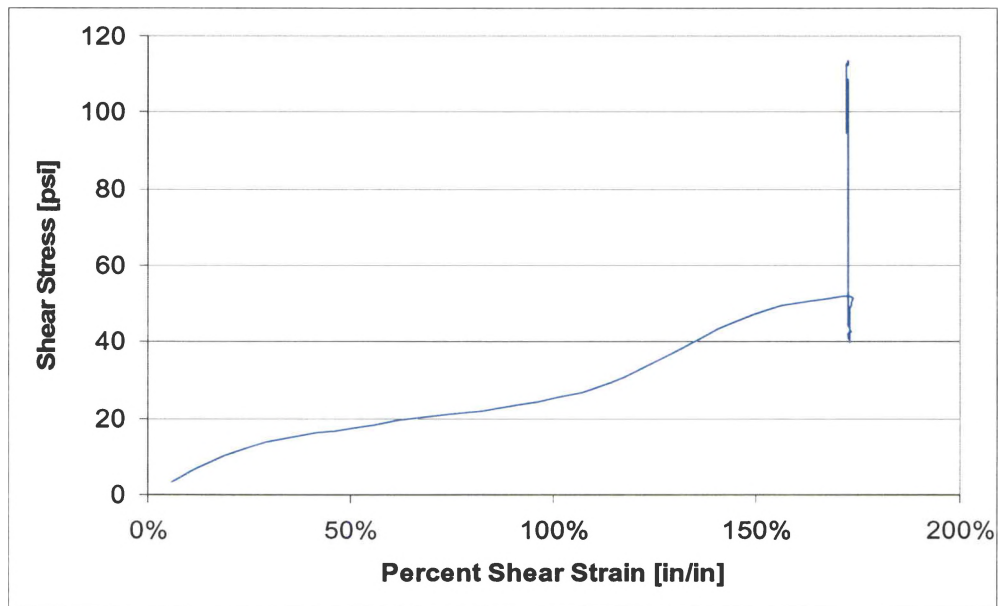
Figure 59: Sample #1 Test1
Note the increase in shear stress (applied force required to hold a position) when the specimen was cooled and held in a particular shape, at the maximum shear strain.
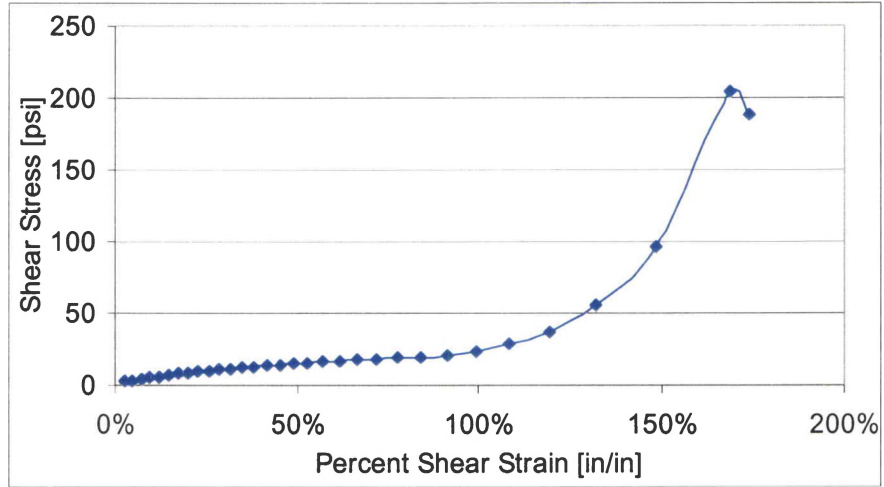
Figure 60: Sample #1 Test2

Material is pinched by the fixture at strains above 100% shear strain, this can be more readily seen by comparing to the plot for Sample #1Test4.
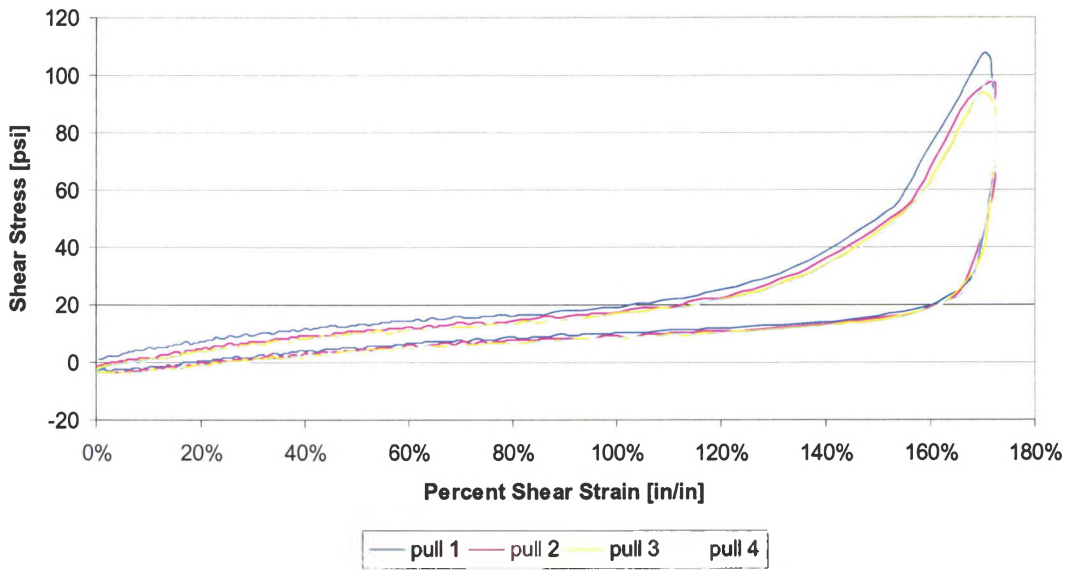
Figure 61: Sample #1 Test3
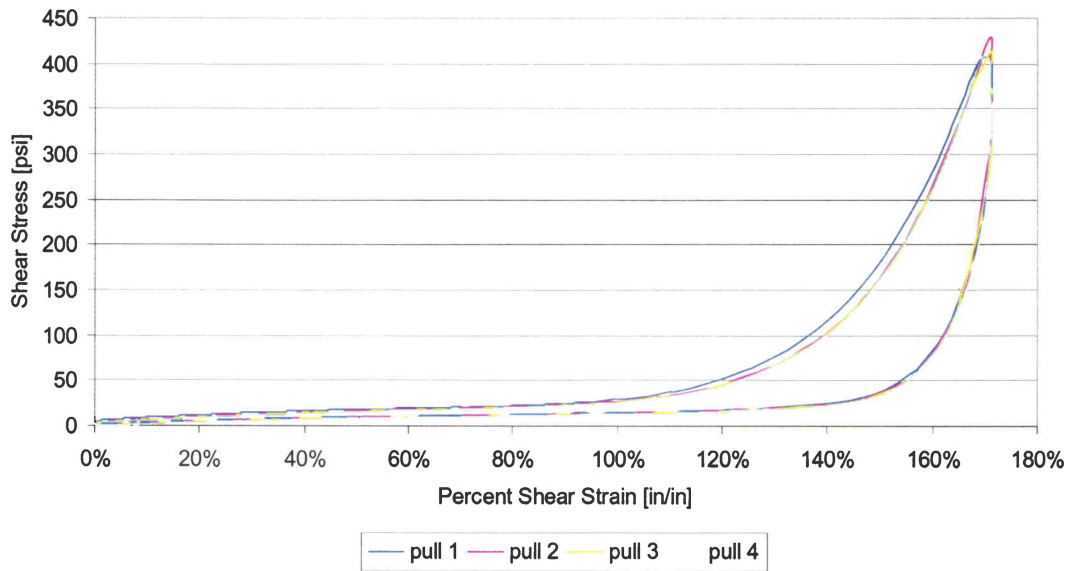
Figure 62: Sample #1 Test4

Note a significantly larger shear stress above 100% shear strain, when compared to most other plots. This is from the material getting pinched by the fixture.
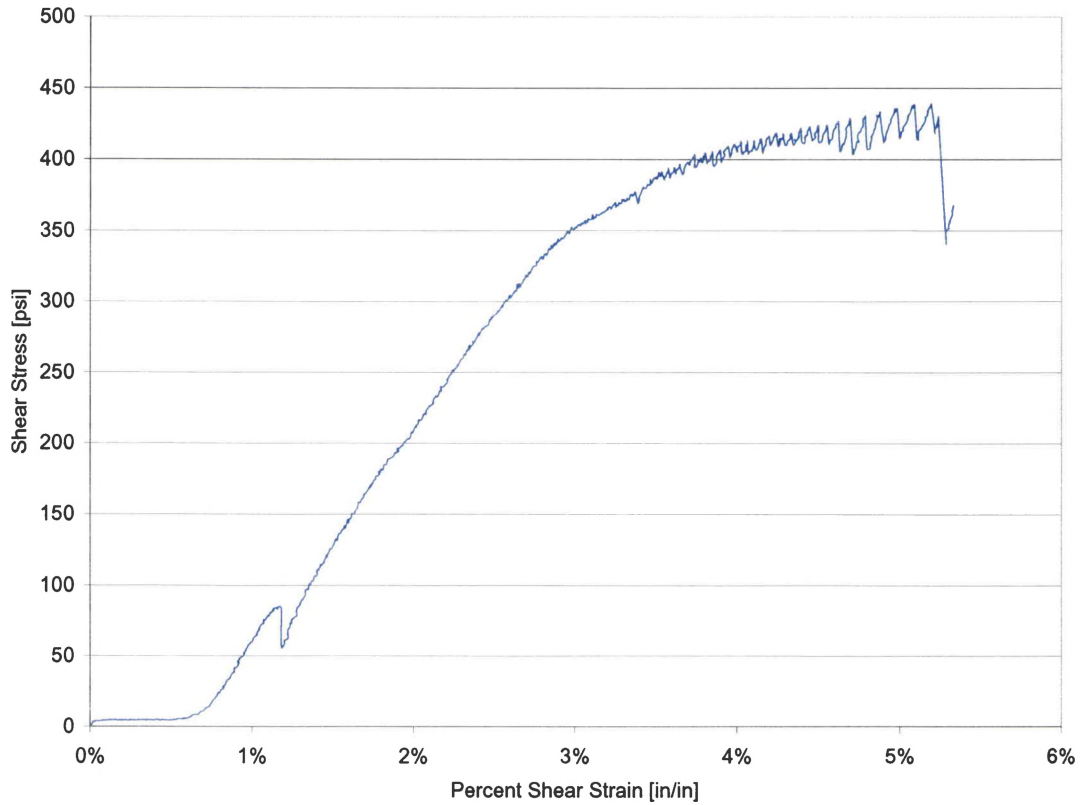
Figure 63: Sample #1 Cold Test

Note the change in shear stress just above 1% shear strain where specimen slipped.

104
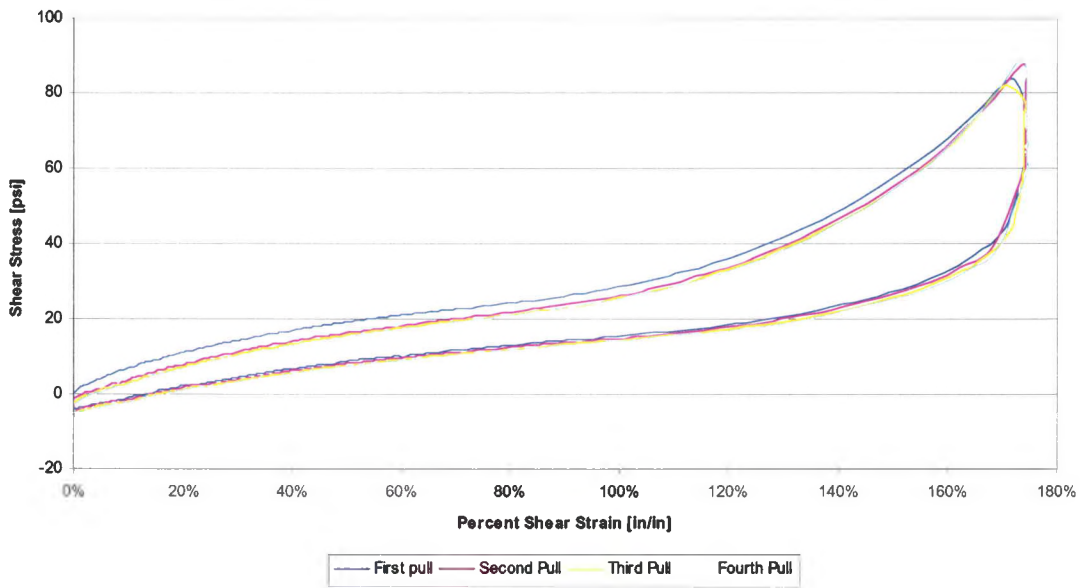
Figure 64: Sample #2 Test2
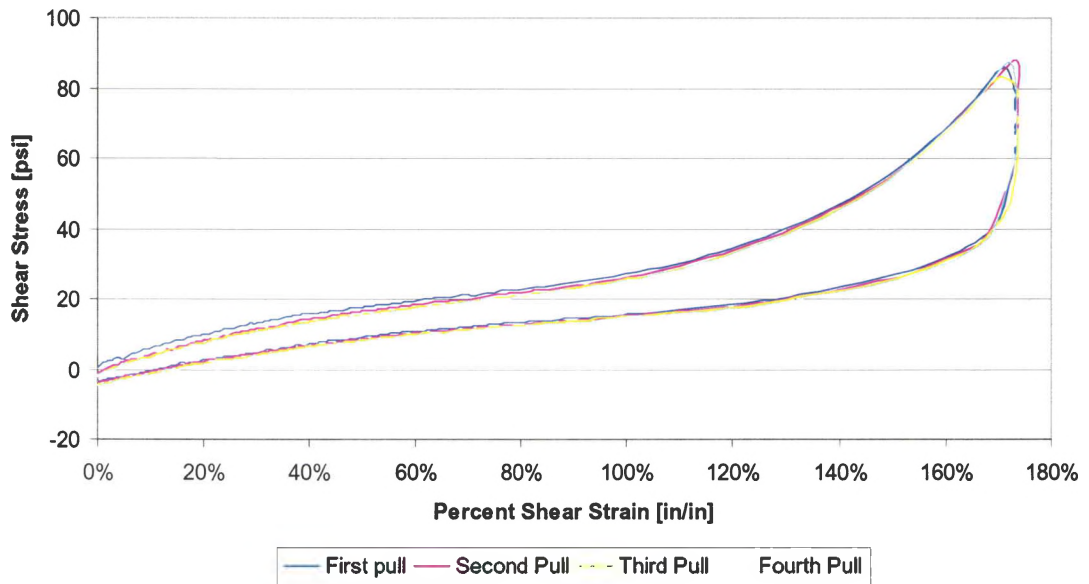
Figure 65: Sample #2 Test3
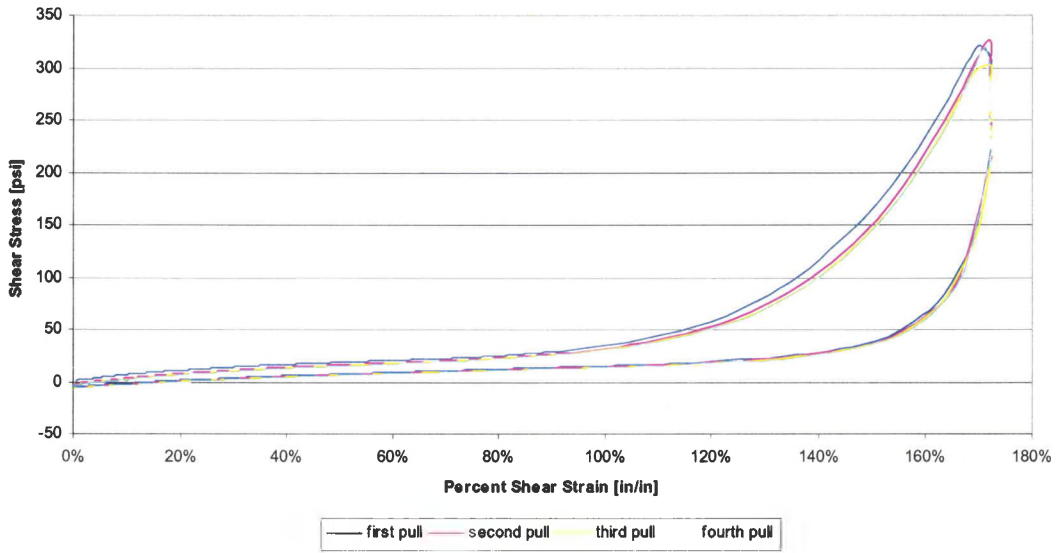
Figure 66: Sample #2 Test4
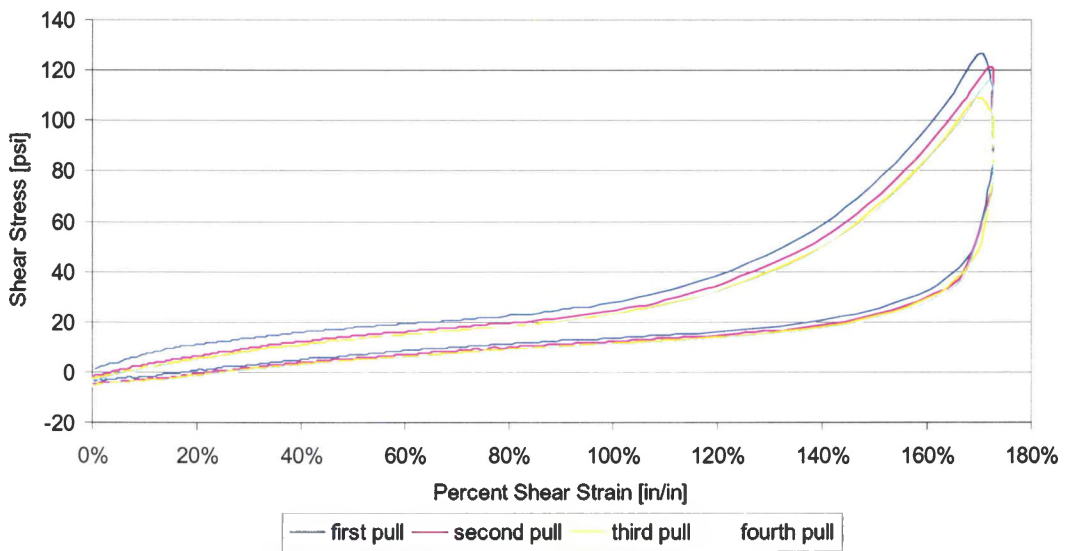
Figure 67: Sample #2 Test5

Specimen pinched by fixture above 100% shear strain.
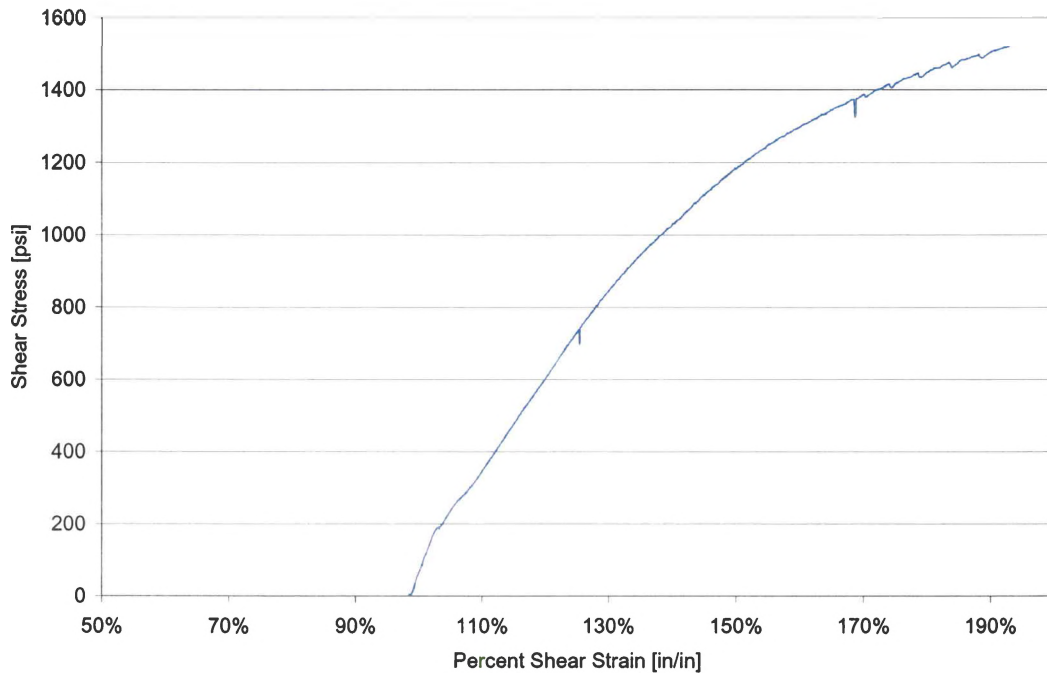
Figure 68: Sample #2 Cold Tension

While deformed the cold SMP could withstand maximum load and deformation allowed by the test equipment without failure.
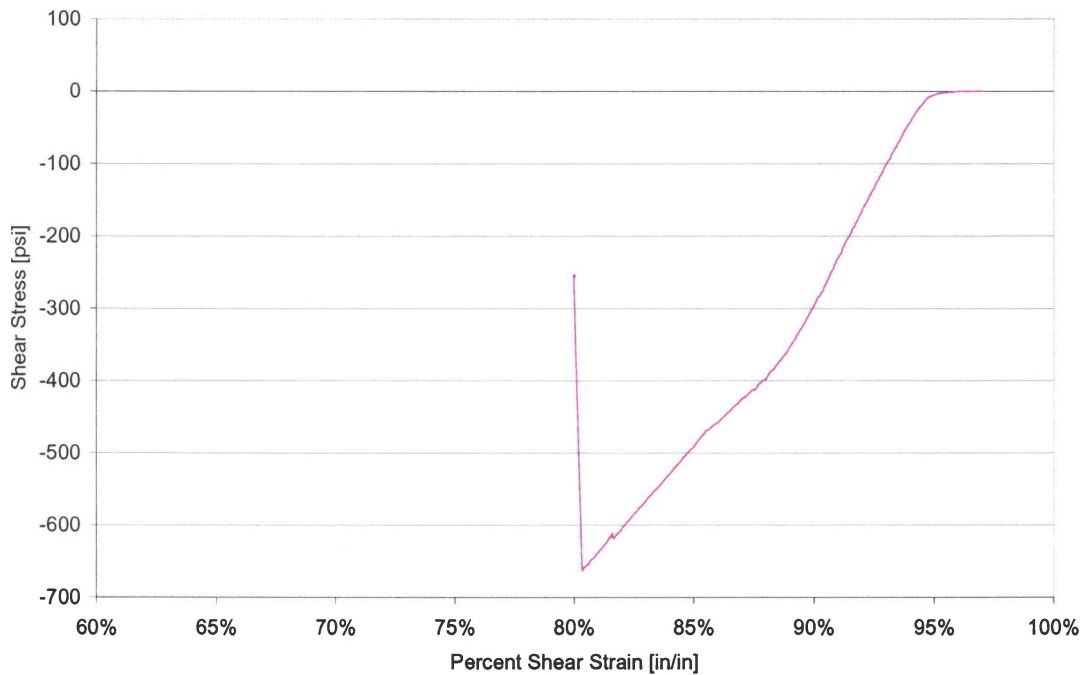
Figure 69: Sample #2 Cold Compression

This is a plot of the cold compression fracture of a deformed specimen. Fracture occurred just above 80% shear strain.
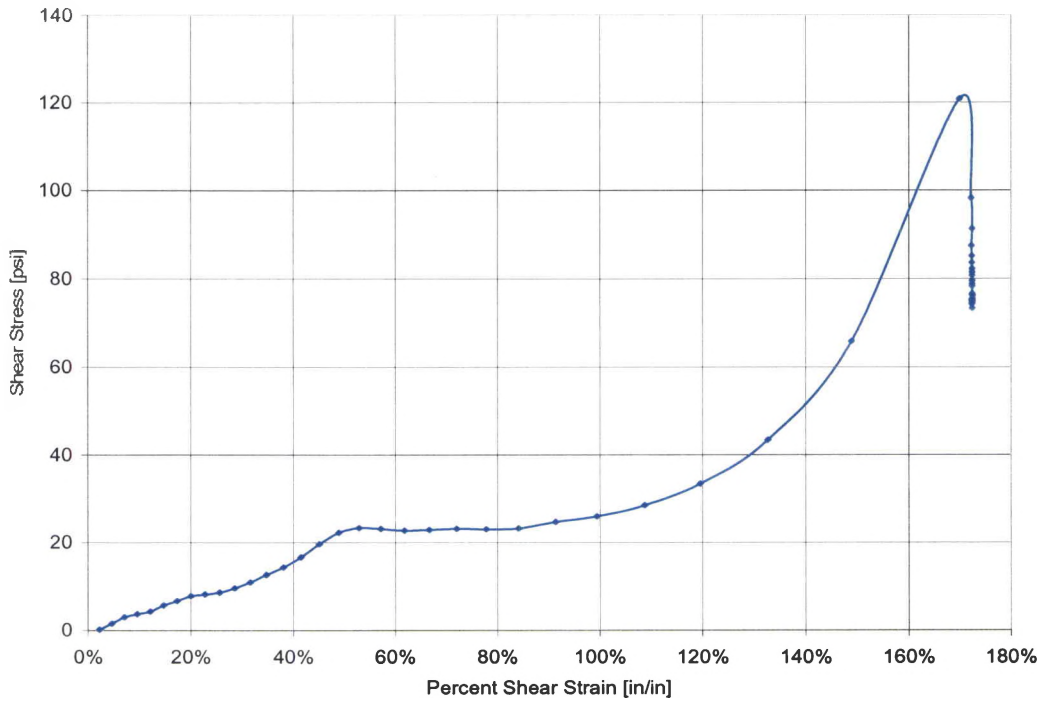
Figure 70: Sample #3 Test1

Knee in data at 50% shear strain indicates where buckling began
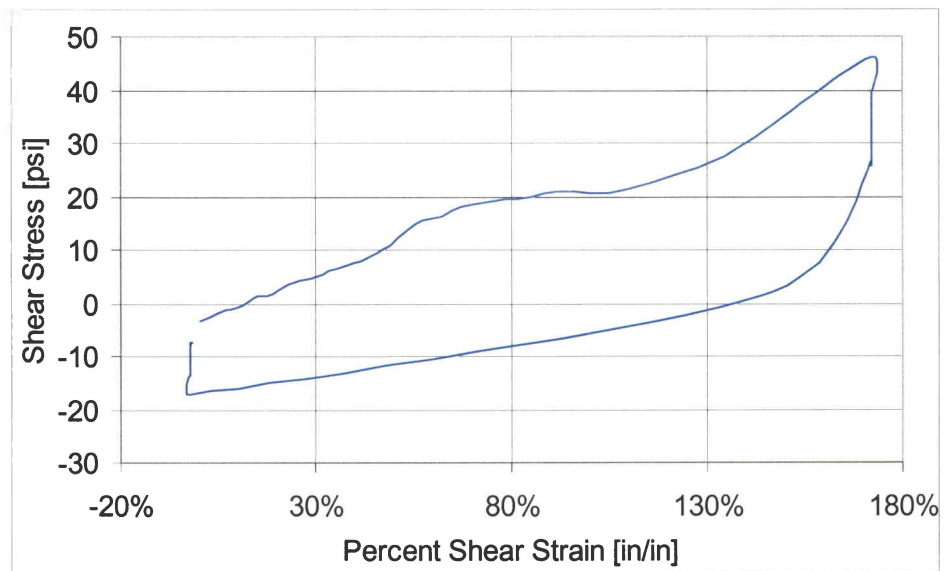
Figure 71: Sample #4 Test1

108
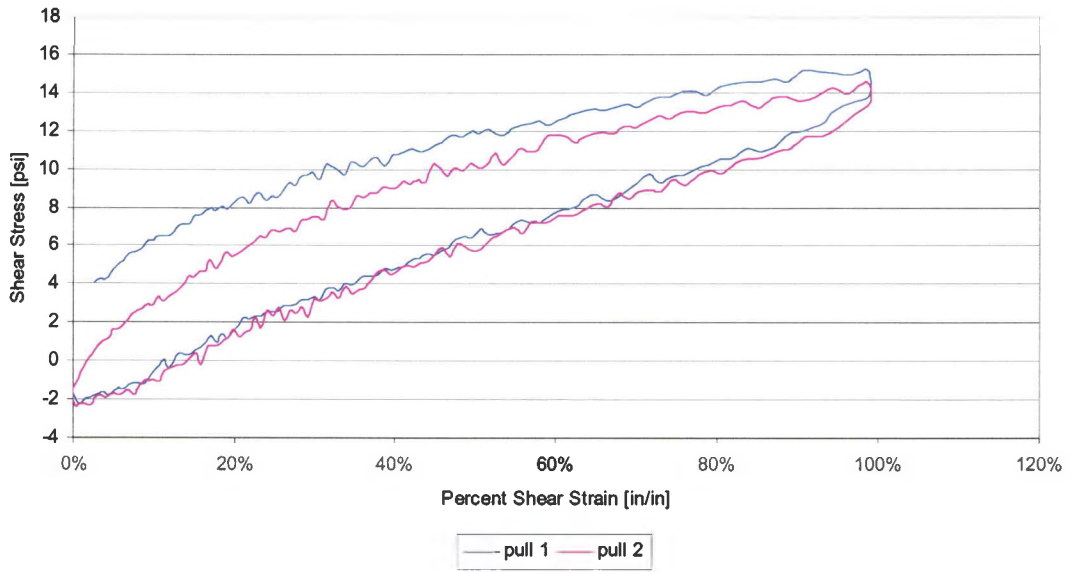
Figure 72: Sample #5 Test1
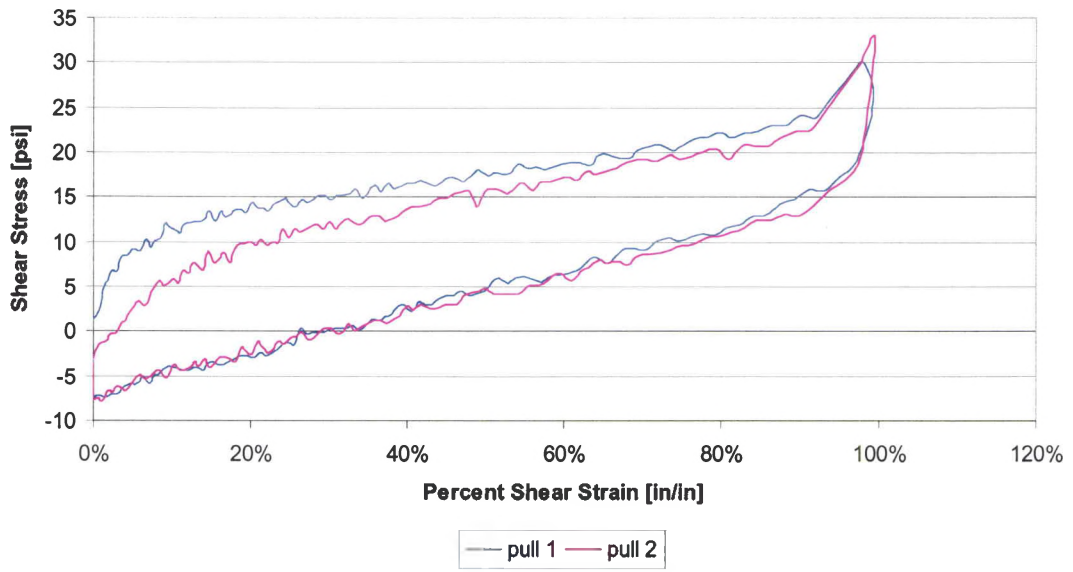
Figure 73: Sample #5 Test2
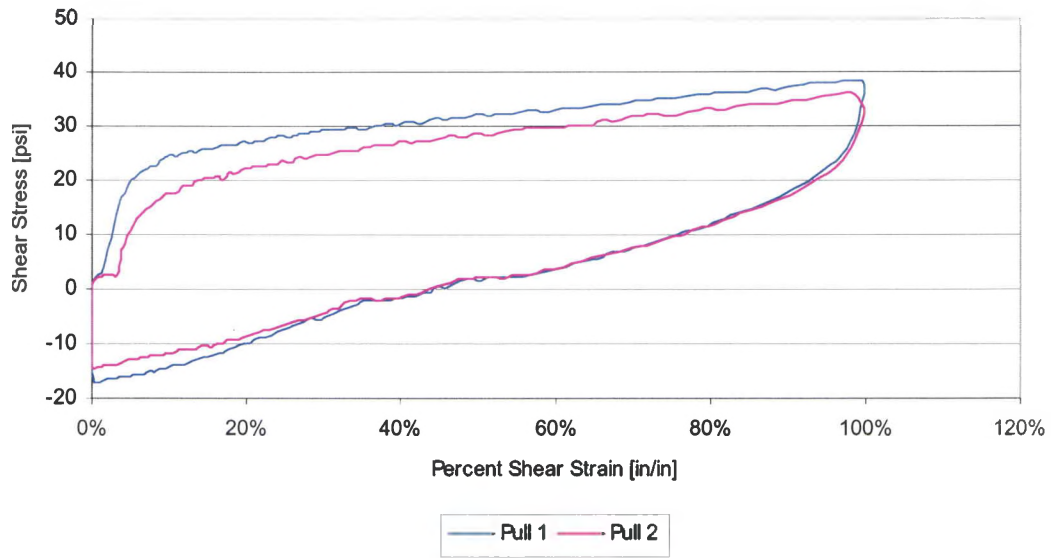
Figure 74: Sample #5 Test3
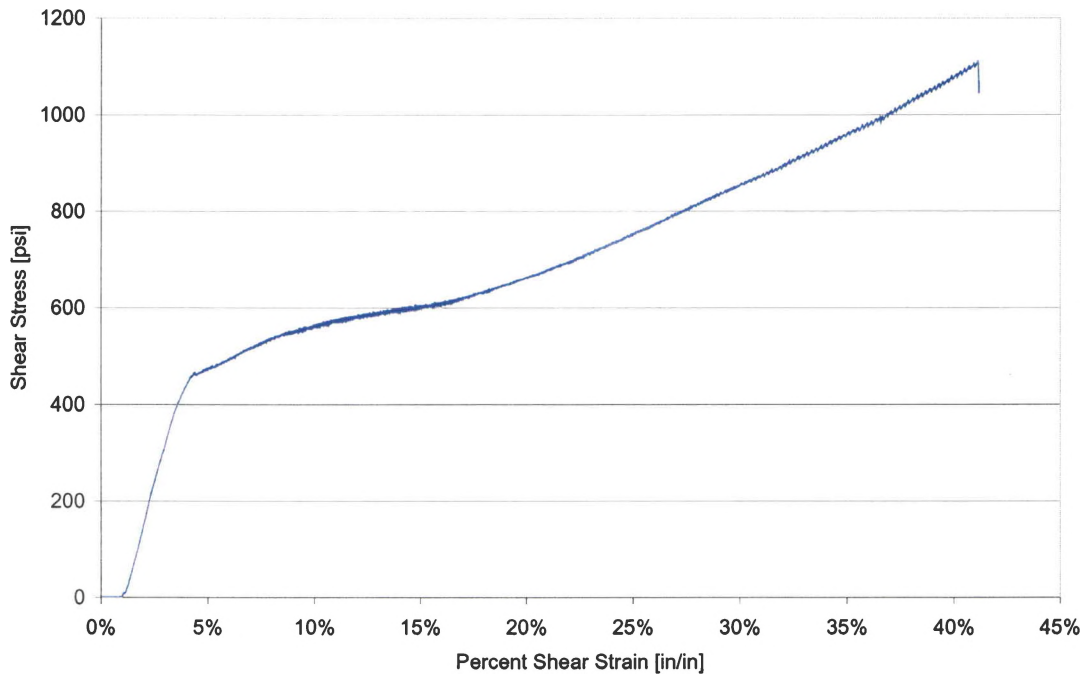
Figure 75: Sample #5 Test4

Cold deformation of the material reached the preset deformation limit of 1.0". The material shows yielding, but no fracture, in cold shear tensile tests.
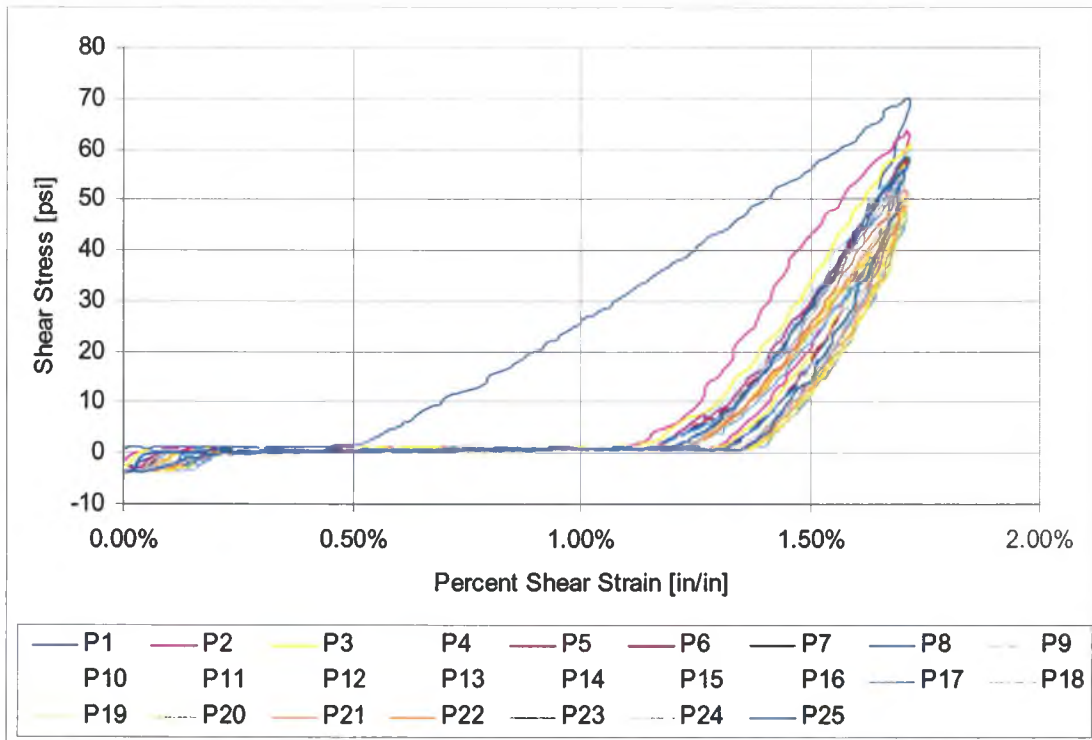
Figure 76: Sample #5 Test5
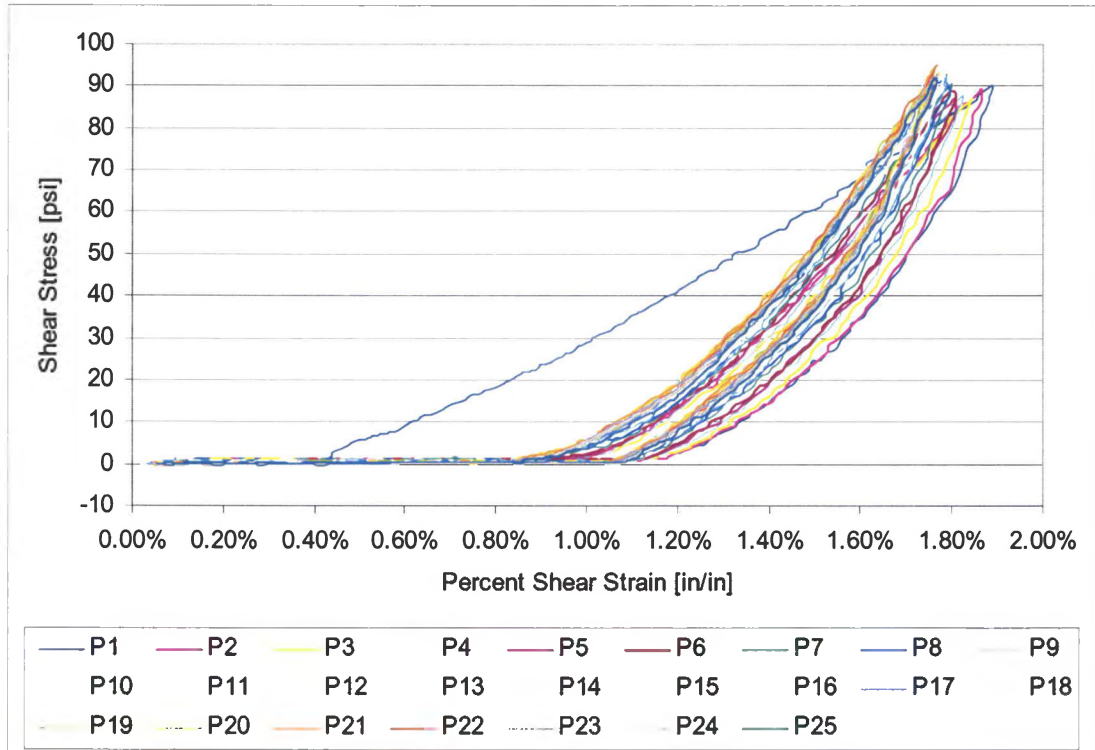
Figure 77: Sample #5 Test6

111
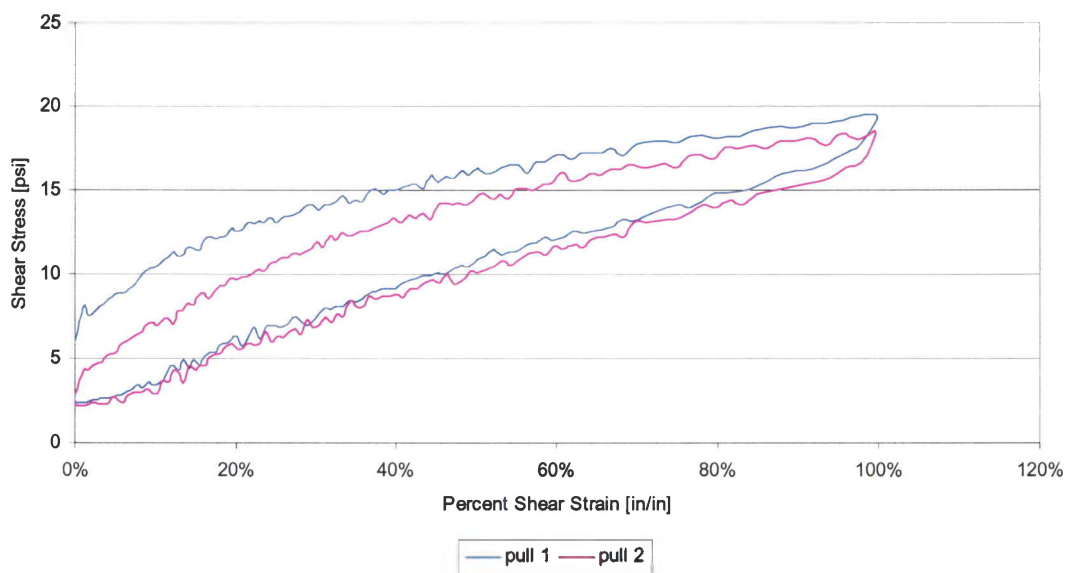
Figure 78: Sample #6 Test1

Figure 79: Sample #6 Test2

112
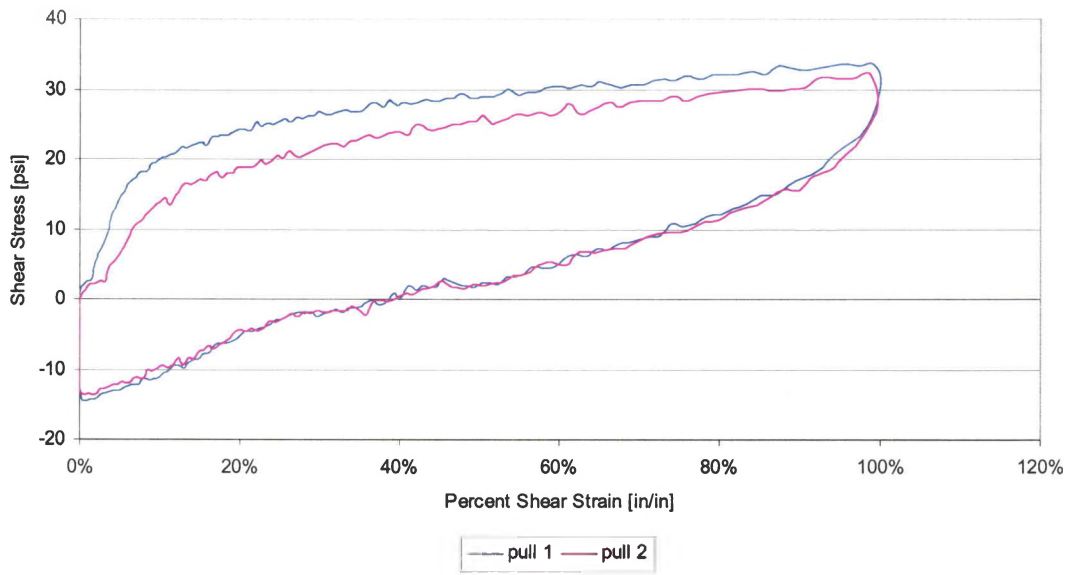
Figure 80: Sample #6 Test3
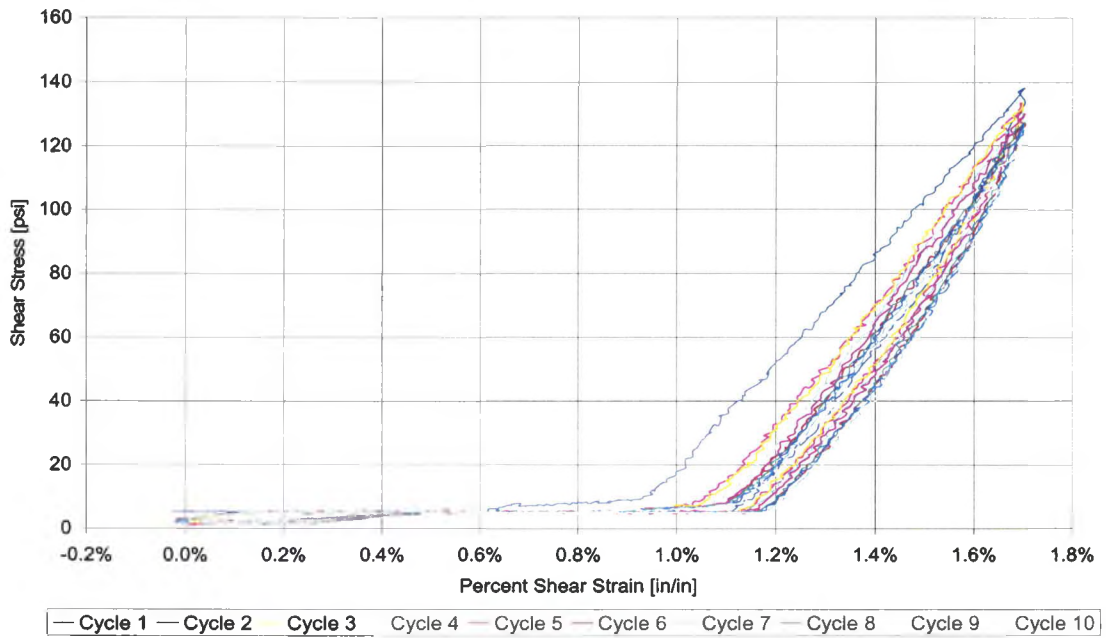
Figure 81: Sample #7 Test1

Cold cycling of undeformed specimen
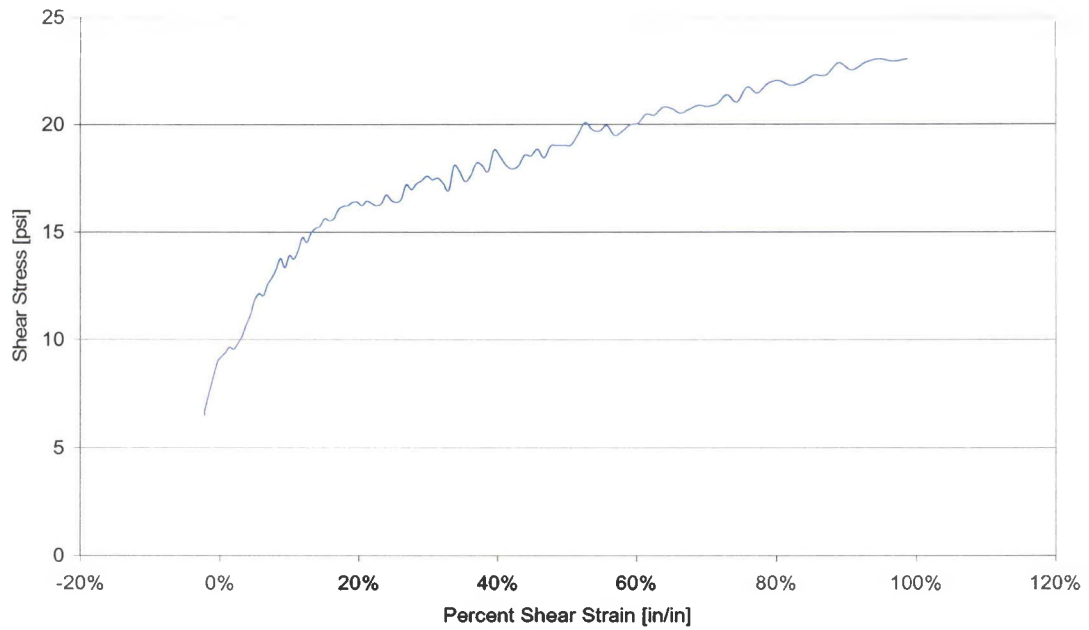
Figure 82: Sample #7 Test2

Heated deformation
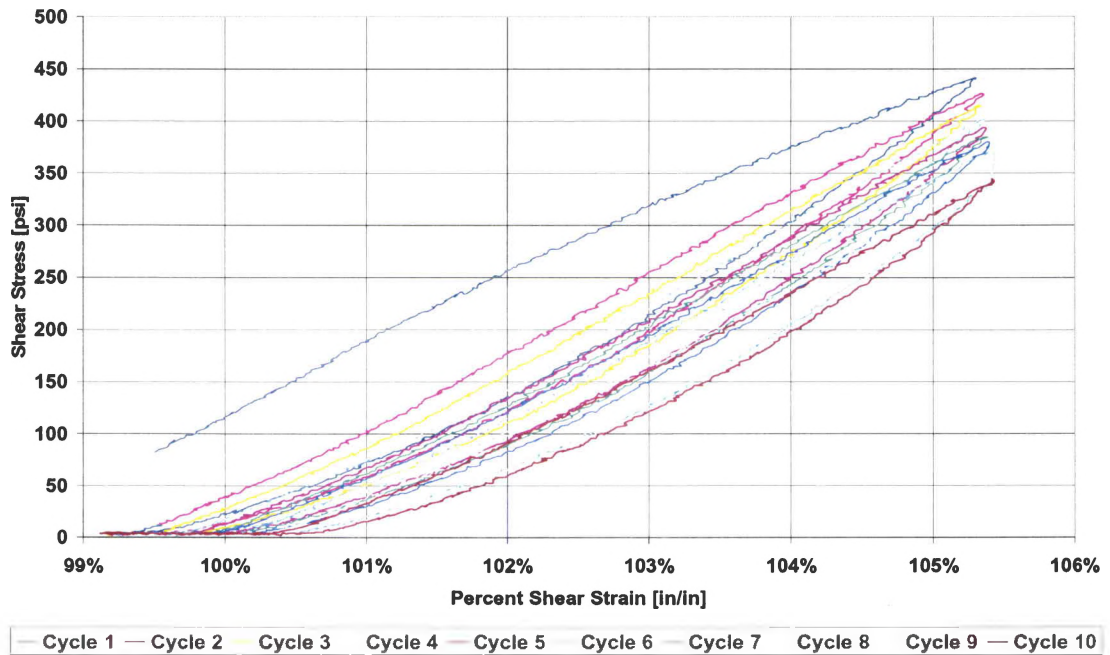
Figure 83: Sample #7 Test3

Cold cycling of deformed specimen

114
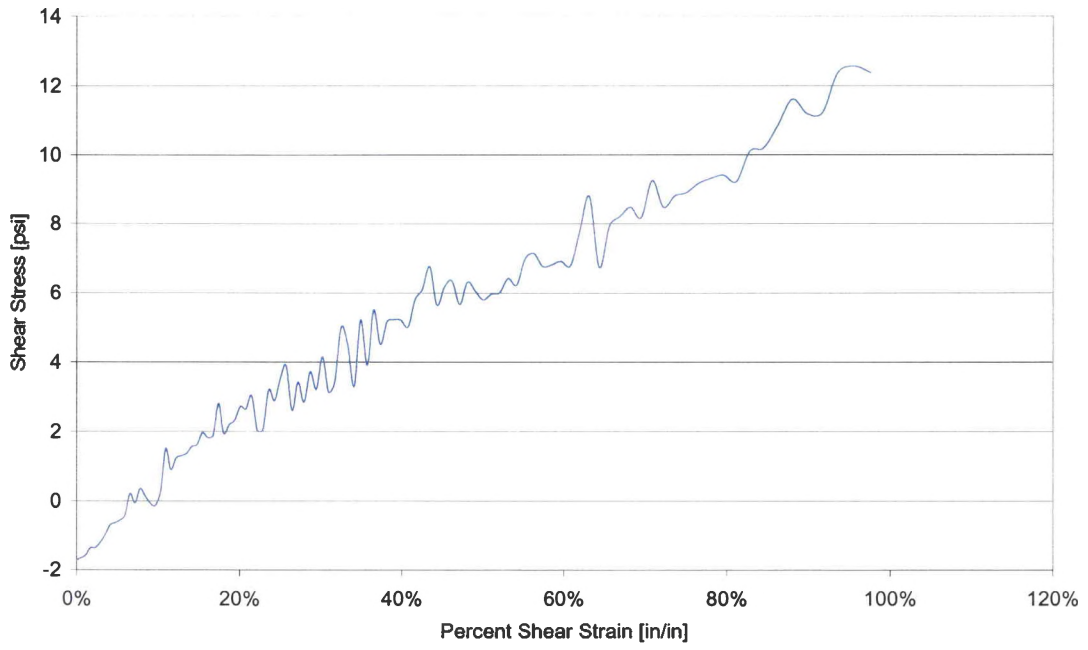
Figure 84: Sample #7 Test4

Heated undeforming to return to initial shape
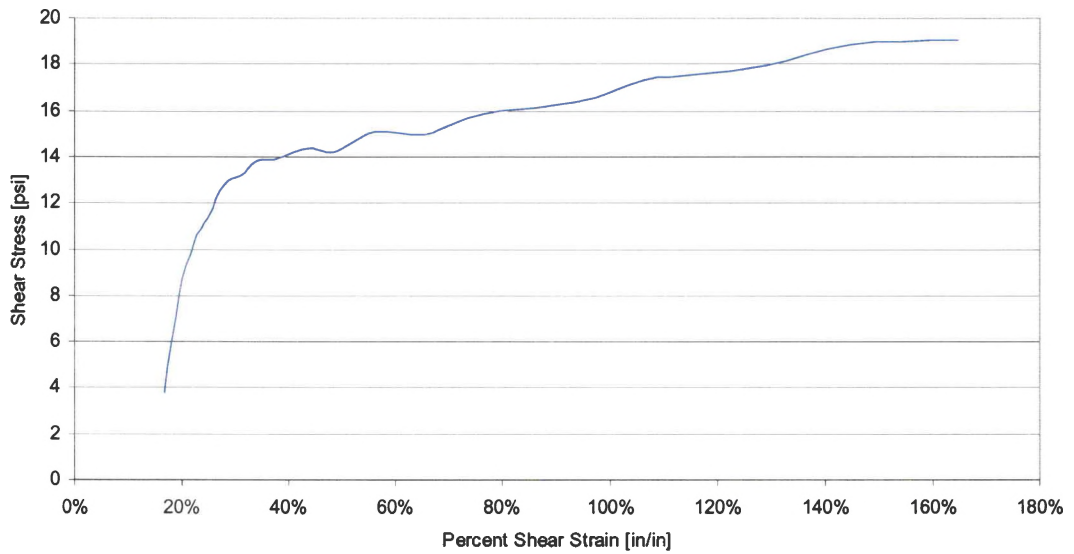
Figure 85: Sample #8 Test1
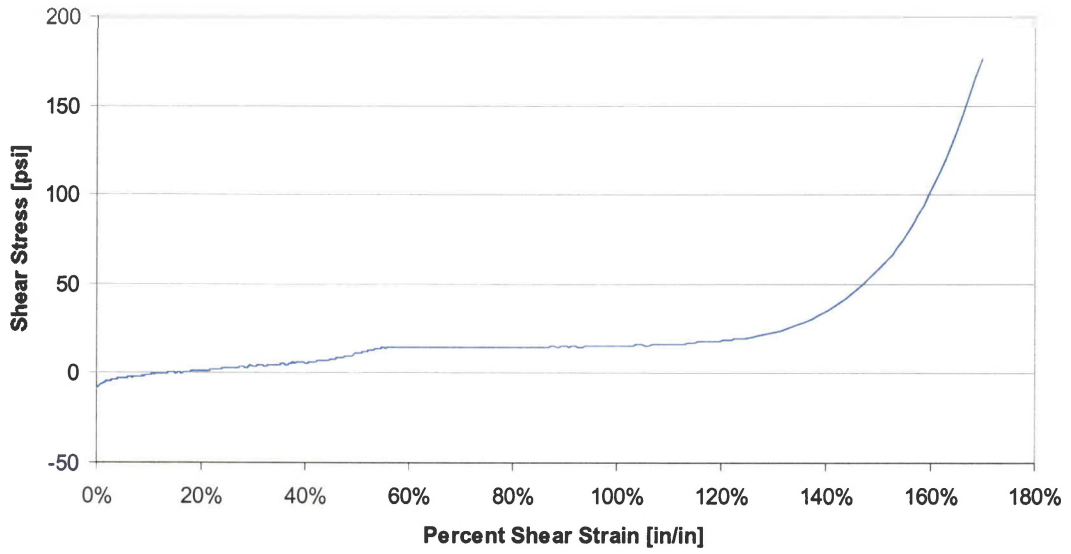
Figure 86: Sample #10 Test1
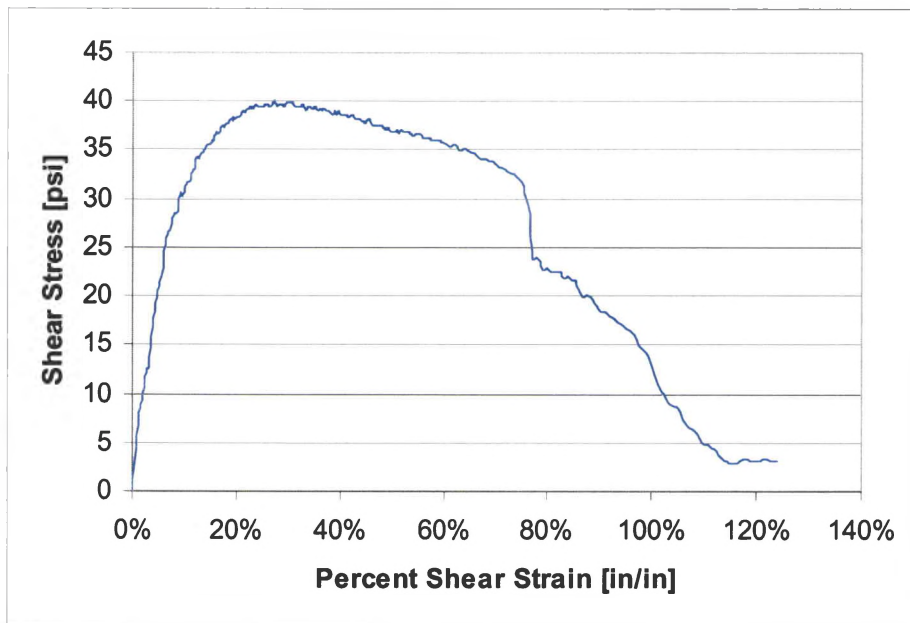
Figure 87: Sample #12 Test1

Specimen tore in fixture

116

APPENDIX C

Prestrain Data

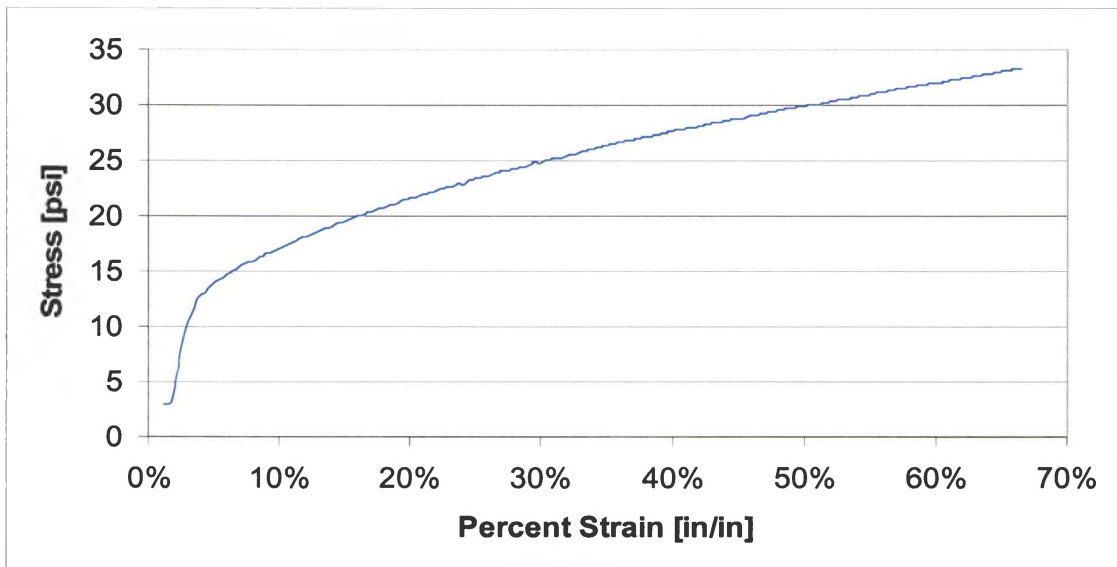This appendix contains the plots of each individual prestraining that was done
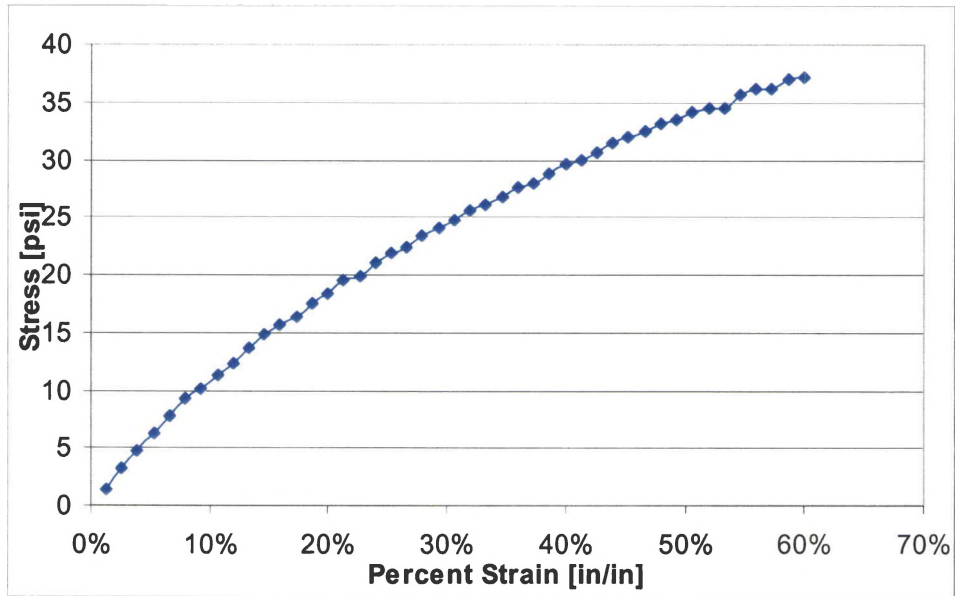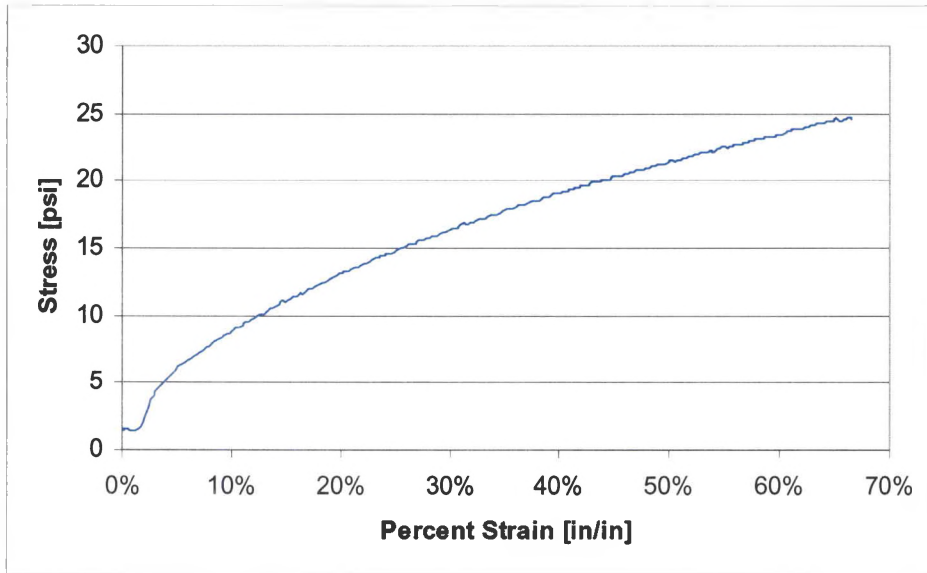

Figure 88: Sample #4

Figure 89: Sample #9
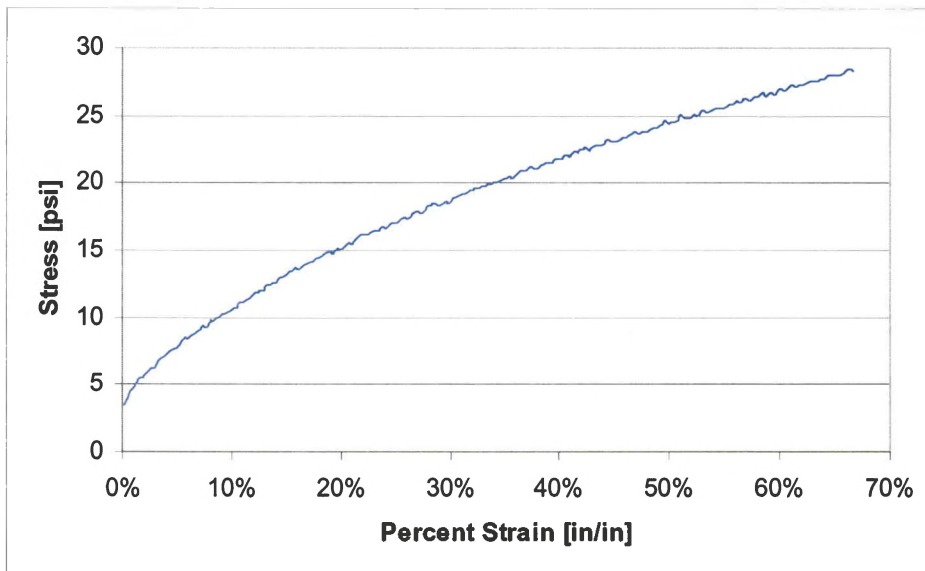
Figure 90: Sample #10

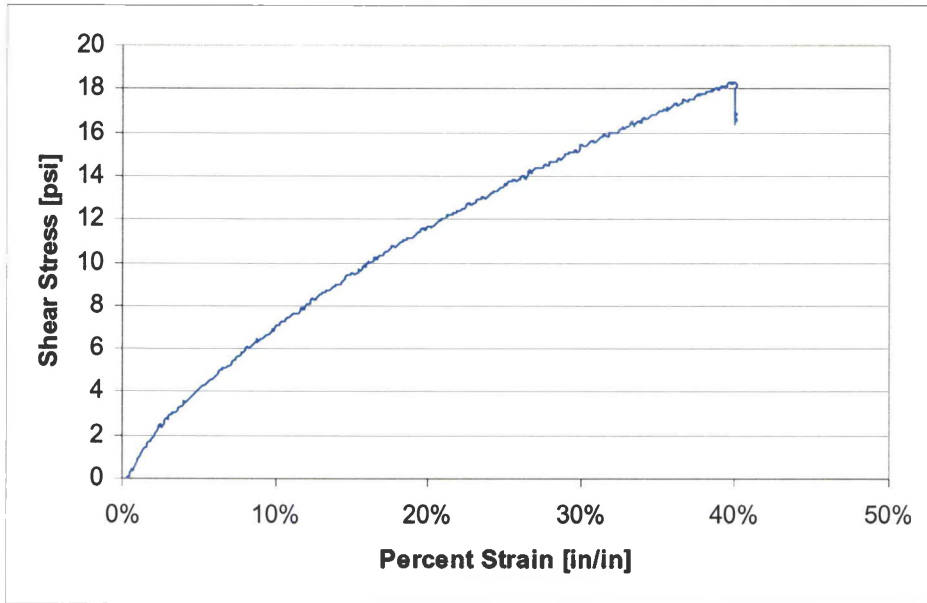**Figure 91: Sample #11**

118

Figure 92: Sample #12

APPENDIX D

Tensile Data

This appendix contains the plots of each individual tensile that was done
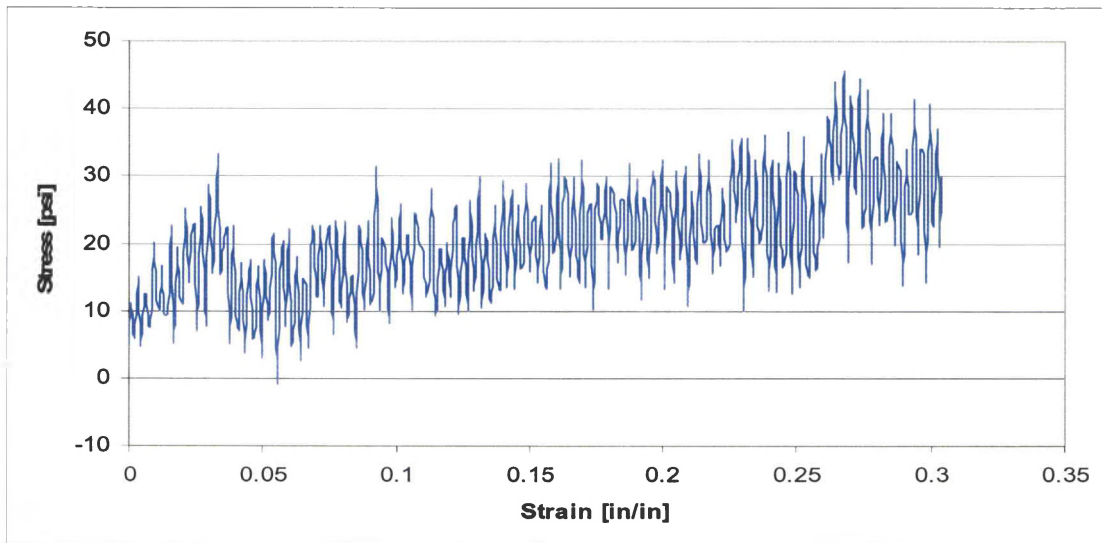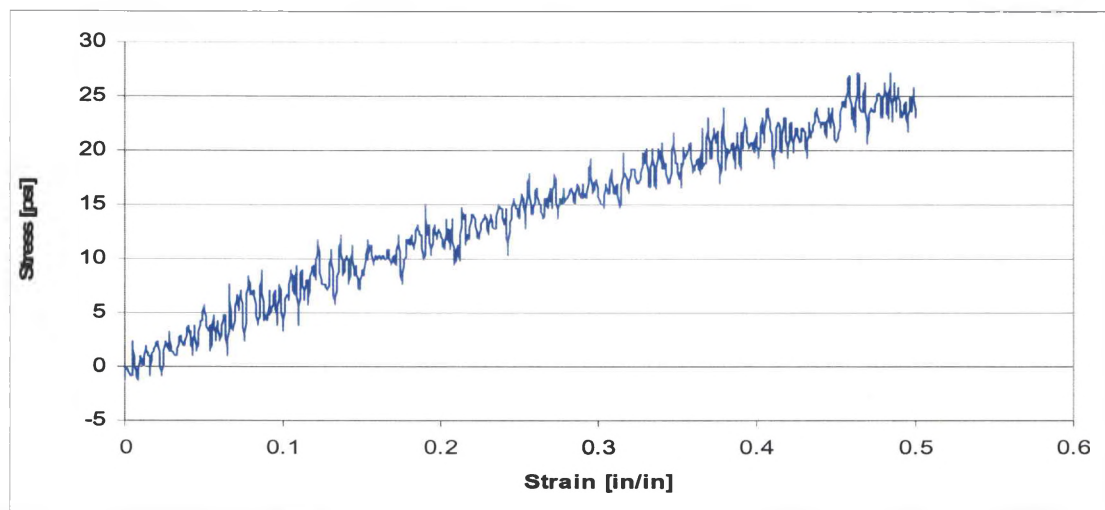

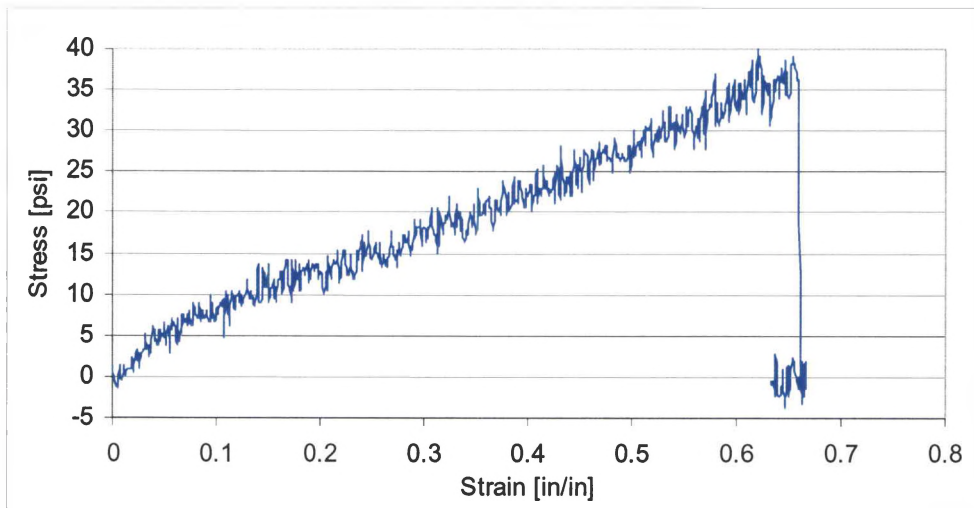**Figure 93: Tensile Specimen #1**

Figure 94: Tensile Specimen #2
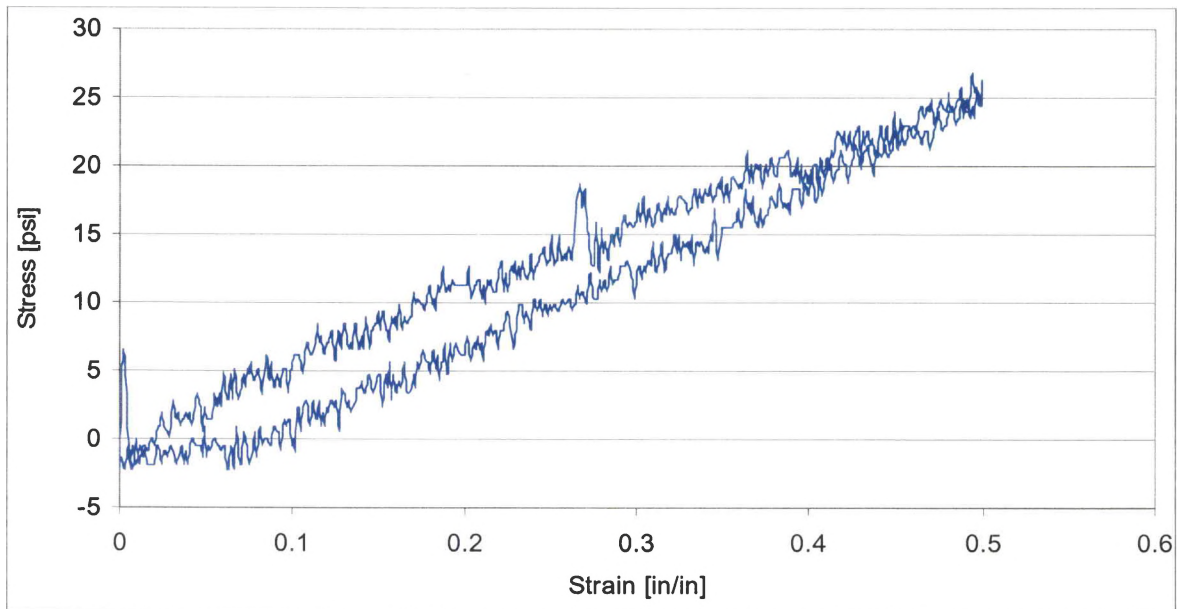
Figure 95: Tensile Specimen #3

Figure 96: Tensile Specimen #4

121

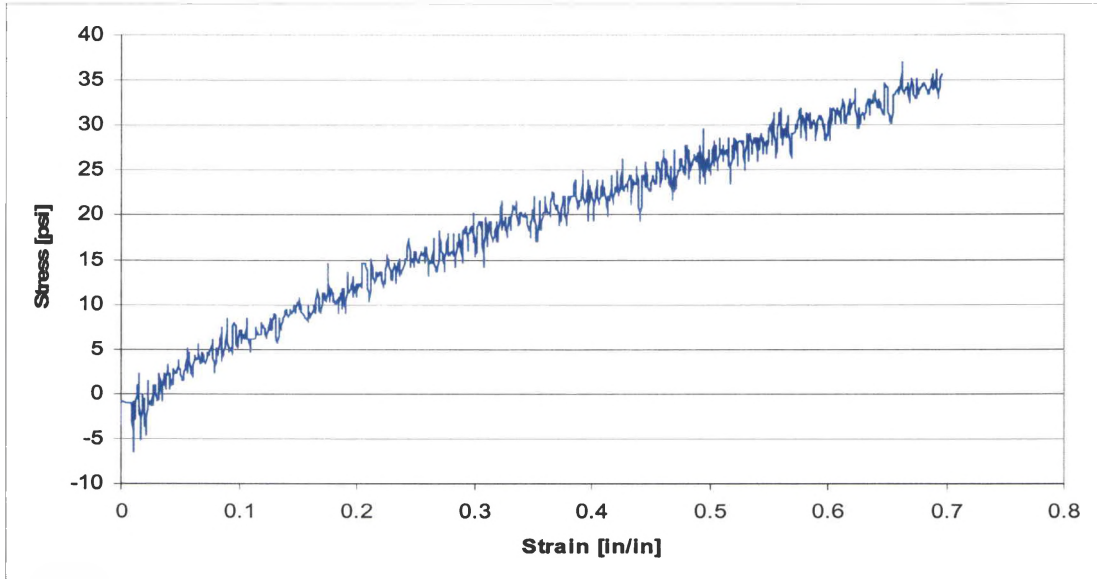**Figure 97: Tensile Specimen #5**
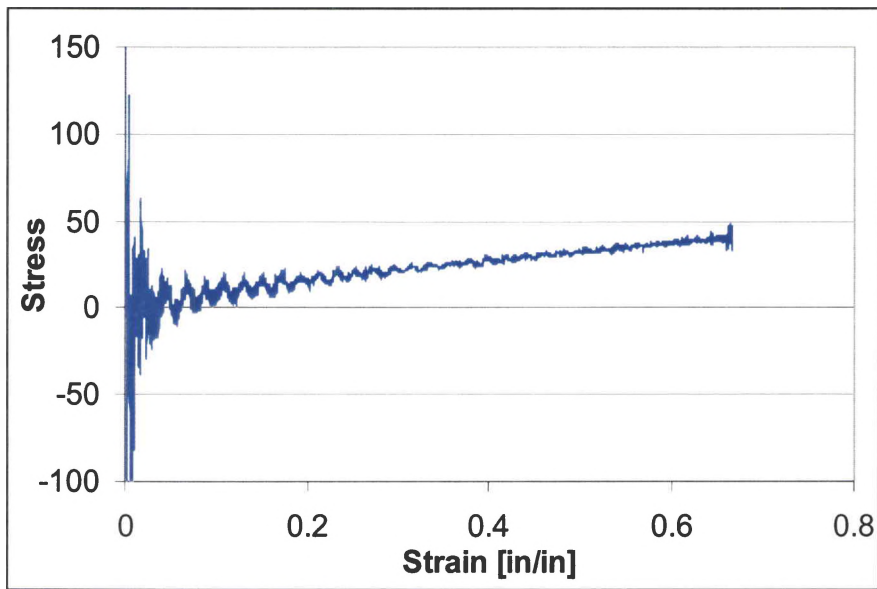
Figure 98: Tensile Specimen #6

122

REFERENCES

Aerodyn.org website: www.aerodyn.org

Aerospaceweb.org website: http://www.aerospaceweb.org/aircraft/bomber/ f111/ pics01.html, 7 April 2005

AIAA website: http://www.aiaa.org/aerospace/Article.cfm?issuetocid =256&ArchiveIssueID=30, 29 March 2005

MTS website: www.mts.com, 25 February 2005

SkyFlash / UGA website: http://www.sky-flash.com, 5 April 2005

ABAQUS. *ABAQUS User's Manual*, Hibbit, Karlsson & Sorensen, Inc., Pawtucket, RI, 1995.

Abrahamson, E. R., Mark S. Lake, Naseem A. Munshi, Ken Gall, 2002. "Shape Memory Polymers for Elastic Memory Composites" AIAA 2002-1562, 43rd Structures, Structural Dynamics, and Materials Conference, April 2002, Denver, CO

Anon., "ASTM Designation D 638 – 03 "Standard Test Method for Tensile Properties of Plastics," 2005, ASTM International, Volume 08.01.

Austin, F., M. J. Rossi, W. Van Nostrand, G. Knowles, A. Jameson, 1994. "Static Shape Control for Adaptive Wings." AIAA Journal 32 (1994) 1895-1901

Campanile, L. F., O. Seack, D. Sachau, 2000. "The Belt-rib Concept for Variable-camber Airfoils: Recent Developments." Proceedings of the SPIE Vol. 3985, 2000, Newport Beach, California.

Cullen, Sean. P., Tim R. Roberts, Tat H. Tong, 2002. "Studies of Shape Memory Behavior of Styrene-Based Network Copolymers." Proceedings of The First World Congress on Biomimetics, 2002, Albuquerque, New Mexico.

Craig, Jr., Roy R.. *Mechanics of Materials, Second Edition.* John Wiley & Sons, New York, NY, 2000

DeCamp, Ronald W., Richard Hardy, Douglas K. Gould, 1987. "Mission-Adaptive Wing." SAE International Pacific Air and Space Technology Conference, Melbourne, Australia 1987.

Dunne, J., D. Pitt, E. White, E. Garcia, 2000. "Ground Demonstration of the Smart Inlet." AIAA 41st Structures, Structural Dynamics, and Materials Conference, Atlanta, Georgia, April 2000.

Frank, Geoffrey. J., Robert A. Brockman, 1998 "A Viscoelastic-viscoplastic Constitutive Model for Glassy Polymers." International Journal of Solids and Structures 38 (2001) 5149-5164

Gall, Ken, Martin L. Dunn, Yiping Liu, Dudley Finch, Mark Lake, Naseem A. Munshi, 2002. "Shape Memory Polymer Nanocomposites." Acta Materialia 50 (2002) 5115-5126

Hjelmstad, Keith D.. *Fundamentals of Structural Mechanics*, Prentice-Hall, Inc., Upper Saddle River, 1997.

Keihl, Michelle. M., Robert S. Bortolin, Brian Sanders, Shiv Joshi, Zeb Tidwell, 2005. "Mechanical Properties of Shape Memory Polymers for Morphing Aircraft Applications." Proceedings of the SPIE... 2005, San Diego, California.

Kikuta, Michael Thomas. "Mechanical Properties of Candidate Materials for Morphing Wings," Master of Science Thesis, Virginia Polytechnic Institute and State University, 2003.

Kudva, J. N., 2004. "Overview of the DARPA/AFRL/NASA Smart Wing Phase 2 Program" Journal of Intelligent Material Systems and Structures 2004 15: 261-267

Lagoudas, Dimitris C., Justin K. Strelec, John Yen, Mohammad A. Khan, 2000. "Intelligent Design Optimization of a Shape Memory Alloy Actuated Reconfigurable Wing." Proceedings of the SPIE Vol. 3984, 2000, Newport Beach, California.

Liu, Changdeng., Seung B. Chun, Patrick T. Mather, Lei Zheng, Elisabeth H. Haley, E. Bryan Coughlin, 2002. "Chemically Cross-Linked Polycyclooctene: Synthesis, Characterization and Shape Memory Behavior." Macromolecules 35 (2002) 9868-9874.

Liu, Yiping. "Thermomechanical Behavior of Shape Memory Polymers," Doctoral Dissertation, University of Colorado, 2004.

Liu, Yiping, Ken Gall, Martin L. Dunn, Patrick McCluskey, 2003. "Thermomechanics of Shape Memory Polymer nanocomposites." Mechanics of Materials 36 (2004) 929-940

McKnight, Geoff, Chris Henry, 2005. "Variable Stiffness Materials for Reconfigurable Surface Applications." Proceedings of the SPIE... 2005, San Diego, California.

Nellutla, Sudeepthi. "Shape Memory Polymers for Elastic Memory Composites" Project Report

Pitt, D. M., J. P. Dunne, E. V. White, E. Garcia, 2001. "SAMPSON Smart Inlet SMA Powered Adaptive Lip Design and Static Test." 42nd AIAA Structures, Structural Dynamics, and Materials Conference, Seattle, Washington, April 2001.

Ram, Arie. *Fundamentals of Polymer Engineering,* Plenum Press, New York, 1997 p 81

Sanders, Brian, Jennifer Chase Fielding. "Kinematically Designed Skins (KiDS)" CSIRF proposal, December 2004

Sanders, Brian, Dave Cowan, Lewes Scherer, 2004. "Aerodynamic Performance of the Smart Wing Control Effectors." Journal of Intelligent Material Systems and Structures 2004 15: 293-303

Snyder, Emily. A., Tat H. Tong, 2005. "Towards Novel Light-Activated Shape Memory Polymer: Thermomechanical Properties of Photo-responsive Polymers." Materials Research Society Spring Meeting 2005, San Francisco, California

Srinivasa, Narayan, Richard Ross, 2005. "An Automated Approach to Design Shape Morphing Strategies for Reconfigurable Surfaces." Proceedings of the SPIE… 2005, San Diego, California.

Strong, A. Brent. *Plastics: Materials and Processing.* Prentice-Hall, Inc., New Jersey, 1996.

Timoshenko, S. P., Gere, J. M.. *Theory of Elastic Stability*, McGraw-Hill Book Company, Inc., New York, 1961.

Bartley-Cho, Jonathan D., Donny P. Wang, Christopher A. Martin, Jayanth N. Kudva, and Mark N. West, 2004. "Development of High-rate, Adaptive Trailing Edge Control Surface for the Smart Wing Phase 2 Wind Tunnel Model." Journal of Intelligent Material Systems and Structures 2004 15: 279-291.

Wang, D. P., J. D. Bartley-Cho, C. A. Martin, B. J. Hallam, J. N. Kudva, B. Sanders, 2001. "Design of a High-Rate, Large Deflection, Control Surface for Vehicle Control." Proceedings of the SPIE... 2001, San Diego, California

VITA

Robert Sebastian Bortolin was born 24 September 1981 in New York City. Robert attended Edgemont High School in Scarsdale, New York from 1995 – 1999. His education continued at the University of Dayton, Dayton, OH, where he graduated 20 December 2003. After spending a month in Italy and some time with family Robert returned to the University of Dayton to continue his studies and received a Master of Science in Aerospace Engineering in August 2005.